Floating Bodies with Surface Tension

by

Hanzhe Chen

A thesis
presented to the University of Waterloo
in fulfillment of the
thesis requirement for the degree of
Master of Mathematics
in
Applied Mathematics

Waterloo, Ontario, Canada, 2016

I hereby declare that I am the sole author of this thesis. This is a true copy of the thesis, including any required final revisions, as accepted by my examiners.

I understand that my thesis may be made electronically available to the public.

Abstract

Capillary phenomena have been studied by mathematicians and physicists for hundreds of years. In this thesis, both two-dimensional($2D$) and three-dimensional($3D$) bodies floating on an unbounded reservoir are studied based on the Young-Laplace equation. We reconsider the $2D$ floating cylinder problem studied in a groundbreaking paper of Bhatnargar and Finn from 2006. We derive the total energy E_T relative to the undisturbed state and the total force in vertical direction and show that $F_T = -\frac{dE_T}{dh}$, where h is the height of the centre of the cylinder relative to the undisturbed fluid level. The number of equilibria, the floating configurations and their stability are also studied. In the $2D$ floating square problem, we rederive the floating configurations and their stability in the no surface tension case. Allowing surface tension, one example with contact angle $\gamma = \frac{\pi}{4}$ is considered. We show that there is one unstable equilibrium of the floating square with a horizontal side. In the $3D$ floating object problem with radial symmetry, the shooting method is applied to obtain the fluid height u and radial distance r from the vertical axis numerically in terms of the inclination angle ψ parameter. In the vertical cylinder problem, the relation between E_T and F_T is found to be consistent with $2D$ cylinder case. In the floating ball problem, a non-monotone relation between height of centre h and the wetting angle ϕ_0 is found. We also give an example of two floating configurations with the same height h. More study of the $3D$ floating ball problem is anticipated.

Acknowledgements

First, I would like to express my deepest gratitude to my supervisor Professor David Siegel. Thank you for your support, guidance, opportunities and encouragement during my master's study in mathematics.

I would like to thank my committee members, Professor Sivabal Sivaloganathan and Professor Marek Stastna, for your suggestions and time. I would like to thank the chair of the defence, Michael Waite, for your time.

Furthermore I would like to thank my office mates Brian Fernandes, Minxin Zhang, Kamran Akbari and Lindsey Daniels for creating the harmonious working environment and your valuable comments for my thesis. I would like to thank to my department colleagues Cesar Ramirez Ibanez and Yangang Chen for the inspiring conversations about the philosophy of mathematics. I would like to thank to my Friends Jian Liang and Naijing Kang for providing me countless free lunch and dinner. I would like to thank to my family for the continued support and unconditional love.

To My Parents and Fiancée

Table of Contents

List of Tables

List of Figures

List of Symbols

We list the descriptions of symbols which will be used later.

Σ The wetted region.

β The relative adhesion coefficient.

γ The contact angle.

κ The capillary constant, where $\kappa = \frac{\rho g}{\sigma}$.

ϕ_0 The wetting angle, the supplementary angle of the azimuthal angle.

ψ The inclination angle.

ψ_0 The inclination angle at contact point.

ρ The density difference of the air and the fluid. Moreover, we assume $\rho_{air} = 0$ thus ρ also represents the density of liquid.

ρ_s The density of the solid or the floating body.

σ Surface tension along the fluid interface.

σ_1 Surface tension between air and solid interface.

σ_2 Surface tension between liquid and solid interface.

a Radius of the cylinder in Chapter 2, side length of the square in Chapter 3 or radius of the ball in Chapter 4.

g The gravity force per unit mass in $2D$ or the gravitational field in $3D$.

h The height of the centre, the displacement from the centre of the cylinder, the square, the vertical cylinder or the ball to the reference fluid level.

m The mass per unit length in $2D$ or the mass in $3D$ of the floating body.

u The fluid height, the displacement from the fluid interface to the reference level.

x The horizontal distance.

y The displacement from free surface level to the bottom of the cylinder.

$E_F, \hat{E}_F$ The fluid potential energy and its dimensionless form.

$E_G, \hat{E}_G$ The body potential energy and its dimensionless form.

$E_T, \hat{E}_T$ The total energy and its dimensionless form.

$E_W, \hat{E}_W$ The wetting energy and its dimensionless form.

$E_\sigma, \hat{E}_\sigma$ The surface tension energy and its dimensionless form.

$F_B, \hat{F}_B$ The buoyant force and its dimensionless form.

$F_G, \hat{F}_G$ The gravitational force and its dimensionless form.

$F_T, \hat{F}_T$ The total force in vertical direction and its dimensionless form.

$F_\sigma, \hat{F}_\sigma$ The surface tension force and its dimensionless form.

$\bar{\phi}_0$ The critical point of E_T, $\bar{\phi}_0 \in (0, \pi)$.

$\mathcal{B}$ The Bond number, where $\mathcal{B} = \kappa a^2$.

$I(\phi_0, \mathcal{C})$ The intersection function of fluid interfaces.

$\bar{\phi}_0$ Equilibrium point of $\hat{F}_T$ if $\hat{F}_T$ admits at most one Equilibrium point.

$\bar{\phi}_{0i}$ Equilibrium points of $\hat{F}_T$ if $\hat{F}_T$ admits two equilibrium points, where $i \in \{1, 2\}$.

$\mathcal{A}$ Dimensionless parameter is defined as $\mathcal{A} = \frac{m}{a^2\rho}$, which is used in Chapter 2.

$\mathcal{A}^*$ $\mathcal{A}^*$ satisfies $\hat{F}_T(\phi_0^*, \mathcal{A}^*) = 0$.

$\mathcal{C}$ Dimensionless parameter is defined as $\mathcal{C} = \sqrt{\kappa}a$, which is used in Chapter 2.

$\mathcal{C}_i(\mathcal{A})$ The boundary curves distingish the number of equilibria in $\mathcal{A}$ vs $\mathcal{C}$ region, where $i \in \{1, 2, 3\}$.

ϕ_0^* The second critical point of $\hat{F}_T$, which satisfies $\phi_0^* > \frac{\pi}{2}$.

$\tilde{\phi}_0$ Satisfying $I(\tilde{\phi}_0, \mathcal{C}) = 0$ for given $\mathcal{C}$.

$(\hat{h}^*, \theta^*)$ The critical point of $\hat{E}_T(\hat{h}, \theta)$.

E_{square} The characteristic energy of the square, where $E_{square} = \rho_s a^3 g$.

α The density ratio $\alpha = \frac{\rho_s}{\rho}$, where ρ_s is the density of solid and ρ is the density of liquid.

$\hat{h}$ Dimensionless centre of height, where $\hat{h} = \frac{h}{a}$.

$\mathcal{S}$ Dimensionless parameter is defined as $\mathcal{S} = \frac{\sigma}{\sqrt{\kappa \rho_s a^3 g}}$.

ψ_1 The inclination angle to the right of the fluid interfaces.

ψ_2 The inclination angle to the left of the fluid interfaces.

ψ_{10} The inclination anlge at the right contact point.

ψ_{20} The inclination angle at the left contact point.

θ The rotational angle clockwise from the vertical axis.

θ^* The critical point of $\hat{E}_T(\theta)$.

h^* The height of centre in force balance.

h_B The displacement of the centroid of buoyance to the reference level.

E_c The characteristic energy in $3D$ vertical cylinder, where $E_c = \pi \sigma a^2$.

F_c The characteristic force in $3D$ vertical cylinder, where $F_c = \pi \sigma a$.

I_0 Modified Bessel function of the first kind.

K_0 Modified Bessel function of the second kind.

$\hat{r}$ The dimensionless radial distance, where $\hat{r} = \frac{r}{a}$.

ω The tangent angle $\omega > 0$, the supplementary angle of ψ.

r The radial distance from the vertical axis.

s The arc length along the fluid interface.

Chapter 1

Introduction

When you walk across a lawn early in the morning, you'll find dew drops attached to the edges of leaf blades. When you read a burette in a chemistry lab, you'll find the liquid surface forms a meniscus. There are countless such capillary phenomena. The records of capillary phenomena can be tracked back to the Renaissance. Leonardo da Vinci[14] described experiments associated with capillary phenomena in his manuscripts. His celebrated work is widely considered the first description of capillary phenomena. Many pioneers such as Newton(1687), Huygens(1690s), Hawksbee(1709), Taylor(1712) and Jurin(1718) have made contributions to the experimental work on capillarity. The description of these pioneers' work can be found in the literature review of capillarity by Lloyd [14]. In 1805, a breakthrough essay [22] by Thomas Young was published by the Royal Society of London. He was the first to present the relation (1.1) between mean curvature H[1] and the pressure difference δp across a fluid interface through balancing δp and surface tension σ, which is assumed to be a constant.

$$\delta p = 2\sigma H, \tag{1.1}$$

He also asserted the contact angle condition (1.2) that the tangential forces along the solid must be balanced. It is also known as "Young's diagram" (see Figures 1.1, 2.7). It leads to

$$\cos \gamma = \frac{\sigma_1 - \sigma_2}{\sigma}, \tag{1.2}$$

---

[1]Young first introduced the notation of mean curvature H, which was precisely defined by Sophie Germain several decades later.

where γ is the contact angle, σ is the surface tension between air and liquid (we say air/liquid surface tension for short.), σ_1 and σ_2 are air/solid and liquid/solid surface tensions, respectively.
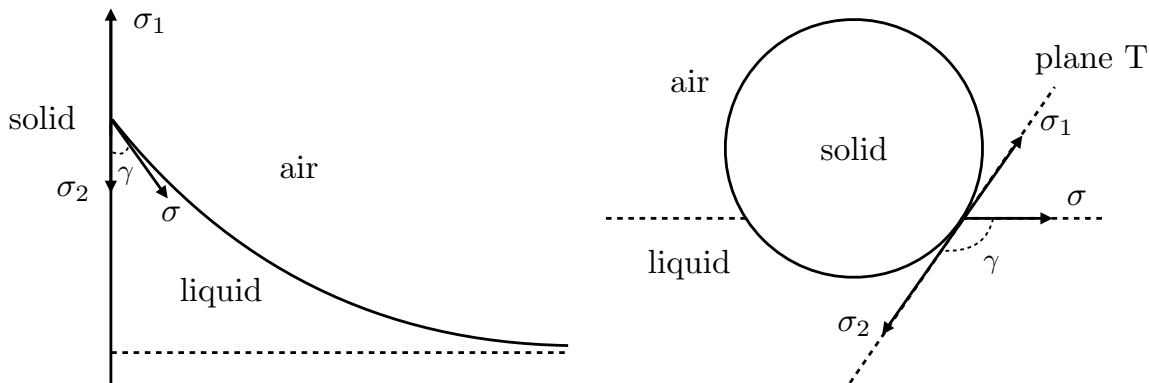
Figure 1.1: Young's diagram for contact angle and a counterexample.

"Young's diagram" is widely used in engineering. In recent years, Finn argues its validity. In paper [6], Finn gives a counterexample of a floating spherical ball in zero gravity (see Figure 1.1). If we follow Young's diagram, the total force in the vertical direction can not be balanced. In [2], Bhatnagar and Finn argue that the surface tension force is only along the fluid interface. In [16], Marchand, Weijs, Snoeijer and Andreotti also criticize Young's diagram and reach the same conclusion about the surface tension force. Related discussions of Young's diagram and Finn's paradox example can also be found in [2], [7], [8], [15] and [18].

Differing from Young's qualitative analysis of capillarity, Laplace reintroduced Young's results with formal mathematical notations in 1806 [5]. Due to their contributions to capillarity, the equation (1.1)[2] was named after Thomas Young and Pierre-Simon Laplace. In 1830, Gauss reproduced the capillary equation and the contact angle condition by reasoning that the energy of this mechanical system is stationary in equilibrium [5].

Gauss' energy method is presented in a general framework by Finn in his celebrated book [5] on capillarity. We now employ Gauss' energy method in a more specific case. Consider a vertical tube with cross section Ω in an infinite reservoir. The density of liquid is ρ_l, the density of air is ρ_{air}, the surface tension of the air/liquid interface is σ, the air/solid interface is σ_1 and the liquid/solid interface is σ_2. With downward acting gravity

---

[2]It is called Young-Laplace Equation or Capillary Equation.
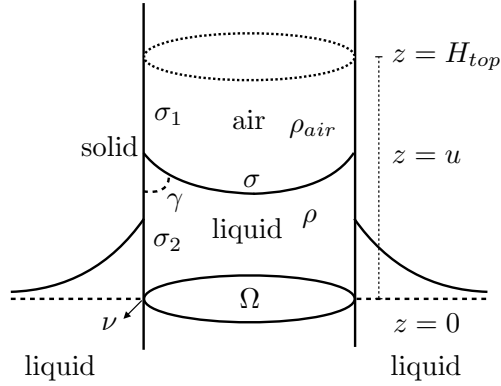
Figure 1.2: A capillary tube.

g and surface tension[3], capillary action causes the air/liquid interface $z = u(x, y)$, where $(x, y) \in \Omega$, which is assumed to be a graph (see Figure 1.2). If we consider the energy in the vertical tube from the fixed height $z = H_{top}$[4] to the reference fluid level $z = 0$, the energy functional can be expressed as

$$\mathcal{E}(u) = \sigma \int_\Omega \sqrt{1 + |\nabla u|^2} d\Omega + \sigma_1 \int_{\partial\Omega} (H_{top} - u) \, ds + \sigma_2 \int_{\partial\Omega} u ds$$
$$+ \rho g \int_\Omega \frac{u^2}{2} d\Omega + \rho_{air} g \int_\Omega \left(\frac{H_{top}^2 - u^2}{2} \right) d\Omega, \tag{1.3}$$

where $\sigma \int_\Omega \sqrt{1 + |\nabla u|^2} d\Omega$ is the surface tension energy of the fluid interface. $\sigma_2 \int_{\partial\Omega} u ds$ and $\sigma_1 \int_{\partial\Omega} (H_{top} - u) \, ds$ are the surface tension energy of liquid/solid interface and air/solid interface, respectively. $\rho g \int_\Omega \frac{u^2}{2} d\Omega$ and $\rho_{air} g \int_\Omega \left(\frac{H_{top}^2 - u^2}{2} \right) d\Omega$ are the potential energy of the liquid and the air in tube from $z = 0$ to $z = H_{top}$.

Minimizing the functional $\mathcal{E}(u)$ results in the capillary equation and contact angle condition:

$$\operatorname{div} \mathsf{T} u \ = \ \kappa u \ \text{in} \ \Omega. \tag{1.4}$$
$$\nu \cdot \mathsf{T} u \ = \ \cos\gamma \ \text{on} \ \partial\Omega. \tag{1.5}$$

---

[3]Surface tension can be interpreted as energy per area.
[4]The surface $z = u$ never touches $z = H_{top}$.

3

Where ν is the outer normal of Ω, $\kappa = \frac{\rho - \rho_{air}}{\sigma} g$ is known as the capillary constant and $\mathsf{T}u = \frac{\nabla u}{\sqrt{1 + |\nabla u|^2}}$. The interface $z = u(x, y)$ meets the tube in the contact angle γ with $\cos \gamma$ given by (1.2). In addition, $\mathrm{div}\, \mathsf{T}u$ has the meaning of twice the mean curvature of the surface u. With hydrostatic pressure in the liquid and air, we see that (1.4) is equivalent to (1.1).

Two symmetric cases are discussed in this thesis. After introducing the inclination angle ψ (see section 2.1), equation (1.4) can be geometrically interpreted for the two-dimensional (2D) cylinder in Chapter 2,

$$\frac{d}{dx} \sin \psi = \kappa u, \tag{1.6}$$

where x is the distance in horizontal axis. The left hand side of (1.6) is the curvature of the interface curve. Moreover, the solution of equation (1.6) is classically known and can be traced back to Laplace and Euler (see Section 2.2).

For three-dimensional(3D) symmetrical floating objects in Chapter 4, if we introduce the radial distance r from the axis, the equation (1.4) becomes as follows,

$$\left(r \sin \psi\right)_r = \kappa r u, \tag{1.7}$$

where ψ is the inclination angle of the radial cross-section.

The equation (1.7) can also be written in parametric form,

$$\frac{du}{d\psi} = \frac{r \sin \psi}{\kappa r u - \sin \psi} \quad \text{and} \quad \frac{dr}{d\psi} = \frac{r \cos \psi}{\kappa r u - \sin \psi}. \tag{1.8}$$

The non-linear first order system (1.8) is also used in the study of both interior problems such as sessile drops [5] and exterior problems such as floating drops [3]. Vogel also gives an analogous representation for the exterior surfaces in [20]. In addition, for the exterior problem, the fluid interface tends asymptotically to the reference level: $u \to 0$ and $\psi \to 0$ as the radial distance $r \to \infty$.

The study of a 2D cylinder floating on an unbounded bath is motivated by Bhatnagar and Finn's work in [2]. They give both energy and force analysis in the study of the floating configurations and their stability. In the force analysis, they discussed different choices in order to include surface tension. We agree with Finn's choice which is inspired by Gifford and Scriven's work in [9]. The surface tension force exists only along the fluid interface instead of along the air/solid or liquid/solid interfaces as depicted in Young's diagram[5].

---

[5]This can be treated as another counterexample to Young's diagram.

When it comes to the buoyant force, the famous Archimedes' principle can not be ignored. In the work "On Floating Bodies", Archimedes stated:

"Any object, wholly or partially immersed in a fluid, is buoyed up by a force equal to the weight of the fluid displaced by the object."

But Archimedes' principle is not in general correct when the air/liquid interface is not flat due to the presence of surface tension. McCuan and Treinen discuss Archimedes' principle and capillarity in [17]. Archimedes' principle is also studied in Appendix B and employed in studying the floating square in Chapter 3. In [2], Bhatnagar and Finn use the principle of virtual work approach. Different from this work which considered infinitesimal changes in the total energy, we give the full expression for the total energy E_T. We also establish the relation between the total force in vertical direction and the total energy in Section 2.6. [2] gives the first example where the floating cylinder admits two equilibrium positions. In the thesis, we correct the stability assertions concerning these two equilibria. Moreover, we give the full study of the total force F_T and the conditions on the number of equilibria the system can admit and their stability.

The study of the $2D$ floating square is motivated by Erdös, Schibler and Herndon's work in [4] and Abolhassani's work in [1]. We rederive the stability conditions of the floating square with the allowance of rotation in absence of surface tension (see Section 3.2). Two parameters are introduced, the centre of mass height h and the clockwise rotation angle θ from the vertical axis. The case with surface tension is complicated. One example with contact angle $\gamma = \frac{\pi}{4}$ is discussed. The result is similar to the case without gravity. Todd and Siegel studied the stability of floating objects with polygonal cross sections without gravity [12]. They concluded that the body cannot have a stable equilibrium with the fluid interface not passing through two of the vertices. Since the stable configuration of the square allowing rotation with surface tension is still an open question, we can only conclude that there is one unstable equilibrium $\theta^* = 0$ of the floating square with a horizontal side in one particular case.

The radial symmetric capillary equation (1.7), (1.8), has received much attention. The study of the $3D$ exterior problem has drawn much attention. The parametric form (1.8) of the capillary equation is employed in the study of liquid bridges [20], floating drops [3] and sessile drops [5]. The non-linear first order system (1.8) does not have an analytical solution. We have to apply the shooting method (see Section 4.2) to compute these. The shooting method for the capillary equation was introduced by Hartland and Hartley in [10]. Elcrat, Treinen and Hemphill also employ shooting method in the study of floating bubbles in [11] and [19]. In the thesis, the shooting method is also applied in the study of

the floating vertical cylinder in Section 4.2. In the study of floating ball by McCuan and Treinen in [17], the arc length parametrization is used instead. Through our numerical computation, the inclination parametrization has better performance (see Section 4.1). Finally, we discuss a challenging $3D$ problem, the floating ball. Differing from the $2D$ cylinder case, a non-monotone relation between the height of h and wetting angle ϕ_0 is found. Moreover, two configurations are displayed with the same height h. The relation between the vertical total force and the total energy is left for future study.

The structure of this thesis is as follows: the $2D$ floating cylinder is discussed in Chapter 2, we focus on Young's diagram, investigating the relation between F_T and E_T and the number of equilibria. The $2D$ floating square with rotation is studied in Chapter 3. The stability conditions are discussed in no surface tension case. With surface tension, one example with contact angle $\gamma = \frac{\pi}{4}$ is studied. In Chapter 4, the floating vertical cylinder and the floating ball are discussed. Finally, conclusions and future work are discussed in Chapter 5.

Chapter 2

Two-Dimensional Cylinder on An Unbounded Bath

The $2D$ cylinder horizontally floating on an unbounded bath is motivated by the ground breaking paper of Bhatnagar and Finn [2]. They studied equilibrium configurations and their stability through considerations of energy and the analysis of the total force. In this chapter, we will follow Bhatnagar and Finn's approach but with some modifications. The three most important contributions are:

1. The relation between the total energy and the total force.

2. How the parameters influence the number of equilibrium configurations and their stability.

3. The limitation of the capillary model due to the possible intersection of fluid interfaces.

In addition, we see limitations in the use of Young's diagram and determine the buoyant force when the fluid interface is not flat.

2.1   Fluid Interface and Configuration

Suppose an infinite reservoir of fluid has its interface at the zero level. Introduce an infinite cylinder of radius a floating horizontally on the infinite reservoir and assume the free fluid

7

level is unchanged. If we admit the presence of surface tension, the fluid will be lifted up or pushed down to the fluid height u.

When the fluid height $u > 0$, the inclination angle is measured counterclockwise from the positive horizontal direction, ψ ranges from $-\pi$ (on the top) to 0 (free fluid level). When the fluid height $u < 0$, ψ ranges from 0 to π.
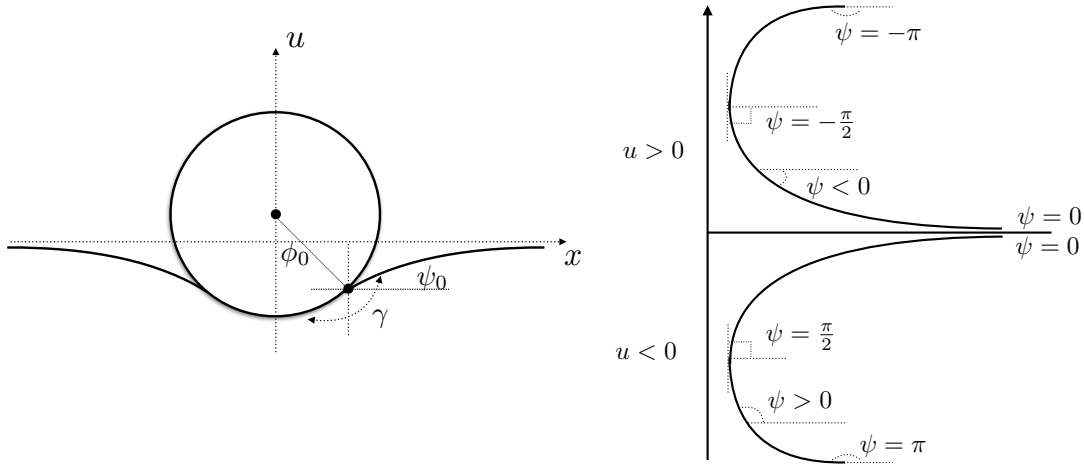
Figure 2.1: Configuration.

Assume that both the fluid and the cylinder are homogeneous. Once a unit length is chosen, our ideal model turns into two-dimensional problem. Viewing the cross section, we set the centre of the cylinder on the vertical axis. At the contact point between the fluid and the cylinder, we can define the contact angle γ, the inclination angle ψ_0 and the wetting angle ϕ_0 at the contact point (see Figure 2.1). Immediately, we obtain the geometric constraint:

$$\psi_0 = \phi_0 + \gamma - \pi. \tag{2.1}$$

Since the configuration is symmetric about the vertical axis, we only need to look at the fluid interface on one side such that the horizontal distance $x > 0$.

2.2 The Capillary Equation

The fluid height u satisfies the one-dimensional capillary equation:

$$\frac{d}{dx} \sin \psi = \kappa u. \tag{2.2}$$

where $\kappa = \frac{\rho g}{\sigma}$ is known as the capillary constant, σ is surface tension along the fluid interface, ρ is the density difference of the fluid and the air, and g is the gravity force per unit mass.

According to our assumption, the fluid height u goes to zero asymptotically as $x \to \pm\infty$.

$$\lim_{x \to \pm\infty} u(x) = 0. \tag{2.3}$$

In this chapter, we will have that the capillary equation (2.2) with boundary condition (2.3) admits the unique symmetric solution $u(x)$. This solution is classically known and can be traced back to Laplace and Euler.
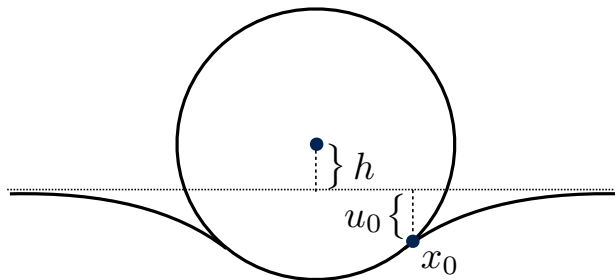
Figure 2.2: Centre height h, $u_0 < 0$ is pictured.

Finn and Bhatnagar in [2] have given the solution where u and x are functions of ψ. We modify the solution to treat $u > 0$ and $u < 0$ simultaneously and to be consistent with our notation.

$$u(\psi) \ = \ -\frac{2}{\sqrt{\kappa}} \sin \frac{\psi}{2}. \tag{2.4}$$

$$x(\psi) \ = \ -\frac{1}{\sqrt{\kappa}} \left[2\cos\frac{\psi}{2} + \ln|\tan\frac{\psi}{4}| - 2\cos\frac{\psi_0}{2} - \ln|\tan\frac{\psi_0}{4}| \right] + a\sin\phi_0. \tag{2.5}$$

At the contact point, the horizontal distance is $x_0 = a\sin\phi_0$, the vertical fluid height at x_0 is $u_0 = u(\psi_0) = -\frac{2}{\sqrt{\kappa}} \sin\frac{\psi_0}{2}$. We define the height of the centre $h = a\cos\phi_0 + u_0$ (see Figure 2.2), therefore

$$h = a\cos\phi_0 - \frac{2}{\sqrt{\kappa}} \sin\frac{\psi_0}{2}. \tag{2.6}$$

9

2.3 Derivation of the Total Energy E_T

In this section, following the method of Gauss [5], we determine all the potential energies of the floating cylinder system. Because of the unboundedness of the exterior fluids, we have to consider the relative energy instead of the full one to avoid the confusion of infinite energy. The types of energies will be expressed explicitly in terms of the contact inclination angle ψ_0 and the wetting angle ϕ_0.

We have the following four types of energy:

- The body potential energy:

  the body potential energy relative to the free fluid level can be expressed as $E_G = mgh$, where $h = a\cos\phi_0 - \frac{2}{\sqrt{\kappa}}\sin\frac{\psi_0}{2}$. E_G is a function in terms of ψ_0 and ϕ_0:

  $$E_G(\psi_0, \phi_0) = mg\left(a\cos\phi_0 - \frac{2}{\sqrt{\kappa}}\sin\frac{\psi_0}{2}\right). \tag{2.7}$$

- The wetting energy:

  the wetting energy is written $E_W = -\beta\sigma|\Sigma|$, where the wetting area per unit length is denoted by $|\Sigma| = 2a\phi_0$. With the relative adhesion coefficient β, E_W only depends on ϕ_0:

  $$E_W(\phi_0) = -2\beta\sigma a\phi_0. \tag{2.8}$$

  In Section 2.4, we will show that β is equal to $\cos\gamma$.

- The surface tension energy:

  surface tension has the interpretation $\frac{energy}{area}$. In order to avoid infinite energy, we define the surface energy E_σ, a relative energy compared with the surface energy of undisturbed fluid surface (Figure 2.3). It has the form:

  $$E_\sigma = 2\sigma \lim_{x_1 \to \infty}\left[\int_{x_0}^{x_1}\sqrt{1 + (\frac{du}{dx})^2}dx - \int_0^{x_1}dx\right]. \tag{2.9}$$

  In Figure 2.3, the fluid surface is a graph. The fluid interface can also have a non-graph shape. The computation of both cases is in Appendix A. E_σ is shown below:

  $$E_\sigma(\psi_0, \phi_0) = \frac{4\sigma}{\sqrt{\kappa}}(1 - \cos\frac{\psi_0}{2}) - 2\sigma a\sin\phi_0. \tag{2.10}$$

10
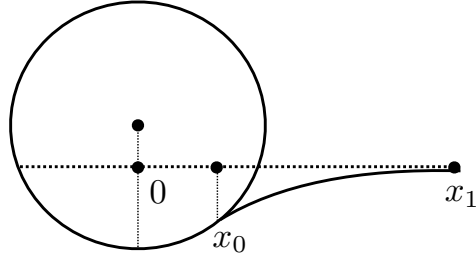
Figure 2.3: Computation relative surface tension energy.

- The fluid potential energy

  the fluid potential energy E_F is also treated as a relative energy compared with the free fluid level as shown on Figure 2.4. A better expression for E_F is to break E_F into two parts E_{F1} and E_{F2}:
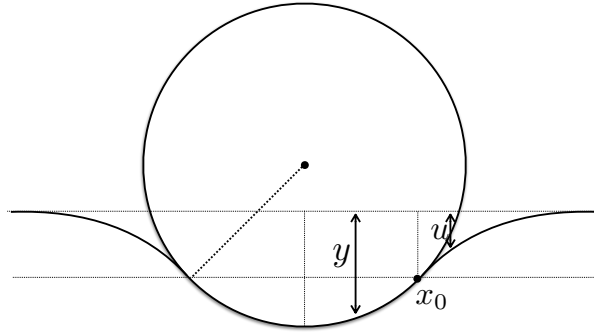
Figure 2.4: Computation of relative potential energy.

$$E_F = \underbrace{2\rho g \int_0^{x_0} \frac{y^2}{2} dx}_{E_{F1}} + \underbrace{2\rho g \int_{x_0}^{\infty} \frac{u^2}{2} dx}_{E_{F2}} . \qquad (2.11)$$

Where y is the vertical height from the free fluid level to the bottom of the cylinder. The calculation of E_F is in Appendix A. E_F is shown below:

11

$$E_F = E_{F_1} + E_{F_2}$$

$$= -\frac{4\sigma}{3\sqrt{\kappa}}\left(1 - 2\cos\frac{\psi_0}{2} + \cos\frac{\psi_0}{2}\cos\psi_0\right) + \frac{1}{12}\rho g a^3 \sin 3\phi_0$$

$$- \rho g a^3 \phi_0 \cos\phi_0 + \frac{3}{4}\rho g a^3 \sin\phi_0 - a^2\sqrt{\sigma\rho g}\sin\frac{\psi_0}{2}\sin 2\phi_0$$

$$+ 2a^2\sqrt{\sigma\rho g}\phi_0 \sin\frac{\psi_0}{2} + 4\sigma a \sin^2\frac{\psi_0}{2}\sin\phi_0. \tag{2.12}$$

The total energy E_T can be expressed of the sum of the above four energies.

$$E_T = E_G + E_W + E_\sigma + E_F. \tag{2.13}$$

The full expression of E_T in terms of ψ_0 and ϕ_0 is:

$$E_T(\psi_0, \phi_0) = mg\left(a\cos\phi_0 - 2\sqrt{\frac{\sigma}{\rho g}}\sin\frac{\psi_0}{2}\right) - 2\beta\sigma a\phi_0 + \frac{8}{3}\sigma\sqrt{\frac{\sigma}{\rho g}}\left(1 - \cos^3\frac{\psi_0}{2}\right)$$

$$- 2\sigma a \sin\phi_0\cos\psi_0 + \frac{1}{12}\rho g a^3\sin 3\phi_0 - \rho g a^3 \phi_0 \cos\phi_0 + \frac{3}{4}\rho g a^3 \sin\phi_0$$

$$- a^2\sqrt{\sigma\rho g}\sin\frac{\psi_0}{2}\sin 2\phi_0 + 2a^2\sqrt{\sigma\rho g}\phi_0\sin\frac{\psi_0}{2}. \tag{2.14}$$

2.4 The Relative Adhesion Coefficient β

Finn argues in a very general setting by a variational argument that $\beta = \cos\gamma$ in [5]. In this section, we will show that minimizing $E_T(\psi_0, \phi_0)$ subject to $h = h_0$ (h_0 is a constant) gives the same result. The Lagrange multiplier is applied.

$$\nabla E_T = \lambda \nabla h, \tag{2.15}$$

$$\frac{\partial E_T}{\partial\phi_0} + \lambda a \sin\phi_0 = 0, \tag{2.16}$$

$$\frac{\partial E_T}{\partial\psi_0} + \frac{\lambda}{\sqrt{\kappa}}\cos\frac{\psi_0}{2} = 0. \tag{2.17}$$

We multiple $\frac{1}{\sqrt{\kappa}}\cos\frac{\psi_0}{2}$ and $a\sin\phi_0$ both sides on (2.16) and (2.17) respectively to obtain:

$$\frac{1}{\sqrt{\kappa}} \cos \frac{\psi_0}{2} \frac{\partial E_T}{\partial \phi_0} = a \sin \phi_0 \frac{\partial E_T}{\partial \psi_0}. \tag{2.18}$$

By substituting total energy E_T into (2.18):

$$
\begin{aligned}
RHS &= -mga\frac{1}{\sqrt{\kappa}} \sin \phi_0 \cos \frac{\psi_0}{2} + 4a\frac{\sigma}{\sqrt{\kappa}} \cos^2 \frac{\psi_0}{2} \sin \frac{\psi_0}{2} \sin \phi_0 \\
&\quad +2\sigma a^2 \sin^2 \phi_0 \sin \psi_0 - \frac{1}{2}a^3\sqrt{\sigma\rho g} \cos \frac{\psi_0}{2} \sin 2\phi_0 \sin \phi_0 + a^3\sqrt{\sigma\rho g}\phi_0 \cos \frac{\psi_0}{2} \sin \phi_0.
\end{aligned}
$$

$$
\begin{aligned}
LHS &= -mga\frac{1}{\sqrt{\kappa}} \sin \phi_0 \cos \frac{\psi_0}{2} - 2\beta a\frac{\sigma}{\sqrt{\kappa}} \cos \frac{\psi_0}{2} - 2a\frac{\sigma}{\sqrt{\kappa}} \cos \phi_0 \cos \psi_0 \cos \frac{\psi_0}{2} \\
&\quad +\frac{1}{4}a^3\sqrt{\sigma\rho g} \cos \frac{\psi_0}{2} \cos 3\phi_0 - a^3\sqrt{\sigma\rho g} \cos \phi_0 \cos \frac{\psi_0}{2} + a^3\sqrt{\sigma\rho g}\phi_0 \sin \phi_0 \cos \frac{\psi_0}{2} \\
&\quad +\frac{3}{4}a^3\sqrt{\sigma\rho g} \cos \phi_0 \cos \frac{\psi_0}{2} - 2\sigma a^2 \sin \frac{\psi_0}{2} \cos \frac{\psi_0}{2} \cos 2\phi_0 + 2\sigma a^2 \sin \frac{\psi_0}{2} \cos \frac{\psi_0}{2}.
\end{aligned}
$$

$$\Rightarrow$$

$$
\begin{aligned}
LHS &= RHS, \\
2a\frac{\sigma}{\sqrt{\kappa}} \sin \psi_0 \cos \frac{\psi_0}{2} \sin \phi_0 &= -2\beta a\frac{\sigma}{\sqrt{\kappa}} \cos \frac{\psi_0}{2} - 2a\frac{\sigma}{\sqrt{\kappa}} \cos \phi_0 \cos \psi_0 \cos \frac{\psi_0}{2}, \\
\sin \psi_0 \sin \phi_0 &= -\beta - \cos \phi_0 \cos \psi_0, \\
\beta &= -\cos(\phi_0 - \psi_0).
\end{aligned}
$$

With the geometric constraint $\psi_0 = \phi_0 + \gamma - \pi$, then $\beta = \cos \gamma$.

2.5 Total Energy with One Parameter $E_T(\phi_0)$ and the Analysis of the Forces

With the geometric constraint $\psi_0 = \phi_0 + \gamma - \pi$ and $\beta = \cos\gamma$, the total energy $E_T(\psi_0, \phi_0)$ can be converted to $E_T(\phi_0)$:

$$E_T(\phi_0) = mg\left(a\cos\phi_0 + 2\sqrt{\frac{\sigma}{\rho g}}\cos\left(\frac{\phi_0 + \gamma}{2}\right)\right) - 2\sigma a\phi_0\cos\gamma + \frac{8}{3}\sigma\sqrt{\frac{\sigma}{\rho g}}\left(1 - \sin^3\left(\frac{\phi_0 + \gamma}{2}\right)\right)$$
$$+ 2\sigma a\sin\phi_0\cos(\phi_0 + \gamma) + \frac{1}{12}\rho g a^3\sin 3\phi_0 - \rho g a^3\phi_0\cos\phi_0 + \frac{3}{4}\rho g a^3\sin\phi_0$$
$$+ a^2\sqrt{\sigma\rho g}\cos\left(\frac{\phi_0 + \gamma}{2}\right)\sin 2\phi_0 - 2a^2\sqrt{\sigma\rho g}\phi_0\cos\left(\frac{\phi_0 + \gamma}{2}\right). \tag{2.19}$$
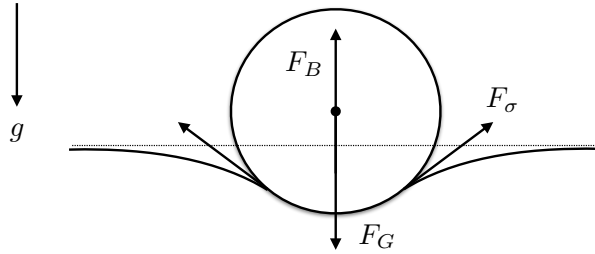
Figure 2.5: Gravitational, buoyant and surface tension forces.

By symmetry the surface tension forces in the horizontal direction cancel so that the net force in the horizontal direction is zero. We only consider forces in the vertical direction. Bhatnagar and Finn give an analysis of the forces in [2], we suppose upward is positive direction and modify the expression of the forces as follows.

- The gravitational force:

  with downward pointed gravitational field g and the mass of a unit length m, the gravitational force can be expressed as

$$F_G = -mg. \tag{2.20}$$

- The buoyant force:

14

the buoyant force rises from the pressure of fluid acting on the floating object. With the outer unit normal of the cylinder $\hat{n}_c$ and the unit vertical upward pointing vector $\hat{k}$, the buoyant force has the form:

$$F_B = \hat{k} \cdot \int_\Sigma \vec{F} ds. \tag{2.21}$$

Where the centripetal component pressure $\vec{F} = \rho g y \hat{n}_c$, Σ is the wetted region.
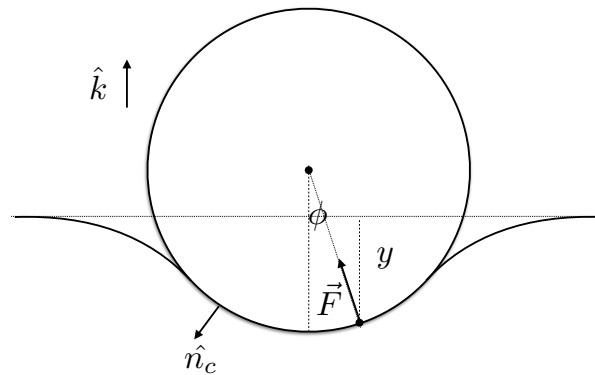
Figure 2.6: Computation of buoyant force.

The buoyant force can also be calculated by integrating with respect to ϕ (see Figure 2.6):

$$
\begin{aligned}
F_B &= 2 \int_0^{\phi_0} \rho g y \cos \phi a \, d\phi \\
&= 2 \int_0^{\phi_0} \rho g (a \cos \phi - h) \cos \phi a \, d\phi \\
&= -4a\sqrt{\sigma \rho g} \cos \left(\frac{\phi_0 + \gamma}{2} \right) \sin \phi_0 - \frac{1}{2} \rho g a^2 \sin 2\phi_0 + \rho g a^2 \phi_0.
\end{aligned}
\tag{2.22}
$$

With no surface tension, the Divergence Theorem leads to Archimedes' principle. But Archimedes' principle is not generally correct when the surface tension is present (See Appendix B).

- The surface tension force:

15

in 1805, Thomas Young derived the formula to determine the contact angle γ in terms of three surface tensions. The Figure 2.7 is known as "Young's diagram". Balancing the forces tangential to the solid gives:

$$\cos\gamma = \frac{\sigma_1 - \sigma_2}{\sigma}. \tag{2.23}$$

Where σ is air/liquid surface tension, σ_1 and σ_2 are air/solid and liquid/solid surface tension, respectively.
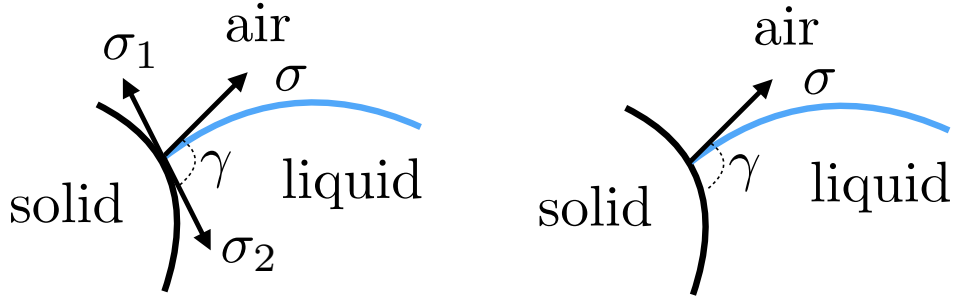
Figure 2.7: Young's diagram and its correction.

The discussion of Young's diagram has gone on for centuries. Recently, Finn gives a counterexample to show the incorrectness of Young's diagram [6]. Instead of applying Young's diagram, we agree with Gifford and Scriven's interpretation [9] of the direction of surface tension acting: the surface tension acts along the fluid interface (see Figure 2.7).

In our case, the vertical component of the surface tension is

$$\begin{aligned} F_\sigma &= 2\sigma \sin\psi_0 \\ &= -2\sigma \sin(\phi_0 + \gamma). \end{aligned} \tag{2.24}$$

The full expression of F_T in terms of ϕ_0 is

$$\begin{aligned} F_T(\phi_0) =& F_G + F_\sigma + F_B \\ =& -mg - 2\sigma\sin(\phi_0 + \gamma) - 4a\sqrt{\sigma\rho g}\cos\left(\frac{\phi_0 + \gamma}{2}\right)\sin\phi_0 \\ & -\frac{1}{2}\rho g a^2 \sin 2\phi_0 + \rho g a^2 \phi_0. \end{aligned} \tag{2.25}$$

16

2.6 Total Energy and Total Force

As minimizing the total energy $E_T(\phi_0)$ is laborious, we introduce a more convenient approach. Firstly, we write h in terms of ϕ_0 by substituting the geometric constraint.

$$h(\phi_0) = a\cos\phi_0 + \frac{2}{\sqrt{\kappa}}\cos\left(\frac{\phi_0 + \gamma}{2}\right). \tag{2.26}$$

The derivative $\frac{dh}{d\phi_0} = -a\sin\phi_0 - \sqrt{\frac{\sigma}{\rho g}}\sin\left(\frac{\phi_0+\gamma}{2}\right) \leq 0$ where equality only holds when $\phi_0 = \gamma = 0$ or $\phi_0 = \gamma = \pi$. Therefore, h and ϕ_0 are in one-to-one correspondence. With the parameters in Bhatnagar and Finn's paper [2] $\{g = 980 \text{ cm/s}^2, m = 1.2 \text{ g}, \rho = 1\text{g/cm}^2, \sigma = 72 \text{ dyn/cm}, \gamma = \frac{\pi}{2}, a = \frac{1}{\sqrt{\pi}} \text{ cm}\}$, the one-to-one correspondence between h and ϕ_0 is shown in Figure 2.8.
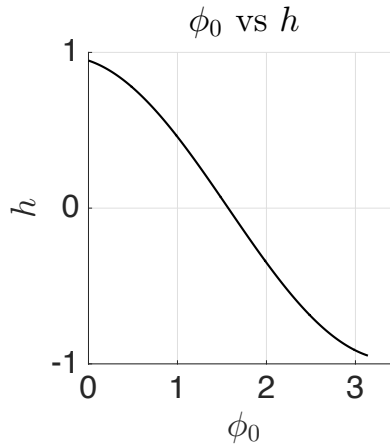
Figure 2.8: ϕ_0 versus h.

When the chain rule is applied, $-\frac{dE_T}{dh}$ and the vertical total force F_T are equal, as expected (see Appendix C).

$$-\frac{dE_T}{dh} = -\frac{dE_T}{d\phi_0}\frac{d\phi_0}{dh} = F_T. \tag{2.27}$$

This leads to the following equivalences.

17

Since $\frac{d\phi_0}{dh} < 0$ (except $\phi_0 = \gamma = 0$ or $\phi_0 = \gamma = \pi$), $\frac{dE_T}{d\phi_0}$ and F_T have the same sign by (2.27):

$$\text{sign}\left(\frac{dE_T}{d\phi_0}\right) = \text{sign}(F_T). \tag{2.28}$$

Assume that $\bar{\phi}_0 \in (0, \pi)$ is the critical point for $E_T(\phi_0)$, then

$$\frac{dE_T}{d\phi_0}(\bar{\phi}_0) = 0 \quad \Leftrightarrow \quad F_T(\bar{\phi}_0) = 0. \tag{2.29}$$

So the critical point $\bar{\phi}_0$ for $E_T(\phi_0)$ is equivalent to the vertical force balance point $F_T(\bar{\phi}_0) = 0$. If we rearrange equation (2.27) and differentiate with respect to ϕ_0, we obtain

$$-\frac{d^2 E_T}{d\phi_0^2} = \frac{dF_T}{d\phi_0}\frac{dh}{d\phi_0} + F_T\frac{d^2 h}{d\phi_0^2}. \tag{2.30}$$

If we plug in $\bar{\phi}_0$, we have the following sign equivalence:

$$\text{sign}\left(\frac{d^2 E_T}{d\phi_0^2}(\bar{\phi}_0)\right) = \text{sign}\left(\frac{dF_T}{d\phi_0}(\bar{\phi}_0)\right). \tag{2.31}$$

$\bar{\phi}_0$ is a local minimum if $\text{sign}\left(\frac{d^2 E_T}{d\phi_0^2}(\bar{\phi}_0)\right) > 0$ and $\bar{\phi}_0$ is a local maximum if $\text{sign}\left(\frac{d^2 E_T}{d\phi_0^2}(\bar{\phi}_0)\right) < 0$, equivalently,

$$\frac{dF_T}{d\phi_0}(\bar{\phi}_0) > 0 \quad \Rightarrow \quad \bar{\phi}_0 \text{ is locally stable.} \tag{2.32}$$

$$\frac{dF_T}{d\phi_0}(\bar{\phi}_0) < 0 \quad \Rightarrow \quad \bar{\phi}_0 \text{ is locally unstable.} \tag{2.33}$$

The cases $\phi_0 = \gamma = 0$ and $\phi_0 = \gamma = \pi$ are not physically realizable, they are in the intersection case, see Section 2.11.

Equipped with the equivalences above, we can focus on F_T instead of E_T to solve the minimization problem. But finding the force balance point is still not easy. Two techniques, non-dimensionalization and Fourier decomposition, are introduced in the following sections.

Remark 2.1. *Bhatnagar and Finn first give an example where the floating cylinder admits two equilibrium positions (we label the equilibria: $\bar{\phi}_{01} < \bar{\phi}_{02}$). With parameters: $\{g = 980 \ cm/s^2, \ m = 1.2 \ g, \ \rho = 1g/cm^2, \ \sigma = 72 \ dyn/cm, \ \gamma = \frac{\pi}{2}, \ a = \frac{1}{\sqrt{\pi}} \ cm\}$, they assert $\bar{\phi}_{01}$ is unstable and $\bar{\phi}_{02}$ is stable. Here, we correct their stability assertion based on (2.32) and (2.33), thus the smaller equilibrium point $\bar{\phi}_{01}$ is stable and the larger equilibrium point $\bar{\phi}_{02}$ is unstable.*

2.7 Two Independent Non-dimensional Parameters

Bhatnagar and Finn introduced two dimensionless parameters in [2]:

$$\mathcal{A} = \tfrac{m}{a^2\rho} \qquad \text{and} \qquad \mathcal{B} = \tfrac{\rho g}{\sigma}a^2.$$

Where $\mathcal{B}$ is known as the Bond number, which is the ratio of gravitational to surface tension forces. It will be more convenient to introduce $\mathcal{C} = \sqrt{\mathcal{B}} = \sqrt{\kappa}a$. The equation of the total force F_T in (2.25) can be expressed as:

$$F_T = \sigma\left[-\mathcal{A}\mathcal{C}^2 - 2\sin(\phi_0 + \gamma) - 4\mathcal{C}\cos\left(\frac{\phi_0 + \gamma}{2}\right)\sin\phi_0 - \frac{1}{2}\mathcal{C}^2\sin 2\phi_0 + \mathcal{C}^2\phi_0\right]. \quad (2.34)$$

If we define a characteristic force as $F_c = 1\sigma$, where 1 is the unit length of the horizontal cylinder. The non-dimensional form total force $\hat{F}_T$ can be expressed as

$$\hat{F}_T = -\mathcal{A}\mathcal{C}^2 - 2\sin(\phi_0 + \gamma) - 4\mathcal{C}\cos\left(\frac{\phi_0 + \gamma}{2}\right)\sin\phi_0 - \frac{1}{2}\mathcal{C}^2\sin 2\phi_0 + \mathcal{C}^2\phi_0. \quad (2.35)$$

Moreover, we require $\mathcal{A} > 0$ and $\mathcal{C} > 0$ to have physical meaning, $\mathcal{A}$ only appears in the constant term, if we increase the value of $\mathcal{A}$, the curve of $\hat{F}_T$ in terms of ϕ_0 shifts down.

2.8 Trigonometric Series

The total force $\hat{F}_T$ in (2.35) is mainly comprised of trigonometric functions sine and cosine. The Fourier decomposition can be applied and the main part of $\hat{F}_T$ can be written as the

trigonometric series in terms of

$$\left\{ \sin \frac{\phi_0}{2}, \cos \frac{\phi_0}{2}, \sin \phi_0, \cos \phi_0, \sin \frac{3\phi_0}{2}, \cos \frac{3\phi_0}{2}, \sin 2\phi_0, \cos 2\phi_0 \right\}. \tag{2.36}$$

The projection formulas give the expression of the coefficients:

$$a_n = \frac{1}{2\pi} \int_0^{4\pi} \hat{F}_T(\phi_0) \cos\left(\frac{n\phi_0}{2}\right) d\phi_0 \quad \text{where} \quad n \in \{1, 2, 3, 4\}. \tag{2.37}$$

$$b_n = \frac{1}{2\pi} \int_0^{4\pi} \hat{F}_T(\phi_0) \sin\left(\frac{n\phi_0}{2}\right) d\phi_0 \quad \text{where} \quad n \in \{1, 2, 3, 4\}. \tag{2.38}$$

Where a_n is the coefficient of $\cos(\frac{n\phi_0}{2})$ and b_n is the coefficient of $\sin(\frac{n\phi_0}{2})$.

The total force equation $\hat{F}_T$ in (2.35) can be transformed to the following:

$$\begin{aligned}
\hat{F}_T(\phi_0) = &- \mathcal{A}\mathcal{C}^2 - 2\mathcal{C} \cos \frac{\gamma}{2} \sin \frac{\phi_0}{2} + 2\mathcal{C} \sin \frac{\gamma}{2} \cos \frac{\phi_0}{2} - 2 \cos \gamma \sin \phi_0 \\
&- 2 \sin \gamma \cos \phi_0 - 2\mathcal{C} \cos \frac{\gamma}{2} \sin \frac{3\phi_0}{2} - 2\mathcal{C} \sin \frac{\gamma}{2} \cos \frac{3\phi_0}{2} \\
&- \frac{1}{2}\mathcal{C}^2 \sin 2\phi_0 + \mathcal{C}^2 \phi_0.
\end{aligned} \tag{2.39}$$

2.9 Stability Behaviors

We wish to study the stability behaviors of our floating cylinder system. First of all, we have to find the equilibria based on the equivalence relation (2.29). We just need to focus on finding the total force balance point $\bar{\phi}_0$, where $\hat{F}_T(\bar{\phi}_0) = 0$.

In the analysis of the total force equation, there are four parameters: ϕ_0, γ, $\mathcal{A}$ and $\mathcal{C}$. We consider two dimensionless parameters $\mathcal{A} > 0$ and $\mathcal{C} > 0$. The contact angle $\gamma \in [0, \pi]$ and $\sigma > 0$. The discussion can be divided into three cases: $\gamma = \frac{\pi}{2}$, $\gamma > \frac{\pi}{2}$ and $\gamma < \frac{\pi}{2}$.

2.9.1 The Case $\gamma = \frac{\pi}{2}$

The following properties are very useful in analyzing the shape of $\hat{F}_T$ curve.

Property 2.1.   *1. $\hat{F}_T$ is centrally symmetric with respect to the point $\left(\frac{\pi}{2}, \hat{F}_T(\frac{\pi}{2})\right)$.*

2. There are two critical points for $\hat{F}_T(\phi_0)$, one is in $(0, \frac{\pi}{2})$ and the other is in $(\frac{\pi}{2}, \pi)$.

Proof.   1. We pick $\phi_0 \in [0, \pi]$ and so $\pi - \phi_0 \in [0, \pi]$.

$$
\begin{aligned}
\hat{F}_T(\pi - \phi_0) &= -\mathcal{A}\mathcal{C}^2 - \sqrt{2}\mathcal{C}\cos\frac{\phi_0}{2} + \sqrt{2}\mathcal{C}\sin\frac{\phi_0}{2} + 2\cos\phi_0 + \sqrt{2}\mathcal{C}\cos\frac{3\phi_0}{2} \\
&\quad + \sqrt{2}\mathcal{C}\sin\frac{3\phi_0}{2} + \frac{1}{2}\mathcal{C}^2\sin 2\phi_0 + \mathcal{C}^2(\pi - \phi_0).
\end{aligned}
$$

Moreover,

$$
\begin{aligned}
\hat{F}_T(\phi_0) + \hat{F}_T(\pi - \phi_0) &= -2\mathcal{A}\mathcal{C}^2 + \mathcal{C}^2\pi \\
&= 2\hat{F}_T\left(\frac{\pi}{2}\right).
\end{aligned}
$$

2. We take the first derivative $\frac{d\hat{F}_T}{d\phi_0}$:

$$
\begin{aligned}
\frac{d\hat{F}_T}{d\phi_0} &= -\frac{\sqrt{2}\mathcal{C}}{2}\cos\frac{\phi_0}{2} - \frac{\sqrt{2}\mathcal{C}}{2}\sin\frac{\phi_0}{2} + 2\sin\phi_0 - \frac{3\sqrt{2}\mathcal{C}}{2}\cos\frac{3\phi_0}{2} \\
&\quad + \frac{3\sqrt{2}\mathcal{C}}{2}\sin\frac{3\phi_0}{2} - \mathcal{C}^2\cos 2\phi_0 + \mathcal{C}^2.
\end{aligned}
$$

Check the end points $\phi_0 = 0, \pi$ and $\phi_0 = \frac{\pi}{2}$.

$$
\frac{d\hat{F}_T}{d\phi_0}(0) = -2\sqrt{2}\mathcal{C} < 0 \quad \text{and} \quad \frac{d\hat{F}_T}{d\phi_0}(\pi) = -2\sigma\mathcal{C} < 0.
$$

$$
\frac{d\hat{F}_T}{d\phi_0}\left(\frac{\pi}{2}\right) = 2\left[1 + \mathcal{C} + \mathcal{C}^2\right] > 0.
$$

That $\frac{d\hat{F}_T}{d\phi_0}$ is strictly increasing on $(0, \frac{\pi}{2})$ follows from:

$$
\begin{aligned}
\frac{d^2\hat{F}_T}{d\phi_0^2} &= \frac{\sqrt{2}\mathcal{C}}{4}\sin\frac{\phi_0}{2} - \frac{\sqrt{2}\mathcal{C}}{4}\cos\frac{\phi_0}{2} + 2\cos\phi_0 + \frac{9\sqrt{2}\mathcal{C}}{4}\sin\frac{3\phi_0}{2} \\
&\quad + \frac{9\sqrt{2}\mathcal{C}}{4}\cos\frac{3\phi_0}{2} + 2\mathcal{C}^2\sin 2\phi_0 > 0.
\end{aligned}
$$

Since $\frac{d\hat{F}_T}{d\phi_0}$ is a continuous function, $\frac{d\hat{F}_T}{d\phi_0}(0) < 0$ and $\frac{d\hat{F}_T}{d\phi_0}(\frac{\pi}{2}) > 0$, so $\hat{F}_T$ admits exactly one critical point in $(0, \frac{\pi}{2})$. With the central symmetry property, $\hat{F}_T$ also admits another critical point in $(\frac{\pi}{2}, \pi)$.

$\square$
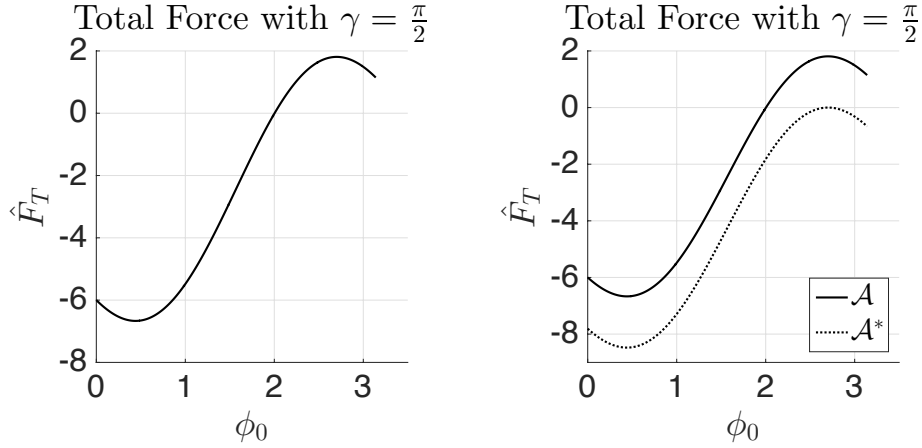
Figure 2.9: Parameters: $\mathcal{A} = 4$, $\mathcal{A}^* = 5.0893$ and $\mathcal{C} = 1$.

Property 2.1 gives the behavior of the $\hat{F}_T(\phi_0)$ curve. $\hat{F}_T$ decreases at the beginning then reaches the first critical point, and then $\hat{F}_T$ increases until reaching the second critical point, finally $\hat{F}_T$ decreases. The Figure 2.9 shows the important result that $\hat{F}_T$ admits at most two equilibrium points (we label the equilibria: $\bar{\phi}_{01} < \bar{\phi}_{02}$). According to the criteria (2.32) and (2.33), the smaller $\bar{\phi}_{01}$ is stable and the larger $\bar{\phi}_{02}$ is unstable.

We consider how the values of $\mathcal{A}$ affect the number of equilibria of $\hat{F}_T$. Since $\mathcal{A}$ only appears in the constant term of $\hat{F}_T$, if the value of $\mathcal{A}$ increases, the curve of $\hat{F}_T$ will shift down (see Figure 2.9). Given the value of $\mathcal{C}$, we define $\mathcal{A}^*$ such that

$$\hat{F}_T(\phi_0^*, \mathcal{A}^*) = 0, \tag{2.40}$$

where $\phi_0^* > \frac{\pi}{2}$ is the second critical point of $\hat{F}_T$. $\mathcal{A}^*$ has to be found numerically. The following table shows the number of equilibria and stability behaviors for different values of $\mathcal{A}$.

The number of equilibria can also be shown in $\mathcal{C}$ vs $\mathcal{A}$ Figures. The details will be discussed in Section 2.12.

Range of $\mathcal{A}$	Number of Equilibria	Stability
$0 < \mathcal{A} < \frac{2}{\mathcal{C}^2} + \pi$	1	stable
$\frac{2}{\mathcal{C}^2} + \pi \leq \mathcal{A} < \mathcal{A}^*$	2	$\bar{\phi}_{01}$ is stable, $\bar{\phi}_{02}$ is unstable
$\mathcal{A} = \mathcal{A}^*$	1	unstable
$\mathcal{A} > \mathcal{A}^*$	0	NA

Table 2.1: Stability Behaviors, Number of Equilibria with Different $\mathcal{A}$.

2.9.2 The Case $\gamma > \frac{\pi}{2}$

When $\gamma > \frac{\pi}{2}$, the stability behaviors of the $\hat{F}_T(\phi_0)$ depend on the sign of $\frac{d\hat{F}_T}{d\phi_0}$ at the end point $\phi_0 = 0$. This leads to the following theorem:

Theorem 2.1. *For $\gamma > \frac{\pi}{2}$, there are two types of behavior of the total force $\hat{F}_T$ curve.*

1. *If $\frac{d\hat{F}_T}{d\phi_0}(0) < 0$, there are two critical points, one lies in $[0, \frac{\pi}{4}]$, the other lies in $[\frac{\pi}{2}, \pi]$. $\hat{F}_T$ decreases to the first critical point, then increases to the second critical point, and then decreases.*

2. *If $\frac{d\hat{F}_T}{d\phi_0}(0) \geq 0$, there is only one critical point in $[\frac{\pi}{2}, \pi]$. $\hat{F}_T$ increases to the only critical point and then decreases.*

Proof. We firstly consider the following two cases for $\phi_0 \in [0, \frac{\pi}{4}]$.

1. If $\frac{d\hat{F}_T}{d\phi_0}(0) < 0$, we have

$$2\mathcal{C}\cos\frac{\gamma}{2} + \cos\gamma > 0 \quad \Leftrightarrow \quad 2\cos\gamma\sin\phi_0 > -4\mathcal{C}\cos\frac{\gamma}{2}\sin\phi_0,$$

where $\gamma \neq \pi$ and $\phi_0 \neq 0$. The latter inequality gives the underlined terms in the following calculation.

$$\frac{d^2\hat{F}_T}{d\phi_0^2} = \frac{\mathcal{C}}{2}\left(\cos\frac{\gamma}{2}\sin\frac{\phi_0}{2} - \sin\frac{\gamma}{2}\cos\frac{\phi_0}{2} + 9\cos\frac{\gamma}{2}\sin\frac{3\phi_0}{2} + 9\sin\frac{\gamma}{2}\cos\frac{3\phi_0}{2}\right)$$
$$+ 2\mathcal{C}^2\sin 2\phi_0 + \underline{2\cos\gamma\sin\phi_0} + 2\sin\gamma\cos\phi_0$$
$$> \frac{\mathcal{C}}{2}\left(\cos\frac{\gamma}{2}\sin\frac{\phi_0}{2} - \sin\frac{\gamma}{2}\cos\frac{\phi_0}{2} - 8\cos\frac{\gamma}{2}\sin\phi_0 + 9\cos\frac{\gamma}{2}\sin\frac{3\phi_0}{2} + 9\sin\frac{\gamma}{2}\cos\frac{3\phi_0}{2}\right)$$
$$2\mathcal{C}^2\sin 2\phi_0 + 2\sin\gamma\cos\phi_0 > 0.$$

23

In the last inequality, the term in parentheses is shown to be positive by graphing it with Matlab.

Moreover, $\frac{d^2\hat{F}_T}{d\phi_0^2} = 4\mathcal{C}\sin\frac{\gamma}{2} + 2\sin\gamma > 0$ when $\phi_0 = 0$. Therefore, $\frac{d\hat{F}_T}{d\phi_0}$ is increasing on $[0, \frac{\pi}{4}]$.

$$
\begin{aligned}
\frac{d\hat{F}_T}{d\phi_0}(\frac{\pi}{4}) &= \mathcal{C}\left(-\cos\frac{\gamma}{2}\cos\frac{\pi}{8} - \sin\frac{\gamma}{2}\sin\frac{\pi}{8} - 3\cos\frac{\gamma}{2}\cos\frac{3\pi}{8} + 3\sin\frac{\gamma}{2}\sin\frac{3\pi}{8}\right) \\
&\quad + \mathcal{C}^2 + \sqrt{2}(\sin\gamma - \cos\gamma) > 0.
\end{aligned}
$$

According to the Intermediate Value Theorem, $\hat{F}_T$ has a critical point, which lies in $[0, \frac{\pi}{4}]$.

2. If $\frac{d\hat{F}_T}{d\phi_0}(0) \geq 0$, we have

$$2\mathcal{C}\cos\frac{\gamma}{2} + \cos\gamma \leq 0. \tag{2.41}$$

Condition in (2.41) implies the monotonicity of $\hat{F}_T$ at $[0, \frac{\pi}{4}]$:

$$
\begin{aligned}
\frac{d\hat{F}_T}{d\phi_0} &= \mathcal{C}^2 - \mathcal{C}^2\cos 2\phi_0 - 2\cos\gamma\cos\phi_0 + 2\sin\gamma\sin\phi_0 \\
&\quad + \mathcal{C}\left(-\cos\frac{\gamma}{2}\cos\frac{\phi_0}{2} - \sin\frac{\gamma}{2}\sin\frac{\phi_0}{2} - 3\cos\frac{\gamma}{2}\cos\frac{3\phi_0}{2} + 3\sin\frac{\gamma}{2}\sin\frac{3\phi_0}{2}\right) \\
&\geq \mathcal{C}^2 - \mathcal{C}^2\cos 2\phi_0 + 2\sin\gamma\sin\phi_0 - 2\cos\gamma\cos\phi_0 + \mathcal{C}\sin\frac{\gamma}{2}\left(3\sin\frac{3\phi_0}{2} - \sin\frac{\phi_0}{2}\right) \\
&\quad + \frac{1}{2}\cos\gamma\cos\frac{\phi_0}{2} + \frac{3}{2}\cos\gamma\cos\frac{3\phi_0}{2} \geq 0.
\end{aligned}
$$

The equality only holds for $\phi_0 = 0$. Therefore, $\hat{F}_T$ increases on $[0, \frac{\pi}{4}]$.

Next we consider $\phi_0 \in [\frac{\pi}{4}, \frac{\pi}{2}]$,

$$
\begin{aligned}
\frac{d\hat{F}_T}{d\phi_0} &= -\mathcal{C}\cos\frac{\gamma}{2}\cos\frac{\phi_0}{2} - \mathcal{C}\sin\frac{\gamma}{2}\sin\frac{\phi_0}{2} - 2\cos\gamma\cos\phi_0 + 2\sin\gamma\sin\phi_0 \\
&\quad - 3\mathcal{C}\cos\frac{\gamma}{2}\cos\frac{3\phi_0}{2} + 3\mathcal{C}\sin\frac{\gamma}{2}\sin\frac{3\phi_0}{2} - \mathcal{C}^2\cos 2\phi_0 + \mathcal{C}^2 > 0.
\end{aligned}
$$

Hence, $\hat{F}_T$ is increasing at $[\frac{\pi}{4}, \frac{\pi}{2}]$.

Finally, we consider $\phi_0 \in [\frac{\pi}{2}, \pi]$. We evaluate $\frac{\hat{F}_T}{d\phi_0}$ at end points $\frac{\pi}{2}, \pi$:

$$\frac{d\hat{F}_T}{d\phi_0}(\pi) = -4\mathcal{C}\sin\frac{\gamma}{2} + 2\cos\gamma < 0.$$

$$\frac{d\hat{F}_T}{d\phi_0}(\frac{\pi}{2}) = \sqrt{2}\mathcal{C}\cos\frac{\gamma}{2} + \sqrt{2}\mathcal{C}\sin\frac{\gamma}{2} + 2\sin\gamma + 2\mathcal{C}^2 > 0.$$

When $\phi_0 \in [\frac{\pi}{2}, \pi]$,

$$\frac{d^2\hat{F}_T}{d\phi_0^2} = \frac{\mathcal{C}}{2}\left(\cos\frac{\gamma}{2}\sin\frac{\phi_0}{2} - \sin\frac{\gamma}{2}\cos\frac{\phi_0}{2} + 9\cos\frac{\gamma}{2}\sin\frac{3\phi_0}{2} + 9\sin\frac{\gamma}{2}\cos\frac{3\phi_0}{2}\right)$$
$$+ 2\mathcal{C}^2\sin 2\phi_0 + 2\cos\gamma\sin\phi_0 + 2\sin\gamma\cos\phi_0 < 0.$$

$\frac{d\hat{F}_T}{d\phi_0}$ is monotone decreasing on $[\frac{\pi}{2}, \pi]$. By the Indermediate Value Theorem, there exists a $\phi^* \in [\frac{\pi}{2}, \pi]$ such that $\frac{d\hat{F}_T}{d\phi_0}(\phi^*) = 0$. Therefore, $\hat{F}_T(\phi_0)$ increases then attaches the critical point, and then decreases on $[\frac{\pi}{2}, \pi]$. $\qquad\square$
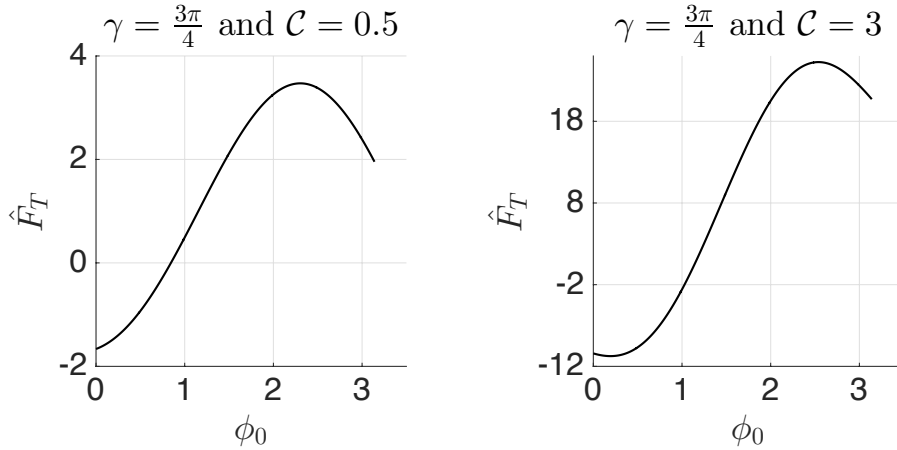
Figure 2.10: Parameter: $\mathcal{A} = 1$.

In summary, there are two behaviors of $\hat{F}_T$: two typical examples of those cases are shown in Figure 2.11.

2.9.3 The Case $\gamma < \frac{\pi}{2}$

When $\gamma < \frac{\pi}{2}$, the stability behaviors of the $\hat{F}_T(\phi_0)$ depend on the sign of $\frac{d\hat{F}_T}{d\phi_0}$ at end point $\phi_0 = \pi$. We obtain the following theorem:

Theorem 2.2. *For $\gamma < \frac{\pi}{2}$, there are two types of behavior of the total force $\hat{F}_T$ curve.*

1. *If $\frac{d\hat{F}_T}{d\phi_0}(\pi) < 0$, there are two critical points, one lies in $[0, \frac{\pi}{2}]$, the other lies in $[\frac{3\pi}{4}, \pi]$. $\hat{F}_T$ decreases to the first critical point, then increases to the second critical point, and then decreases.*

2. *If $\frac{d\hat{F}_T}{d\phi_0}(\pi) \geq 0$, there is only one critical point in $[\frac{3\pi}{4}, \pi]$. $\hat{F}_T$ decreases to the only critical point and then increases.*

Proof. With $\gamma < \frac{\pi}{2}$,

$$\frac{d\hat{F}_T}{d\phi_0}(0) = -4\mathcal{C}\cos\frac{\gamma}{2} - 2\cos\gamma < 0.$$

$$\frac{d\hat{F}_T}{d\phi_0}(\frac{\pi}{2}) = \sqrt{2}\mathcal{C}\cos\frac{\gamma}{2} + \sqrt{2}\mathcal{C}\sin\frac{\gamma}{2} + 2\sin\gamma + 2\mathcal{C}^2 > 0.$$

$\hat{F}_T$ always decreases at the beginning. We first consider $\phi_0 \in [0, \frac{\pi}{2}]$,

$$\frac{d^2\hat{F}_T}{d\phi_0{}^2} = 2\mathcal{C}^2\sin 2\phi_0 + 2\cos\gamma\sin\phi_0 + 2\sin\gamma\cos\phi_0$$

$$+ \frac{\mathcal{C}}{2}\left(\cos\frac{\gamma}{2}\sin\frac{\phi_0}{2} - \sin\frac{\gamma}{2}\cos\frac{\phi_0}{2} + 9\cos\frac{\gamma}{2}\sin\frac{3\phi_0}{2} + 9\sin\frac{\gamma}{2}\cos\frac{3\phi_0}{2}\right) \geq 0.$$

The equality only holds for both ϕ_0 and γ being 0. Therefore, $\frac{d\hat{F}_T}{d\phi_0}$ increases on $[0, \frac{\pi}{2}]$. By the Intermediate Value Theorem, there exists $\phi^* \in [0, \frac{\pi}{2}]$ such that $\frac{d\hat{F}_T}{d\phi_0}(\phi^*) = 0$. As a result, $\hat{F}_T(\phi_0)$ decreases then reaches the critical point, and then increases.

Next, we consider $\phi_0 \in [\frac{\pi}{2}, \frac{3\pi}{4}]$,

$$\frac{d\hat{F}_T}{d\phi_0} = \mathcal{C}^2 - \mathcal{C}^2\cos 2\phi_0 - 2\cos\gamma\cos\phi_0 + 2\sin\gamma\sin\phi_0$$

$$+ \mathcal{C}\left(-\cos\frac{\gamma}{2}\cos\frac{\phi_0}{2} - \sin\frac{\gamma}{2}\sin\frac{\phi_0}{2} - 3\cos\frac{\gamma}{2}\cos\frac{3\phi_0}{2} + 3\sin\frac{\gamma}{2}\sin\frac{3\phi_0}{2}\right) > 0.$$

26

Therefore, $\hat{F}_T(\phi_0)$ increases on $[\frac{\pi}{2}, \frac{3\pi}{4}]$.

Finally, we consider $\phi_0 \in [\frac{3\pi}{4}, \pi]$. We distinguish the cases as follows:

1. If $\frac{d\hat{F}_T}{d\phi_0}(\pi) \geq 0$, we have

$$\cos\gamma \geq 2\mathcal{C}\sin\frac{\gamma}{2} \quad \Leftrightarrow \quad -\mathcal{C} \geq -\frac{\cos\gamma}{2\sin\frac{\gamma}{2}} \quad \text{with} \quad \gamma \neq 0. \tag{2.42}$$

The inequality in (2.42) leads the following result:

$$
\begin{aligned}
\frac{d\hat{F}_T}{d\phi_0} &= \mathcal{C}^2 - \mathcal{C}^2\cos 2\phi_0 - 2\cos\gamma\cos\phi_0 + 2\sin\gamma\sin\phi_0 \\
&\quad \underline{-\mathcal{C}}\left(\cos\frac{\gamma}{2}\cos\frac{\phi_0}{2} + \sin\frac{\gamma}{2}\sin\frac{\phi_0}{2} + 3\cos\frac{\gamma}{2}\cos\frac{3\phi_0}{2} - 3\sin\frac{\gamma}{2}\sin\frac{3\phi_0}{2}\right) \\
&\geq \mathcal{C}^2 - \mathcal{C}^2\cos 2\phi_0 - 2\cos\gamma\cos\phi_0 + 2\sin\gamma\sin\phi_0 \\
&\quad \underline{-\frac{\cos\gamma}{2\sin\frac{\gamma}{2}}}\left(\cos\frac{\gamma}{2}\cos\frac{\phi_0}{2} + \sin\frac{\gamma}{2}\sin\frac{\phi_0}{2} + 3\cos\frac{\gamma}{2}\cos\frac{3\phi_0}{2} - 3\sin\frac{\gamma}{2}\sin\frac{3\phi_0}{2}\right) > 0.
\end{aligned}
$$

Moreover, if $\gamma = 0$, $\frac{d\hat{F}_T}{d\phi_0} > 0$ as well. Hence $\hat{F}_T$ increases on $[\frac{3\pi}{4}, \pi]$.

2. If $\frac{d\hat{F}_T}{d\phi_0}(\pi) < 0$, $\frac{d^2\hat{F}_T}{d\phi_0^2}$ is monotone decreasing on $[\frac{3\pi}{4}, \pi]$. At the other end point $\frac{d\hat{F}_T}{d\phi_0}(\frac{3\pi}{4}) > 0$. By the Intermediate Value Theorem, $\hat{F}_T$ admits one critical point $\phi^* \in [\frac{3\pi}{4}, \pi]$. Therefore $\hat{F}_T(\phi_0)$ increases and reaches the critical point, then decreases at $[\frac{3\pi}{4}, \pi]$.

$\square$

In summary, there are two behaviors of $\hat{F}_T$, two typical examples of those cases are shown in Figure 2.11.

2.10 Asymptotic Behavior of $\mathcal{A}^*$ and ϕ_0^* for $\gamma = \frac{\pi}{2}$

As we discussed, for $\gamma = \frac{\pi}{2}$, ϕ_0^* and $\mathcal{A}^*$ in (2.40) have to be found numerically. But there do exist asymptotic equations of $\phi_0^*(\mathcal{C})$ and $\mathcal{A}^*(\mathcal{C})$ as both $\mathcal{C} \to \infty$ and $\mathcal{C} \to 0$. In this section, we will find these asymptotic series. We first state a special case of the Real Analytic Implicit Function Theorem [13]:
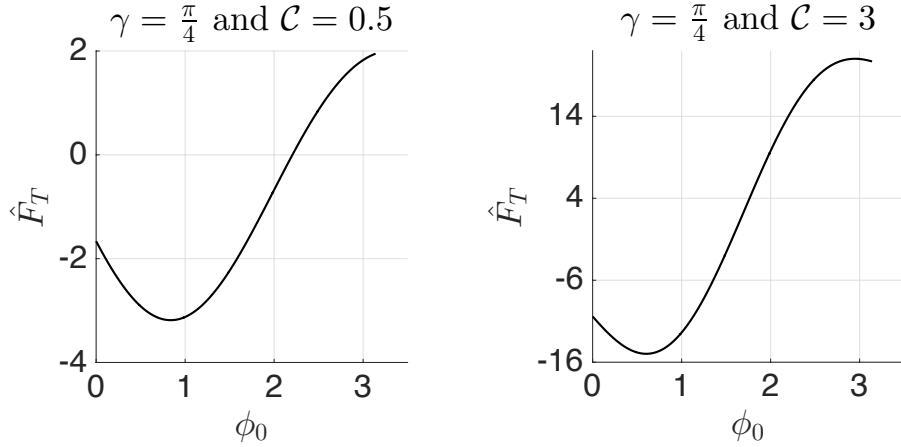
Figure 2.11: Parameter: $\mathcal{A} = 1$.

Theorem 2.3. *Let $\varphi(x, \epsilon)$ be a real valued function analytic at $(x_0, 0)$, that is, $\varphi(x, \epsilon)$ has a two-variable power series in powers of $x - x_0$ and ϵ which converges in a ball about $(x_0, 0)$. Let $\varphi(x_0, 0) = 0$ and $\varphi_x(x_0, 0) \neq 0$. Then there is an $\epsilon_0 > 0$ and a unique analytic function $x = x(\epsilon)$ defined for all $|\epsilon| \leq \epsilon_0$, that is, $x(\epsilon)$ has a power series in ϵ which converges for $|\epsilon| \leq \epsilon_0$, such that*

$$\varphi\left(x(\epsilon), \epsilon\right) = 0 \quad and \quad x(0) = x_0. \tag{2.43}$$

2.10.1   As $\mathcal{C} \to 0$

We notice that $\frac{d}{d\phi_0}\hat{F}_T(\pi; 0) = 0$ and $\frac{d^2}{d\phi_0^2}\hat{F}_T(\pi; 0) \neq 0$. By the Implicit Function Theorem 2.3, there exists $\phi_0^* = g(\mathcal{C})$ with $g(0) = \pi$, where g is a analytic about $\mathcal{C} = 0$. Therefore, there exists an analytic function $\phi_0^*(\mathcal{C})$ in terms of $\mathcal{C}$ near $\mathcal{C} = 0$ satisfying $\frac{d}{d\phi_0}\hat{F}_T(\phi_0^*(\mathcal{C}); \mathcal{C}) = 0$.

Consider the regular asymptotic series $\phi_0^* = \pi + a_1\mathcal{C} + a_2\mathcal{C}^2 + ...$ After tedious calculations, we obtain:

$$\mathcal{A}^* = \frac{2}{\mathcal{C}^2} + 2 + \pi - 2\sqrt{2}\mathcal{C} + \mathcal{O}(\mathcal{C}^2). \tag{2.44}$$

$$\phi_0^* = \pi - \sqrt{2}\mathcal{C} + 2\mathcal{C}^2 - \frac{7}{12}\sqrt{2}\mathcal{C}^3 + \mathcal{O}(\mathcal{C}^4). \tag{2.45}$$

As $\mathcal{C} \to 0$ (see details in Appendix D).

28

2.10.2   As $\mathcal{C} \to \infty$

The regular asymptotic series doesn't work in this case, we have to reconsider the series. Rearranging $\frac{d\hat{F}_T}{d\phi_0} = 0$,

$$2\sin^2\phi_0 + \frac{1}{\mathcal{C}}\frac{\sqrt{2}}{2}\left\{-\cos\frac{\phi_0}{2} - \sin\frac{\phi_0}{2} - 3\cos\frac{3\phi_0}{2} + 3\sin\frac{3\phi_0}{2}\right\} + \frac{2}{\mathcal{C}^2}\sin\phi_0 = 0. \quad (2.46)$$

We define a function $K(\phi_0, \mathcal{C})$:

$$K(\phi_0, \mathcal{C}) = \sin\phi_0 - \left[\frac{1}{\mathcal{C}}\frac{\sqrt{2}}{4}\left\{\cos\frac{\phi_0}{2} + \sin\frac{\phi_0}{2} + 3\cos\frac{3\phi_0}{2} - 3\sin\frac{3\phi_0}{2}\right\} - \frac{1}{\mathcal{C}^2}\sin\phi_0\right]^{\frac{1}{2}}.$$
$$(2.47)$$

The solutions of $K = 0$ and $\frac{d\hat{F}_T}{d\phi_0} = 0$ are equivalent. Let $\mathcal{D} = \frac{1}{\sqrt{\mathcal{C}}}$,

$$K(\phi_0, \mathcal{D}) = \sin\phi_0 - \mathcal{D}\left[\frac{\sqrt{2}}{4}\left\{\cos\frac{\phi_0}{2} + \sin\frac{\phi_0}{2} + 3\cos\frac{3\phi_0}{2} - 3\sin\frac{3\phi_0}{2}\right\} - \mathcal{D}^2\sin\phi_0\right]^{\frac{1}{2}}.$$
$$(2.48)$$

We have $K(\pi, 0) = 0$ and $\frac{\partial K}{\partial\phi_0}(\pi, 0) = -1$. According to the Implicit Function Theorem 2.3, there exists $\phi_0^* = g(\mathcal{D})$ with $g(0) = \pi$, where g is a analytic about $\mathcal{D} = 0$. We can consider $\phi^* = \pi + a_1\mathcal{D} + a_2\mathcal{D}^2 + a_3\mathcal{D}^3 + ...$ (equivalently $\phi_0^* = \pi + \frac{a_1}{\mathcal{C}^{\frac{1}{2}}} + \frac{a_2}{\mathcal{C}} + \frac{a_3}{\mathcal{C}^{\frac{3}{2}}} + ...$) and plug the series into $\frac{d\hat{F}_T}{d\phi_0}(\phi_0^*) = 0$ (see details in Appendix D).

As $\mathcal{C} \to \infty$,

$$\mathcal{A}^* = \pi + \frac{\frac{4}{3}2^{\frac{3}{4}}}{\mathcal{C}^{\frac{3}{2}}} + \mathcal{O}(\mathcal{C}^{-\frac{1}{2}}).$$

$$\phi_0^* = \pi - \frac{2^{\frac{1}{4}}}{\mathcal{C}^{\frac{1}{2}}} + \frac{\frac{\sqrt{2}}{2}}{\mathcal{C}} + \frac{\frac{7}{24}2^{-\frac{1}{4}}}{\mathcal{C}^{\frac{3}{2}}} + \mathcal{O}(\mathcal{C}^{-2}).$$

The following Figures in 2.12 give the performance of the asymptotic series.

2.11   Intersection Condition

There is a possibility that interfaces on the two sides of the cylinder intersect, invalidating our model. Consider $\psi < 0$ case, we find that the intersection of the fluid interfaces happens if all of the following three conditions are satisfied:
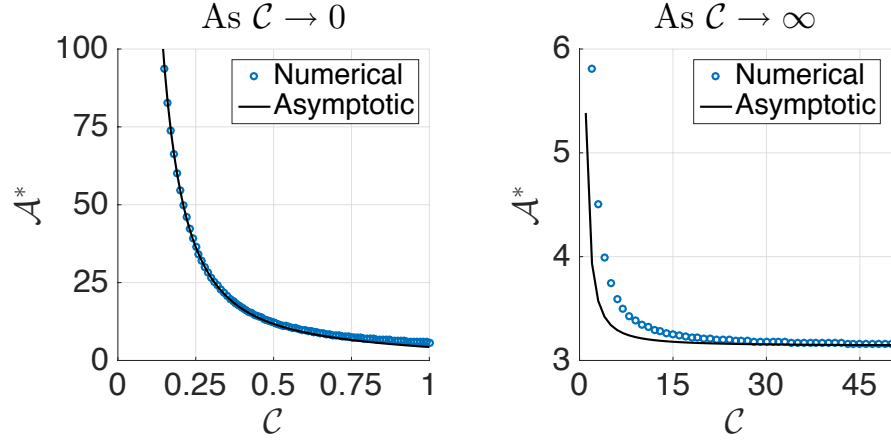
Figure 2.12: The performance of asymptotic series compared with numerical results.

- $-\pi \leq \psi_0 < -\frac{\pi}{2} \quad \Leftrightarrow \quad 0 \leq \phi_0 + \gamma < \frac{\pi}{2}$.

- $h > a \quad \Leftrightarrow \quad \cos \phi_0 + \frac{2}{\mathcal{C}} \cos(\frac{\phi_0 + \gamma}{2}) > 1$.

- $x(-\frac{\pi}{2}) \leq 0 \quad \Leftrightarrow \quad \sqrt{2} + \ln(\tan \frac{\pi}{8}) - 2 \sin(\frac{\phi_0 + \gamma}{2}) - \ln\left[-\tan(\frac{\phi_0 + \gamma - \pi}{4})\right] \geq \mathcal{C} \sin \phi_0$.

Actually the third condition implies the second condition. Our conditions are:

- Angle constraint:
$$0 \leq \phi_0 + \gamma < \frac{\pi}{2}, \quad \text{where } \gamma \in [0, \frac{\pi}{2}).$$

- The inequality:

$$\mathcal{C} \leq \frac{\sqrt{2} + \ln(\tan \frac{\pi}{8}) - 2 \sin(\frac{\phi_0 + \gamma}{2}) - \ln\left[-\tan(\frac{\phi_0 + \gamma - \pi}{4})\right]}{\sin \phi_0}.$$

For the $\psi > 0$ case, the following conditions are needed:

- $\frac{\pi}{2} < \psi_0 \leq \pi \quad \Leftrightarrow \quad \frac{3\pi}{2} < \phi_0 + \gamma \leq 2\pi$.

- $-h > a$.

30
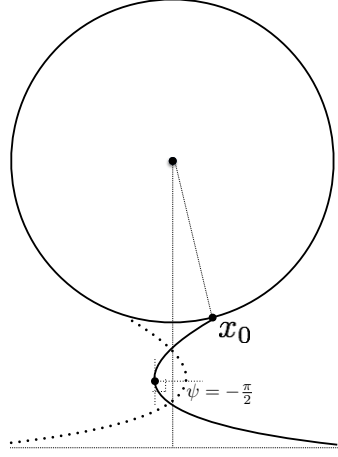
Figure 2.13: Intersection for the $\psi < 0$ case.

- $x(\frac{\pi}{2}) \leq 0$.

Similar to the conditions above, we have:

- Angle constraint:

$$\frac{3\pi}{2} < \phi_0 + \gamma \leq 2\pi, \ \text{ where } \ \gamma \in (\frac{\pi}{2}, \pi] \ \text{ and } \ \phi_0 \in [0, \pi].$$

- The inequality:

$$\mathcal{C} \leq \frac{\sqrt{2} + \ln(\tan\frac{\pi}{8}) - 2\sin(\frac{\phi_0+\gamma}{2}) - \ln\left[\tan(\frac{\phi_0+\gamma-\pi}{4})\right]}{\sin\phi_0}.$$

We define the intersection function $I(\phi_0, \mathcal{C})$ as follows:

$$I(\phi_0, \mathcal{C}) = \mathcal{C}\sin\phi_0 - \sqrt{2} - \ln(\tan\frac{\pi}{8}) + 2\sin(\frac{\phi_0+\gamma}{2}) + \ln\left[\pm\tan(\frac{\phi_0+\gamma-\pi}{4})\right], \quad (2.49)$$

where " $+$ " sign works for $\gamma \in [0, \frac{\pi}{2})$, $\phi_0 \in (0, \frac{\pi}{2} - \gamma]$ and " $-$ " sign works for $\gamma \in (\frac{\pi}{2}, \pi]$, $\phi_0 \in [\frac{3\pi}{2} - \gamma, \pi)$. In addition, $I(\phi_0, \mathcal{C}) = 0$ is the boundary curve between the intersection region[1] and the non-intersection region, and we have the pair $(\phi_0, \mathcal{C})$ lies in the non-intersection region if and only if $I(\phi_0, \mathcal{C}) > 0$.

---

[1]The intersection region means the region that the fluid interfaces intersect.

In Figure 2.21, the intersection of fluid interfaces happens in the shaded region. The two cases are: $\gamma = \frac{\pi}{4}$, $\phi_0 \in [0, \frac{\pi}{4})$ and $\gamma = \frac{3\pi}{4}$, $\phi_0 \in (\frac{3\pi}{4}, \pi]$.
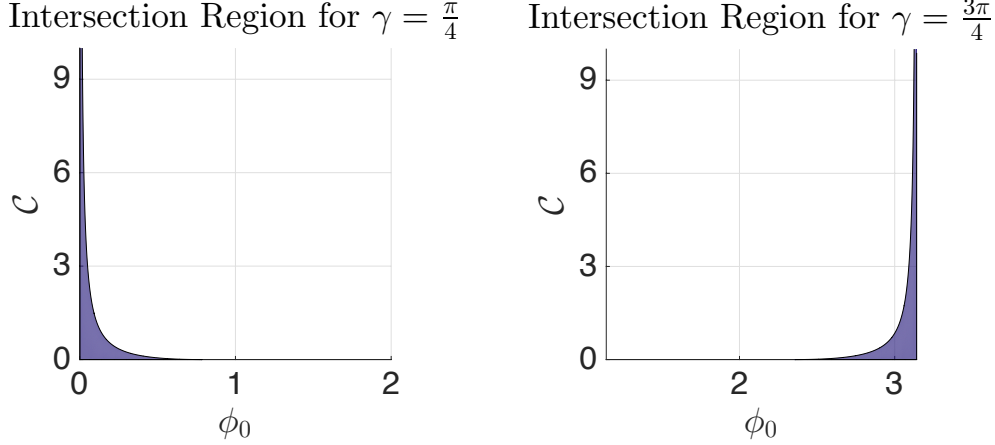
Figure 2.14: Intersection regions for $\gamma = \frac{\pi}{4}$ and $\gamma = \frac{3\pi}{4}$.

When $\gamma = \frac{\pi}{2}$, there is always no intersection. Moreover, we are also interested in the number of the equilibrium points for $\gamma \neq \frac{\pi}{2}$. If the floating cylinder could admit two equilibrium points, we would like to know whether or not the equilibrium points lie in the intersection region.

Remark 2.2. *We expect that the stable point would never lie in the intersection region, while the unstable point might or might not lie in the intersection region. We will discuss the details in next section.*

2.12 $\mathcal{C}$ vs $\mathcal{A}$: Regions with Different Numbers of Equilibria

$\mathcal{A}$, $\mathcal{C}$ and contact angle γ will affect the number of equilibria of our floating system. So plotting $\mathcal{C}$ vs $\mathcal{A}$ region will be helpful and clear. Examples with typical contact angles,$\gamma = 0, \frac{\pi}{4}, \frac{\pi}{2}, \frac{3\pi}{4}$ and π, will be discussed. In $\mathcal{C}$ vs $\mathcal{A}$, we define $\mathcal{C}_i(\mathcal{A})$ as the boundary curves between the regions with different number of equilibria. According to the discussion of the types of behavior of the $\hat{F}_T$ curve in Section 2.9, sign of $\hat{F}_T(\pi)$, sign of $\hat{F}_T(\phi_0^*)$ and sign of $\hat{F}_T(\tilde{\phi}_0)$ play important roles in changing the number of equilibria. The boundary curves $\mathcal{C}_i(\mathcal{A})$ can be expressed as follows:

1. $\mathcal{C}_1(\mathcal{A}) : \hat{F}_T(\pi) = 0 \iff (\mathcal{A} - \pi)\mathcal{C}^2 = 2\sin\gamma$.

2. $\mathcal{C}_2(\mathcal{A}) : \hat{F}_T(\phi_0^*) = 0$ where $\phi_0^* > \frac{\pi}{2}$ satisfying $\frac{d\hat{F}_T}{d\phi_0}(\phi_0^*) = 0$.

3. $\mathcal{C}_3(\mathcal{A}) : \hat{F}_T(\tilde{\phi}_0) = 0$ where $\tilde{\phi}_0$ satisfying $I(\tilde{\phi}_0, \mathcal{C}) = 0$, $I(\phi_0, C)$ is the intersection function (2.49).

Only $\mathcal{C}_1(\mathcal{A})$ can be solved analytically such that $\mathcal{C}_1(\mathcal{A}) = \sqrt{\frac{2\sin\gamma}{\mathcal{A} - \pi}}$ (for $\gamma \neq 0, \pi$). While, the critical point of $\frac{d\hat{F}_T}{d\phi_0}$, ϕ_0^* and the angle $\tilde{\phi}_0$ can be solved by Fzero in Matlab. In the following, we will analyze the boundary curves $\mathcal{C}_i(\mathcal{A})$ and plot the $\mathcal{C}$ vs $\mathcal{A}$ region.

2.12.1 Example One: $\gamma = 0$

When $\gamma = 0$, we have $\frac{d\hat{F}_T}{d\phi_0}(\pi) = 2\sigma > 0$ such that $\hat{F}_T$ has at most one equilibrium point, denoted as $\bar{\phi}_0$ if it exists. Therefore, $\mathcal{C}_1(\mathcal{A})$ the boundary between the zero equilibrium point region and the one equilibrium point region has the following expression:

$$\hat{F}_T(\pi) = 0 \iff \mathcal{A} = \pi. \tag{2.50}$$

Theorem 2.4 tells us $\bar{\phi}_0$ never lies in the intersection region if the equilibrium point $\bar{\phi}_0$ exists. Figure 2.15 shows the $\mathcal{C}$ vs $\mathcal{A}$ region, the one equilibrium point region is to the left of $\mathcal{C}_1(\mathcal{A})$ and the no equilibrium point region is to the right of $\mathcal{C}_1(\mathcal{A})$.

Theorem 2.4. *For $\gamma = 0$, if there exists $\bar{\phi}_0$ such that $\hat{F}_T(\bar{\phi}_0) = 0$, then $I(\bar{\phi}_0, \mathcal{C}) > 0$ for any given $\mathcal{C}$.*

Proof. See Appendix E. $\qquad\square$

2.12.2 Example Two: $\gamma = \frac{\pi}{4}$

When $\gamma = \frac{\pi}{4}$, sign $\left(\frac{d\hat{F}_T}{d\phi_0}(\pi)\right)$ can be either nonnegative or negative. We have:
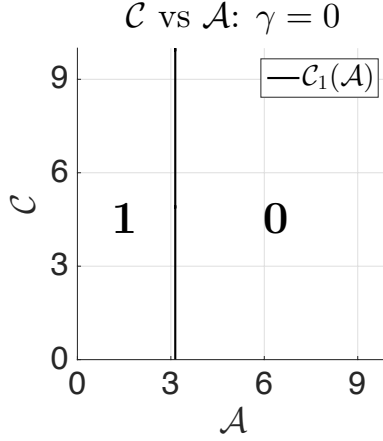
$\mathcal{C}$ vs $\mathcal{A}$: $\gamma = 0$

Figure 2.15: $\mathcal{C}$ vs $\mathcal{A}$: $\gamma = 0$. **0** indicates the zero equilibrium point region and **1** indicates the one equilibrium point region. The boundary curve between region **0** and region **1** is $\mathcal{A} = \pi$.

- Case 1: $\frac{d\hat{F}_T}{d\phi_0}(\pi) \geq 0 \quad \Leftrightarrow \quad -4\mathcal{C}\sin\frac{\gamma}{2} + 2\cos\gamma \geq 0.$

  The inequality above implies $\mathcal{C} \in [0, \mathcal{C}_0]$ where $\mathcal{C}_0 = \frac{\cos\gamma}{2\sin\frac{\gamma}{2}}$. In this case, $\hat{F}_T$ has at most one equilibrium point, denoted as $\bar{\phi}_0$ if it exists. $I(\bar{\phi}_0, \mathcal{C}) > 0$ can be checked numerically, hence the intersection never happens.

  When $\mathcal{C} \in [0, \mathcal{C}_0]$, the boundary curve $\mathcal{C}_{11}(\mathcal{A})$ is

  $$\hat{F}_T(\pi) = 0 \iff \mathcal{C}_{11}(\mathcal{A}) = \sqrt{\frac{\sqrt{2}}{\mathcal{A} - \pi}}, \tag{2.51}$$

  where $\mathcal{A} \in [\mathcal{A}_0, \infty)$ and $\mathcal{A}_0$ satisfies $\mathcal{C}_{11}(\mathcal{A}_0) = \mathcal{C}_0$. Moreover, $\mathcal{C}_{11}(\mathcal{A})$ is the boundary curve between the zero equilibrium point region and the one equilibrium point region. The zero equilibrium point region is above $\mathcal{C}_{11}(\mathcal{A})$ and the one equilibrium point region is below $\mathcal{C}_{11}(\mathcal{A})$.

- Case 2: $\frac{d\hat{F}_T}{d\phi_0}(\pi) < 0 \quad \Leftrightarrow \quad -4\mathcal{C}\sin\frac{\gamma}{2} + 2\cos\gamma < 0.$

34

$\frac{d\hat{F}_T}{d\phi_0}(\pi) < 0$ implies $\mathcal{C} > \mathcal{C}_0$. In this case, $\hat{F}_T$ has at most two equilibrium points, denoted as $\bar{\phi}_{01}$ and $\bar{\phi}_{02}$ if they exist. Both $I(\bar{\phi}_{01}, \mathcal{C}) > 0$ and $I(\bar{\phi}_{02}, \mathcal{C}) > 0$ can be tested numerically, so the equilibria never lie in the intersection region.

When $\mathcal{C} > \mathcal{C}_0$, the boundary curve $\mathcal{C}_{12}(\mathcal{A})$ is

$$\hat{F}_T(\pi) = 0 \iff \mathcal{C}_{12}(\mathcal{A}) = \sqrt{\frac{\sqrt{2}}{\mathcal{A} - \pi}} \text{ where } \mathcal{A} \in (\pi, \mathcal{A}_0]. \tag{2.52}$$

Since $\frac{d\hat{F}_T}{d\phi_0}(\pi) < 0$, $\mathcal{C}_{12}(\mathcal{A})$ is the boundary curve between the one equilibrium point region and the two equilibrium points region. The one equilibrium point region is to the left of $\mathcal{C}_{12}(\mathcal{A})$ and the two equilibrium points region is to the right of $\mathcal{C}_{12}(\mathcal{A})$. Moreover, $\mathcal{C}_{11}(\mathcal{A})$ in (2.51) and $\mathcal{C}_{12}(\mathcal{A})$ in (2.52) can be combined together, giving $\mathcal{C}_1(\mathcal{A})$:

$$\mathcal{C}_1(\mathcal{A}) = \sqrt{\frac{\sqrt{2}}{\mathcal{A} - \pi}} \text{ where } \mathcal{A} \in (\pi, \infty). \tag{2.53}$$

To obtain $\mathcal{C}_2(\mathcal{A})$, we need $\phi_0^* > \frac{\pi}{2}$, which belongs to the $\frac{d\hat{F}_T}{d\phi_0}(\pi) < 0$ case.

In Figure 2.16, The region between the curve $\mathcal{C}_1(\mathcal{A})$ and $\mathcal{C}_2(\mathcal{A})$ is the two equilibrium points region with $\mathcal{A} \in (\pi, \mathcal{A}_0]$. The one equilibrium region is below $\mathcal{C}_1(\mathcal{A})$ and the zero equilibrium region is above $\mathcal{C}_{12}(\mathcal{A})$ and $\mathcal{C}_2(\mathcal{A})$ curves.
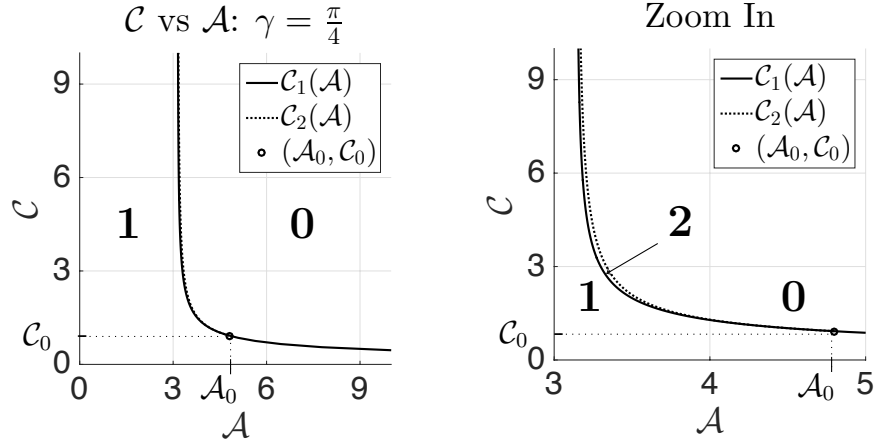
Figure 2.16: $\mathcal{C}$ vs $\mathcal{A}$: $\gamma = \frac{\pi}{4}$. **0** indicates the zero equilibrium point region, **1** indicates the one equilibrium point region and **2** indicates the two equilibrium points region. The boundary curve ends at point $(\mathcal{A}_0, \mathcal{C}_0) = \left(\pi + \frac{4\sqrt{2}}{2+\sqrt{2}}, \frac{\sqrt{2+\sqrt{2}}}{2} \right)$.

2.12.3 Example Three: $\gamma = \frac{\pi}{2}$

When $\gamma = \frac{\pi}{2}$, intersection of the fluid interfaces never happens. We have the explicit expression for the boundary $\mathcal{C}_1(\mathcal{A}) = \sqrt{\frac{2}{\mathcal{A} - \pi}}$. And the boundary curve $\mathcal{C}_2(\mathcal{A}^*)$ can be obtained numerically. It is the inverse of $\mathcal{A}^*(\mathcal{C})$ curve. We change notation, using $\mathcal{A}$ instead of $\mathcal{A}^*$. Moreover, we have discussed the asymptotic series of $\mathcal{A}^*$ for both $\mathcal{C} \to 0$ and $\mathcal{C} \to \infty$ in Section 2.10.

In Figure 2.17 $\gamma = \frac{\pi}{2}$ case, the zero equilibrium point region is above $\mathcal{C}_2(\mathcal{A})$, the two equilibrium points region is between $\mathcal{C}_1(\mathcal{A})$ and $\mathcal{C}_2(\mathcal{A})$. The one equilibrium point region is below $\mathcal{C}_1(\mathcal{A})$.
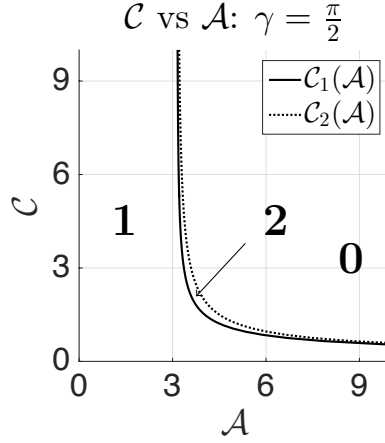
Figure 2.17: $\mathcal{C}$ vs $\mathcal{A}$: $\gamma = \frac{\pi}{2}$. **0** indicates the zero equilibrium point region, **1** indicates the one equilibrium point region and **2** indicates the two equilibrium points region.

Remark 2.3. *When $\gamma \leq \frac{\pi}{2}$, the intersection of fluid interface never happens. Therefore $\mathcal{C}_3(\mathcal{A})$ does not exist. If $\hat{F}_T$ only admits one equilibrium point $\bar{\phi}_0$, $\bar{\phi}_0$ is always stable. And if the system admits two equilibria $\bar{\phi}_{01}$ and $\bar{\phi}_{02}$, $\bar{\phi}_{01}$ is stable and $\bar{\phi}_{02}$ is unstable.*

2.12.4 Example Four: $\gamma = \frac{3\pi}{4}$

For $\gamma > \frac{\pi}{2}$, $\frac{d\hat{F}_T}{d\phi_0}(\pi) < 0$. When $\gamma = \frac{3\pi}{4}$, $\hat{F}_T$ can admit at most two equilibria, denoted as $\bar{\phi}_{01}$ and $\bar{\phi}_{02}$ if they exist. If $\bar{\phi}_{01}$ and $\bar{\phi}_{02} \in [\frac{3\pi}{4}, \pi]$, $I(\phi_0, \mathcal{C})$ is needed to test their validity[2]. Therefore $\mathcal{C}_3(\mathcal{A})$ is the boundary curve between the one valid and one invalid equilibrium points region and the two equilibrium points region.

If $\hat{F}_T(\pi) > 0$, $\hat{F}_T$ admits exact one equilibrium point $\bar{\phi}_0$. Since $I(\bar{\phi}_0, \mathcal{C}) > 0$, the equilibrium point never lies in intersection region. When $\hat{F}_T(\pi) = 0$, $\bar{\phi}_0 = \pi$ is also a equilibrium point, but it's invalid ($I(\pi, \mathcal{C}) < 0$). Therefore, $\mathcal{C}_1(\mathcal{A})$ is the boundary curve between the one equilibrium point region and the one valid, one invalid equilibrium points region. Explicitly, we have the form $\mathcal{C}_1(\mathcal{A}) = \sqrt{\frac{\sqrt{2}}{\mathcal{A} - \pi}}$.

In Figure 2.18, the one equilibrium point region is below $\mathcal{C}_1(\mathcal{A})$, the zero equilibrium point region is above $\mathcal{C}_2(\mathcal{A})$. The one valid and one invalid equilibrium points region is bounded by $\mathcal{C}_1(\mathcal{A})$ and $\mathcal{C}_3(\mathcal{A})$. The two equilibrium points region is bounded by $\mathcal{C}_2(\mathcal{A})$ and $\mathcal{C}_3(\mathcal{A})$.

---

[2]Valid means the no intersection case.
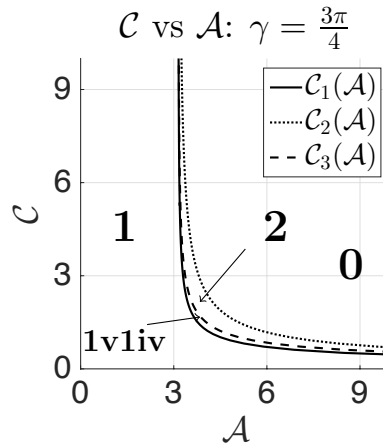
Figure 2.18: $\mathcal{C}$ vs $\mathcal{A}$: $\gamma = \frac{3\pi}{4}$. **0** indicates the zero equilibrium point region, **1** indicates the one equilibrium point region, **1v1iv** indicates the one valid, one invalid equilibrium points region and **2** indicates the two equilibrium points region.
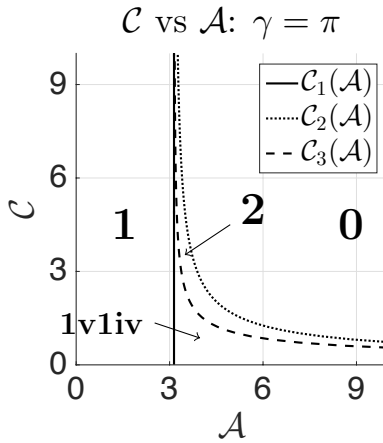
Figure 2.19: $\mathcal{C}$ vs $\mathcal{A}$: $\gamma = \pi$. **0** indicates the zero equilibrium point region, **1** indicates the one equilibrium point region, **1v1iv** indicates the one valid, one invalid equilibrium points region and **2** indicates the two equilibrium points region. $\mathcal{C}_1(\mathcal{A})$ curve is $\mathcal{A} = \pi$.

2.12.5   Example Five: $\gamma = \pi$

When $\gamma = \pi$, the results are similar to the previous case, $\gamma = \frac{3\pi}{4}$. The same strategy is applied to obtain $\mathcal{C}_2(\mathcal{A})$ and $\mathcal{C}_3(\mathcal{A})$. The only difference is that the boundary curve $\mathcal{C}_1(\mathcal{A})$

between the one equilibrium point region and the one valid, one invalid equilibrium points region is $\mathcal{A} = \pi$ (see Figure 2.19).

2.13 An Example That Admits Two Configurations

In this section, we will give an example that admits two configurations. With contact angle $\gamma = \frac{\pi}{2}$, $\mathcal{A} = 3.8$ and $\mathcal{C} = 2$, total force curve can be shown as follows:
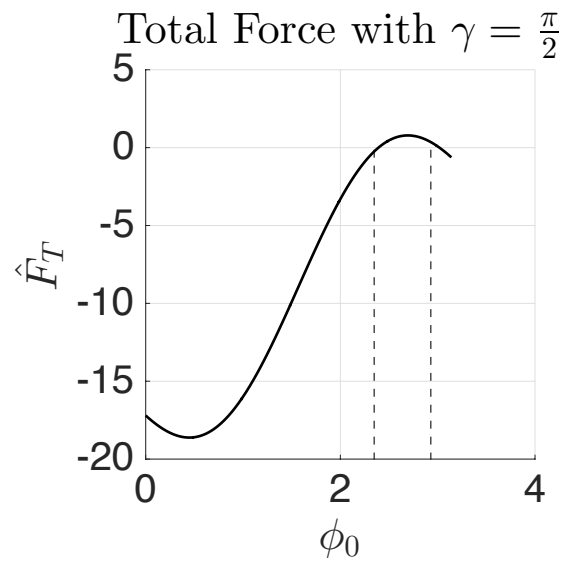
Figure 2.20: Two Equilibrium points: $\bar{\phi}_{01} = 2.3915$ and $\bar{\phi}_{02} = 3.0178$.

We obtain two equilibrium points $\bar{\phi}_{01} = 2.3915$ and $\bar{\phi}_{02} = 3.0178$. The following shows their configurations:
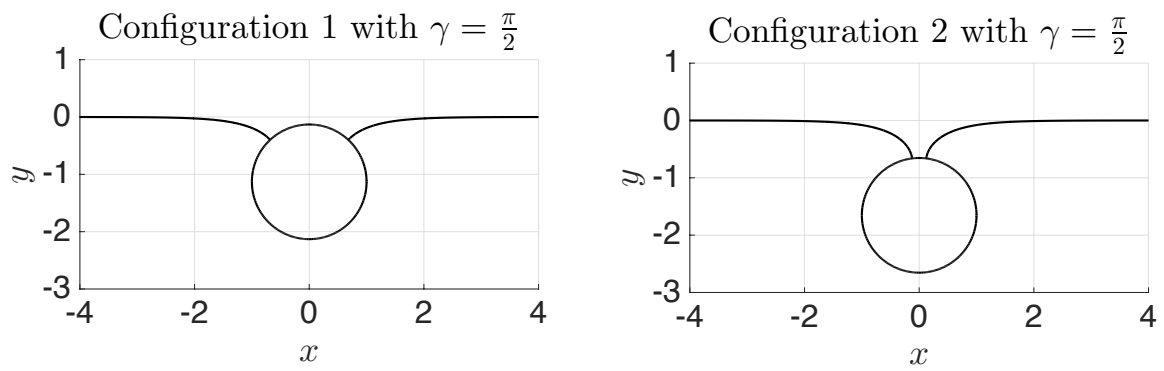
Figure 2.21: Parameters: $\gamma = \frac{\pi}{2}$, $\mathcal{A} = 3.8$, $\mathcal{C} = 2$ and radius $a = 1$.

Chapter 3

Two-Dimensional Floating Square

We introduce a $2D$ floating square allowing rotation in this chapter. Physically, we mean a horizontal cylinder with square cross-section. In Kemp and Siegel's work [12], they discuss the stability of floating objects with polygonal cross-sections in absence of gravity. They show that the only stable floating configurations occur when the fluid interfaces intersect two corners of the polygon. In this chapter, the energy method is applied in the study of floating square with rotation. In no surface tension case, we rederive the stability conditions of the floating square with the allowance of rotation. Our derivation is slightly different from Erdös, Schibler and Herndon's work [4] and Abolhassani's work [1]. Archimedes' principle is applied in the energy function. In the presence of surface tension case, an example with contact angle $\frac{\pi}{4}$ is discussed.

3.1   Configurations with No Surface Tension

Suppose the square with side length a is floating on the liquid with two vertices immersed, and the bottom parallel to the horizontal reference level. Different from floating cylinder, the square is not rotationally invariant. We introduce the rotational angle θ, which is clockwise from the vertical axis, and the height of centre h. The homogeneous square has a density of ρ_s and liquid has a density of ρ. We define the density ratio as $\alpha = \frac{\rho_s}{\rho}$. For $\alpha > 1$, floating is not possible. For $\frac{1}{2} < \alpha \leq 1$, by reflecting the square with respect to the fluid level and replacing α by $1 - \alpha$, we have the same energy, see [4]. Thus it is sufficient to discuss only $\alpha \in (0, \frac{1}{2}]$.

When we restrict $\theta \in [0, \frac{\pi}{4}]$ and $\alpha \in (0, \frac{1}{2}]$, there are two types of configurations (see Figure 3.1 and Figure 3.2).

3.1.1   Two Corners Immersed

Suppose two vertices C and D are immersed in the fluid and centre of the square G is set to be the origin, and η is an included angle between the diagonal line of the square and the horizontal axis through the origin G. The geometric constraint is as follows:

$$\theta + \eta = \frac{\pi}{4}. \tag{3.1}$$

The coordinates of vertices C_G and D_G (with G as the origin) can be obtained:

$$C_G = \left(-\frac{\sqrt{2}}{2} a \cos \eta, \, -\frac{\sqrt{2}}{2} a \sin \eta \right), \tag{3.2}$$

$$D_G = \left(\frac{\sqrt{2}}{2} a \sin \eta, \, -\frac{\sqrt{2}}{2} a \cos \eta \right). \tag{3.3}$$
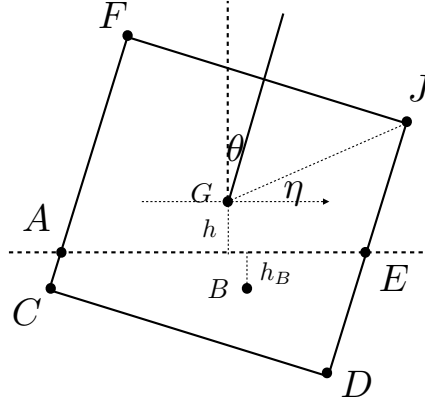
Figure 3.1: Two corners immersed.

Our two corners immersed configuration is obtained by shifting G up vertically by h. Therefore, the coordinates for vertices C and D are:

$$C = (C_x, C_y) = \left(-\frac{a}{2}(\cos\theta + \sin\theta), h - \frac{a}{2}(\cos\theta - \sin\theta)\right), \tag{3.4}$$

$$D = (D_x, D_y) = \left(\frac{a}{2}(\cos\theta - \sin\theta), h - \frac{a}{2}(\cos\theta + \sin\theta)\right). \tag{3.5}$$

The coordinates of the other two vertices F and J are:

$$F = (F_x, F_y) = (C_x + a\sin\theta, C_y + a\cos\theta), \tag{3.6}$$

$$J = (J_x, J_y) = (D_x + a\sin\theta, D_y + a\cos\theta). \tag{3.7}$$

A and E are the points that the square and the fluids intersect at, with coordinates:

$$A = (A_x, A_y) = \left(-\frac{a}{2}\cos\theta - \frac{a}{2}\sin\theta\tan\theta - h\tan\theta, 0\right), \tag{3.8}$$

$$E = (E_x, E_y) = \left(\frac{a}{2}\cos\theta + \frac{a}{2}\sin\theta\tan\theta - h\tan\theta, 0\right). \tag{3.9}$$

With two corners immersed, we require $C_y < 0$ and $J_y > 0$ or equivalently,

$$\frac{a}{2}(\sin\theta - \cos\theta) < h < \frac{a}{2}(\cos\theta - \sin\theta). \tag{3.10}$$

Archimedes' principle (see Appendix B) implies the height of centre in force balance h^*. If we consider one unit length, the weight of the square is equal to the weight of liquid displaced:

$$\begin{aligned} M_{square} &= M_{liquid}, \\ \rho_s a^2 &= \rho\,\text{Area}_{ACDE}. \end{aligned} \tag{3.11}$$

Where the area of the trapezoid $ACDE$ is:

$$\begin{aligned} \text{Area}_{ACDE} &= \frac{1}{2}\left(|AC| + |DE|\right)|CD| \\ &= \frac{1}{2}a\left(\frac{-C_y}{\cos\theta} + \frac{-D_y}{\cos\theta}\right) \\ &= \frac{a^2}{2} - \frac{ah}{\cos\theta}. \end{aligned} \tag{3.12}$$

43

Equations (3.11) and (3.12) imply

$$h^* = a(\frac{1}{2} - \alpha) \cos\theta. \tag{3.13}$$

With $0 < \alpha \leq \frac{1}{2}$ and $|h| \leq \frac{a}{2}(\cos\theta - \sin\theta)$,

$$0 \leq \theta \leq \arctan(2\alpha), \quad \text{where } \alpha \in \left(0, \frac{1}{2}\right]. \tag{3.14}$$

3.1.2   One Corner Immersed

Another configuration has only the vertex D immersed. Compared with the two corners immersed case, the expressions of the coordinates of the vertices and the intersection points are the same except for vertex A.

$$A = \left(\frac{C_y}{\tan\theta} - \frac{a}{2}(\cos\theta + \sin\theta), 0\right), \quad \text{where } \theta \neq 0. \tag{3.15}$$
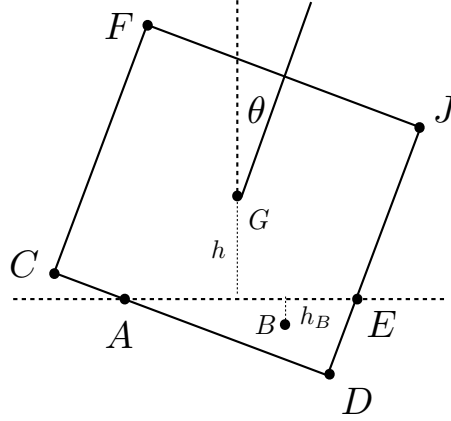
Figure 3.2: One corner immersed.

With one corner immersed, we require $C_y \geq 0$ and $D_y < 0$ or equivalently,

$$\frac{a}{2}(\cos\theta - \sin\theta) \leq h < \frac{a}{2}(\cos\theta + \sin\theta). \tag{3.16}$$

44

Archimedes' principle implies

$$
\begin{aligned}
M_{square} &= M_{liquid}, \\
\rho_s a^2 &= \rho \text{Area}_{ADE},
\end{aligned}
\tag{3.17}
$$

where

$$
\begin{aligned}
\text{Area}_{ADE} &= \frac{1}{2}|AD||DE| \\
&= \frac{1}{2}\left(a - \frac{C_y}{\sin\theta}\right)\left(\frac{-D_y}{\cos\theta}\right).
\end{aligned}
\tag{3.18}
$$

Combining (3.17) and (3.18), we have the height of centre in force balance

$$
h^* = \frac{a}{2}(\cos\theta + \sin\theta) \pm a\sqrt{\alpha \sin 2\theta}.
\tag{3.19}
$$

Since $D_y < 0$, only "$-$" sign is valid, and therefore,

$$
h^* = \frac{a}{2}(\cos\theta + \sin\theta) - a\sqrt{\alpha \sin 2\theta}.
\tag{3.20}
$$

With $\frac{a}{2}(\cos\theta - \sin\theta) \leq h < \frac{a}{2}(\cos\theta + \sin\theta)$,

$$
\arctan(2\alpha) \leq \theta \leq \frac{\pi}{4}, \quad \text{where } \alpha \in \left(0, \frac{1}{2}\right].
\tag{3.21}
$$

Remark 3.1. *The three corners immersed case only happens when $\alpha > \frac{1}{2}$, and can be obtained by reflecting the square with respect to the fluid level in the one corner immersed case and replacing α by $1 - \alpha$.*

3.2   Energy Point of View

To study the stability behaviour of our floating square with rotation, the energy method is employed again as in Section 2.3. Without surface tension, the total energy E_T is consists of the body potential energy E_G and the fluid potential energy E_F. E_T depends on both h and θ. If we consider E_T in force balance, E_T only depends on the rotational angle θ.

3.2.1 Total Energy $E_T(\theta)$ in Force Balance

- The body potential energy E_G:

  with the downward pointing gravity g, E_G depends on variable h^*:

  $$E_G(h^*) = \rho_s a^2 g h^*.\tag{3.22}$$

- Fluid potential energy E_F:

  We treat E_F differently than in the $2D$ floating cylinder case by expressing it in terms of the centre of buoyancy. h_B is the centroid of ADE. We obtain:

  $$\begin{aligned}
  E_F &= \rho g \int_\Sigma \frac{y^2}{2} ds \\
  &= -\rho g |\Sigma| h_B,
  \end{aligned}\tag{3.23}$$

  where Σ is the wetted region, ds is the element of the wetted region, y is the vertical displacement from the reference level to Σ and h_B is the vertical component of the centre of buoyancy[1].

  If there are two corners immersed, the enclosed region $\Sigma \cup |AE|$ is a trapezoid, and the vertical component of the centre of buoyancy is

  $$\begin{aligned}
  h_B &= \frac{1}{6\text{Area}_{ACDE}} \Big[(A_y + C_y)(A_x C_y - C_x A_y) + (C_y + D_y)(C_x D_y - D_x C_y) \\
  &\quad + (D_y + E_y)(D_x E_y - E_x D_y) + (E_y + A_y)(E_x A_y - A_x E_y) \Big].
  \end{aligned}\tag{3.24}$$

  Provided $h^* = a(\frac{1}{2} - \alpha)\cos\theta$, h_B in force balance can be expressed as

  $$h_B = -a \left(\frac{1}{2}\alpha\cos\theta + \frac{1}{24\alpha}\sin\theta\tan\theta \right).\tag{3.25}$$

  If there is one corner immersed, the enclosed region $\Sigma \cup |AE|$ is a triangle, and the vertical component of the centroid of buoyancy is

  $$\begin{aligned}
  h_B &= \frac{1}{3}(A_y + E_y + D_y) \\
  &= -\frac{1}{3}a\sqrt{\alpha}\sin 2\theta.
  \end{aligned}\tag{3.26}$$

---

[1]The formulas of centroid of polygons are provided in [21]

Therefore, the total energy E_T in force balance has the expression:

- In the two corners immersed case,

$$
\begin{aligned}
E_T(\theta) &= \rho_s a^2 g h^* - \rho g |\Sigma| h_B \\
&= \rho_s a^2 g h^* - \frac{1}{2}\rho a^2 g(\frac{h^*}{\cos\theta} - \frac{a}{2})(\alpha\cos\theta + \frac{1}{12\alpha}\sin\theta\tan\theta) \\
&= \rho_s a^3 g\left[\frac{1}{2}\cos\theta(1-\alpha) + \frac{1}{24\alpha}\sin\theta\tan\theta\right],
\end{aligned}
\tag{3.27}
$$

where $0 < \theta \leq \arctan(2\alpha)$, and $\alpha \in (0, \frac{1}{2}]$.

- In the one corner immersed case,

$$
\begin{aligned}
E_T(\theta) &= \rho_s a^2 g h^* + \rho g \frac{1}{2}\left(a - \frac{h^* - \frac{a}{2}(\cos\theta - \sin\theta)}{\sin\theta}\right)\left(\frac{\frac{a}{2}(\cos\theta + \sin\theta) - h^*}{\cos\theta}\right)(\frac{1}{3}a\sqrt{\alpha}\sin 2\theta) \\
&= \rho_s a^3 g\left[\frac{1}{2}(\cos\theta + \sin\theta) - \frac{2}{3}\sqrt{\alpha\sin 2\theta}\right],
\end{aligned}
\tag{3.28}
$$

where $\arctan(2\alpha) \leq \theta \leq \frac{\pi}{4}$, and $\alpha \in (0, \frac{1}{2}]$.

3.2.2 Stability Analysis of Two Corners Immersed Case

So far, we obtained the expression of total energy in force balance $E_T(\theta)$,

$$
E_T(\theta) = \rho_s a^3 g\left[\frac{1}{2}\cos\theta(1-\alpha) + \frac{1}{24\alpha}\sin\theta\tan\theta\right],
$$

where $0 \leq \theta \leq \arctan(2\alpha)$, and $\alpha \in (0, \frac{1}{2}]$.

The following theorem gives the stability of the floating square with rotation for two corners immersed case.

Theorem 3.1. *Total energy E_T admits two critical points $\theta^* = 0$ and $\theta^* = \arccos\left(\frac{1}{\sqrt{12\alpha - 12\alpha^2 - 1}}\right)$.*

1. *When $\theta^* = 0$, θ^* is stable if $0 < \alpha \leq \frac{1}{2} - \frac{1}{2\sqrt{3}}$ and θ^* is unstable if $\frac{1}{2} - \frac{1}{2\sqrt{3}} < \alpha \leq \frac{1}{2}$.*

2. *When $\theta^* = \arccos\left(\frac{1}{\sqrt{12\alpha - 12\alpha^2 - 1}}\right)$, α is only valid on $[\frac{1}{2} - \frac{1}{\sqrt{6}}, \frac{1}{4}]$ and θ^* is stable.*

Proof. First, we compute the critical points,

$$\frac{dE_T}{d\theta}(\theta) = \rho_s a^3 g \left[\frac{1}{2}(\alpha - 1)\sin\theta + \frac{1}{24\alpha}\left(\sin\theta + \frac{\sin\theta}{\cos^2\theta} \right) \right] = 0. \qquad (3.29)$$

This leads to $\theta^* = 0$ or $\cos^2\theta^* = \frac{1}{12\alpha - 12\alpha^2 - 1}$.

The inequality $12\alpha - 12\alpha^2 - 1 \geq 0$ gives $\alpha \geq \frac{1}{2} - \frac{1}{\sqrt{6}}$. Therefore, $\theta^* = \arccos\left(\frac{1}{\sqrt{12\alpha - 12\alpha^2 - 1}} \right)$. In order to require the two corners immersed, we need $\theta^* \leq \arctan(2\alpha)$, or equivalently, $\alpha \leq \frac{1}{4}$. Thus, if we have $\theta^* = \arccos\left(\frac{1}{\sqrt{12\alpha - 12\alpha^2 - 1}} \right)$, α ranges from $(\frac{1}{2} - \frac{1}{\sqrt{6}})$ to $\frac{1}{4}$.

Next, we calculate $\frac{d^2 E_T}{d\theta^2}(\theta)$,

$$\frac{d^2 E_T}{d\theta^2}(\theta) = \rho_s a^3 g \left[\frac{1}{2}(\alpha - 1)\cos\theta + \frac{1}{24\alpha}\left(\cos\theta + \frac{\sin^2\theta}{\cos^3\theta} + \frac{1}{\cos^3\theta} \right) \right]. \qquad (3.30)$$

1. If $\theta^* = 0$,
$$\frac{d^2 E_T}{d\theta^2}(0) = \rho_s a^3 g \left[-\frac{1}{2} + \frac{1}{2}\alpha + \frac{1}{12\alpha} \right] = 0.$$

   Therefore, $\theta^* = 0$ is stable if
   $$\frac{d^2 E_T}{d\theta^2}(0) \geq 0 \quad \Leftrightarrow \quad 0 < \alpha \leq \frac{1}{2} - \frac{1}{2\sqrt{3}},$$

   and $\theta^* = 0$ is unstable if
   $$\frac{d^2 E_T}{d\theta^2}(0) < 0 \quad \Leftrightarrow \quad \frac{1}{2} - \frac{1}{2\sqrt{3}} < \alpha \leq \frac{1}{2}.$$

2. If $\theta^* = \arccos\left(\frac{1}{\sqrt{12\alpha - 12\alpha^2 - 1}} \right)$,

$$\frac{d^2 E_T}{d\theta^2}(\theta^*) = \rho_s a^3 g \left\{ \frac{\alpha - 1}{2\sqrt{12\alpha - 12\alpha^2 - 1}} + \frac{1}{24\alpha}\left[\frac{1}{\sqrt{12\alpha - 12\alpha^2 - 1}} - \sqrt{12\alpha - 12\alpha^2 - 1} \right. \right.$$
$$\left. \left. + 2\left(\sqrt{12\alpha - 12\alpha^2 - 1} \right)^3 \right] \right\} \geq 0. \qquad (3.31)$$

   Therefore, $\theta^* = \arccos\left(\frac{1}{\sqrt{12\alpha - 12\alpha^2 - 1}} \right)$ is stable if $\frac{1}{2} - \frac{1}{\sqrt{6}} \leq \alpha \leq \frac{1}{4}$.

   $\square$

48

3.2.3   Stability Analysis of One Corner Immersed Case

With one corner immersed, the total energy in force balance E_T is

$$E_T(\theta) = \rho_s a^3 g \left[\frac{1}{2}(\cos\theta + \sin\theta) - \frac{2}{3}\sqrt{\alpha\sin 2\theta} \right],$$

where $\arctan(2\alpha) \le \theta \le \frac{\pi}{4}$, and $\alpha \in (0, \frac{1}{2}]$.

For one corner immersed case, the following theorem shows the stability behaviour of the floating square with rotation.

Theorem 3.2. *Total energy E_T admits two critical points $\theta^* = \frac{\pi}{4}$ and $\theta^* = \frac{1}{2}\arcsin(\frac{16\alpha}{9-16\alpha})$.*

1. *When $\theta^* = \frac{\pi}{4}$, θ^* is stable if $\frac{9}{32} \le \alpha \le \frac{1}{2}$ and θ^* is unstable if $0 < \alpha < \frac{9}{32}$.*

2. *When $\theta^* = \frac{1}{2}\arcsin(\frac{16\alpha}{9-16\alpha})$, α must belong to the interval $[\frac{1}{4}, \frac{9}{32}]$ and θ^* is stable.*

Proof. We compute the critical points:

$$\frac{dE_T}{d\theta}(\theta) = \rho_s a^3 g \left(\frac{1}{2}(-\sin\theta + \cos\theta) - \frac{2\sqrt{\alpha}}{3}\frac{\cos 2\theta}{\sqrt{\sin 2\theta}} \right) = 0. \tag{3.32}$$

This leads to $\theta^* = \frac{\pi}{4}$ and $\theta^* = \frac{1}{2}\arcsin(\frac{16\alpha}{9-16\alpha})$. Since $\arctan(2\alpha) \le \theta^* \le \frac{\pi}{4}$, α ranges from $\frac{1}{4}$ to $\frac{9}{32}$ when $\theta^* = \frac{1}{2}\arcsin(\frac{16\alpha}{9-16\alpha})$.

We compute the second derivative:

$$\frac{d^2 E_T}{d\theta^2}(\theta) = \rho_s a^3 g \left\{ -\frac{1}{2}(\sin\theta + \cos\theta) + \frac{2\sqrt{\alpha}}{3}\left(2\sqrt{\sin 2\theta} + \frac{\cos^2 2\theta}{\sqrt{\sin^3 2\theta}} \right) \right\}. \tag{3.33}$$

1. When $\theta^* = \frac{\pi}{4}$,

$$\frac{d^2 E_T}{d\theta^2}\left(\frac{\pi}{4}\right) = \rho_s a^3 g \left(\frac{4\sqrt{\alpha}}{3} - \frac{\sqrt{2}}{2} \right). \tag{3.34}$$

Therefore, $\theta^* = \frac{\pi}{4}$ is stable if

$$\frac{d^2 E_T}{d\theta^2}\left(\frac{\pi}{4}\right) \ge 0 \quad \Leftrightarrow \quad \frac{9}{32} \le \alpha \le \frac{1}{2},$$

and $\theta^* = \frac{\pi}{4}$ is unstable if

$$\frac{d^2 E_T}{d\theta^2}\left(\frac{\pi}{4}\right) < 0 \quad \Leftrightarrow \quad 0 < \alpha < \frac{9}{32}.$$

2. When $\theta^* = \frac{1}{2}\arcsin(\frac{16\alpha}{9-16\alpha})$,

$$\frac{d^2 E_T}{d\theta^2}(\theta^*) = \rho_s a^3 g\left(\frac{1 + \frac{4096}{135}(\alpha - \frac{9}{64})^2}{96\alpha\sqrt{9-16\alpha}}\right) > 0. \tag{3.35}$$

Therefore, $\theta^* = \frac{1}{2}\arcsin\left(\frac{16\alpha}{9-16\alpha}\right)$ is stable if $\frac{1}{4} \le \alpha \le \frac{9}{32}$.

$\square$

Remark 3.2. *Detailed conclusions in Theorem 3.1 and Theorem 3.2 are the same as those in [4].*

3.3   Floating Square With Rotation and Surface Tension

With surface tension, the configurations of the floating square with a rotation become complicated. In this section, we are going to give a typical example of two corners immersed square when surface tension is present and contact angle $\gamma = \frac{\pi}{4}$.

3.3.1   Configuration With $\gamma = \frac{\pi}{4}$
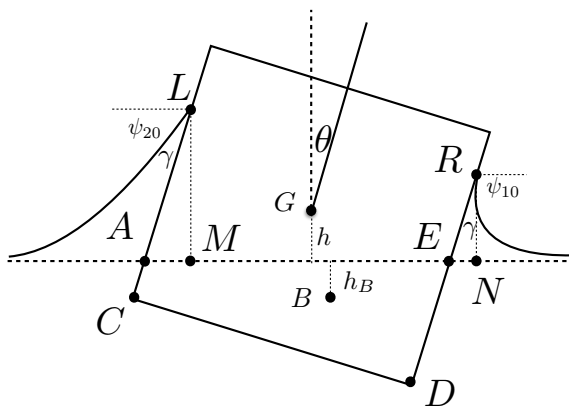
Figure 3.3: The floating square when surface tension is present.

We consider the configuration in Figure 3.3, the floating square has two corners immersed and is rotated clockwise by θ. The liquid is lifted up, with contact angle $\gamma = \frac{\pi}{4}$,

to the square. We define two inclination angles to parametrize the fluid interfaces: $\psi_1 \in [\psi_{10}, 0]$ is to the right and $\psi_2 \in [\psi_{20}, 0]$ is to the left, where $\psi_{10}, \psi_{20} < 0$. We have the following geometric constraints:

$$2\gamma - \pi = \psi_{10} + \psi_{20}, \tag{3.36}$$

$$-\psi_{20} + \gamma + \theta = \frac{\pi}{2}, \tag{3.37}$$

$$-\psi_{10} + \gamma - \theta = \frac{\pi}{2}. \tag{3.38}$$

Solutions of the capillary equation in Section 2.2 can also be employed in this case. We denote $u_1(\psi)$ and $u_2(\psi)$ as the height of fluid interfaces to the right and to the left, respectively:

$$u_1(\psi_1) = -\frac{2}{\sqrt{\kappa}} \sin \frac{\psi_1}{2} \quad \text{and} \quad u_2(\psi_2) = -\frac{2}{\sqrt{\kappa}} \sin \frac{\psi_2}{2}. \tag{3.39}$$

Based on the fluid heights at the contact points $u_1(\psi_{10})$ and $u_2(\psi_{20})$, we can compute the horizontal distances of the contact points x_{10} and x_{20}:

$$N_x = E_x + u_{10} \tan \theta \quad \text{and} \quad M_x = A_x + u_{20} \tan \theta. \tag{3.40}$$

Moreover, the left fluid interface has positive slope $\frac{du_2}{dx} = -\tan \psi_2$ and the right fluid interface has negative slope $\frac{du_1}{dx} = \tan \psi_1$. Given $\frac{dx}{d\psi_2} = \frac{\cos \psi_2}{\kappa u_2}$ and $\frac{dx}{d\psi_1} = -\frac{\cos \psi_1}{\kappa u_1}$, we integrate the ψ_2 and ψ_1, respectively. Then the parametric solutions for $x(\psi_1)$ and $x(\psi_2)$ can be expressed as follows:

$$
\begin{aligned}
x(\psi_1; \psi_{10}, \theta, h) &= -\frac{1}{\sqrt{\kappa}} \left[2 \cos \frac{\psi_1}{2} + \ln \left| \tan \frac{\psi_1}{4} \right| + 2 \cos \frac{\psi_{10}}{2} + \ln \left| \tan \frac{\psi_{10}}{4} \right| \right] \\
&\quad + \frac{a}{2} \cos \theta + \frac{a}{2} \sin \theta \tan \theta - h \tan \theta - \frac{2}{\sqrt{\kappa}} \sin \frac{\psi_{10}}{2},
\end{aligned} \tag{3.41}
$$

$$
\begin{aligned}
x(\psi_2; \psi_{20}, \theta, h) &= \frac{1}{\sqrt{\kappa}} \left[2 \cos \frac{\psi_2}{2} + \ln \left| \tan \frac{\psi_2}{4} \right| - 2 \cos \frac{\psi_{20}}{2} - \ln \left| \tan \frac{\psi_{20}}{4} \right| \right] \\
&\quad - \frac{a}{2} \cos \theta - \frac{a}{2} \sin \theta \tan \theta - h \tan \theta - \frac{2}{\sqrt{\kappa}} \sin \frac{\psi_{20}}{2}.
\end{aligned} \tag{3.42}
$$

51

3.3.2 Total Energy $\hat{E}_T$ and Stability Analysis for $\gamma = \frac{\pi}{4}$

The dimensionless total energy $\hat{E}_T$ can be expressed in terms of $\hat{h}$ and θ, where $\hat{h} = \frac{h}{a}$. In order to avoid the contact points L, R hitting the vertices of the square, we choose $\hat{h} \in \left[-\frac{1}{2} + \frac{u_0}{a}, \frac{1}{2} + \frac{u_0}{a} \right]$ if $\theta = 0$. Since our configuration is also symmetric with respect to the rotational angle θ, $E_T(\hat{h}, -\theta)$ and $E_T(\hat{h}, \theta)$ give the same energy. Moreover, $\theta \in \left[-\frac{\pi}{4}, \frac{\pi}{4} \right]$. We introduce a characteristic energy E_{square} and a dimensionless variable S as follows:

$$E_{square} = \rho_s a^3 g \quad \text{and} \quad S = \frac{\sigma}{\sqrt{\kappa \rho_s a^3 g}}. \tag{3.43}$$

The dimensionless form of the total energy can be expressed as follows:

$$\hat{E}_T(\hat{h}, \theta; S, \theta) = \hat{E}_G + \hat{E}_W + \hat{E}_\sigma + \hat{E}_F, \tag{3.44}$$

where,

1. The body potential energy is:
$$\hat{E}_G = \hat{h}. \tag{3.45}$$

2. The wetting energy is:
$$\hat{E}_W = 2\cos\gamma \left[\sqrt[3]{\frac{S^2}{\alpha}} \left(\frac{\hat{h}}{\cos\theta} - 1 \right) + \sqrt{2} S \frac{\cos\frac{\theta}{2}(\sin\frac{\gamma}{2} - \cos\frac{\gamma}{2})}{\cos\theta} \right]. \tag{3.46}$$

3. The surface tension energy is:
$$\begin{aligned} \hat{E}_\sigma &= 2S \left[2 - \sqrt{2}\cos\frac{\theta}{2} \left(\sin\frac{\gamma}{2} + \cos\frac{\gamma}{2} \right) \right] - \sqrt[3]{\frac{S^2}{\alpha}} \left(\cos\theta + \sin\theta\tan\theta \right) \\ &\quad -2\sqrt{2} S \tan\theta \sin\frac{\theta}{2} \left(\sin\frac{\gamma}{2} + \cos\frac{\gamma}{2} \right). \end{aligned} \tag{3.47}$$

4. The fluid potential energy is:
$$\begin{aligned} \hat{E}_F &= -S \left[\frac{4}{3} - \sqrt{2}\cos\frac{\theta}{2} \left(\sin\frac{\gamma}{2} + \cos\frac{\gamma}{2} \right) + \frac{\sqrt{2}}{3}\cos\frac{3\theta}{2} \left(\sin\frac{3\gamma}{2} - \cos\frac{3\gamma}{2} \right) \right] \\ &\quad + \frac{4}{3} S \tan\theta \left[\sin^3(\frac{\gamma + \theta}{2} - \frac{\pi}{4}) - \sin^3(\frac{\gamma - \theta}{2} - \frac{\pi}{4}) \right] \\ &\quad + \frac{1}{\alpha} \left[\frac{1}{12\cos\theta} + \frac{\hat{h}^2}{2\cos\theta} - \frac{\hat{h}}{2} + \frac{\cos 2\theta}{24\cos\theta} \right]. \end{aligned} \tag{3.48}$$
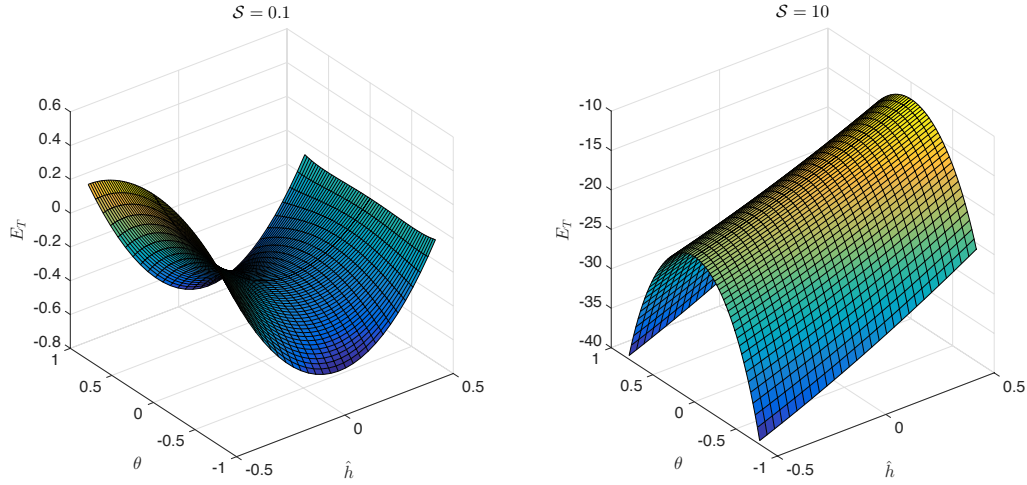
Figure 3.4: Two examples with $\gamma = \frac{\pi}{4}$ and $\alpha = \frac{1}{4}$.

The calculation details are shown in Appendix F.

Minimizing the total energy $\hat{E}_T$ is complicated and numerical computation will be sufficient. We choose $\gamma = \frac{\pi}{4}$, $\alpha = \frac{1}{4}$ and $\mathcal{S} \in [0, 100]$. According to our numerical computation, there are two typical examples $\mathcal{S} = 0.1$ and $\mathcal{S} = 10$ (see Figure 3.4).

- When $\mathcal{S} = 0.1$,

$$\frac{\partial \hat{E}_T}{\partial \hat{h}} = 0 \text{ and } \frac{\partial \hat{E}_T}{\partial \theta} = 0.$$

$$\Rightarrow \quad \hat{h}^* = \frac{1}{2} - \frac{10 + 2\sqrt{2}\sqrt[3]{5}}{40} \approx 0.129 > 0 \text{ and } \theta^* = 0. \tag{3.49}$$

Since the valid interval for $\hat{h}$ is $[-0.395, 0.605]$ with $u_0 \approx 0.524$, $\hat{h}^* \in [-0.395, 0.605]$, $(\hat{h}^*, \theta^*)$ is a critical point. The test discriminant is

$$D|_{(\hat{h}^*, \theta^*)} = \left(\frac{\partial^2 \hat{E}_T}{\partial \hat{h}^2}\right)\left(\frac{\partial^2 \hat{E}_T}{\partial \theta^2}\right) - \left(\frac{\partial^2 \hat{E}_T}{\partial \hat{h}\partial \theta}\right) < 0. \tag{3.50}$$

Thus, $(\hat{h}^*, \theta^*)$ is an unstable equilibrium point by the second derivative test. The following Figure 3.5 shows the unstable configuration in this case.

An Unstable Equilibrium
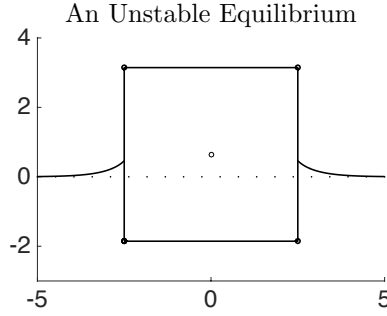
Figure 3.5: Parameters: $\mathcal{S} = 0.1$, $\alpha = \frac{1}{4}$, $\gamma = \frac{\pi}{4}$ and $a = 5$.

Remark 3.3. *Allowing only vertical motion, the configuration in Figure 3.5 is stable.*

- When $\mathcal{S} = 10$,

$$\frac{\partial \hat{E}_T}{\partial \hat{h}} = 0 \text{ and } \frac{\partial \hat{E}_T}{\partial \theta} = 0.$$

$$\Rightarrow \quad \hat{h}^* = \frac{1}{2} - \frac{1 + 2^{\frac{11}{6}} 5^{\frac{2}{3}}}{4} \approx -2.355 \text{ and } \theta^* = 0. \tag{3.51}$$

Since the valid interval for $\hat{h}$ is $[-0.477, 0.523]$ with $u_0 \approx 0.113$, $\hat{h}^* \notin [-0.477, 0.523]$, there is no critical point in this case. Moreover, this case is not physically realizable.

Chapter 4

Three-dimensional Floating Objects

In this chapter, two cases of $3D$ radial symmetric objects floating on an infinite reservoir are studied. One is a floating vertical cylinder and the other is a floating ball. The following three questions are discussed:

1. How to solve for radially symmetric exterior capillary surfaces, the nonlinear system (4.6)?

2. In $3D$ problems, does the relation $-\frac{dE_T}{dh} = F_T$ still hold?

3. Can we find stable configurations?

4.1 Governing Equation

We define r as the radial distance from the axis of symmetry. The fluid height $u(r)$ can be obtained by solving the radial symmetric capillary equation:

$$\left(\frac{ru'}{\sqrt{1 + (u')^2}} \right)' = \kappa r u. \tag{4.1}$$

Through the scaling transformation

$$u(r) = \frac{1}{\sqrt{\kappa}} w(\sqrt{\kappa} r), \tag{4.2}$$

the capillary equation (4.1) can be transformed to

$$\left(\frac{\bar{r} w_{\bar{r}}}{\sqrt{1+(w_{\bar{r}})^2}}\right)_{\bar{r}} = \bar{r} w, \tag{4.3}$$

where $\bar{r} = \sqrt{\kappa} r$. The equations (4.1) and (4.3) are equivalent when $\kappa = 1$ and thus, the capillary equation with any value of κ can be transformed to one with $\kappa = 1$. In addition, the capillary equation (4.1) can be written as

$$(r \sin \psi)_r = \kappa r u, \tag{4.4}$$

with the inclination angle ψ introduced in Chapter 2. Equation (4.4) can be converted into a system of DEs with the parameter ψ:

$$(r \sin \psi)_r \equiv \sin \psi + r \cos \psi \frac{d\psi}{dr} = \kappa r u$$

$$\Rightarrow \quad \frac{dr}{d\psi} = \frac{r \cos \psi}{\kappa r u - \sin \psi}. \tag{4.5}$$

Equation (4.5) and $\frac{du}{dr} = \tan \psi$ imply that

$$\frac{du}{d\psi} = \frac{r \sin \psi}{\kappa r u - \sin \psi} \quad \text{and} \quad \frac{dr}{d\psi} = \frac{r \cos \psi}{\kappa r u - \sin \psi}. \tag{4.6}$$

With our
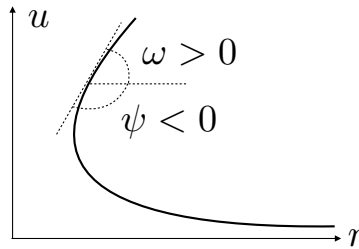
Figure 4.1: Tangent angles ψ and ω.

An analogous representation is used in the study of the liquid bridges in [20], sessile drops in [5] and floating drops in [3], shown as follows:

$$\frac{du}{d\omega} = \frac{-r \sin \omega}{\kappa r u + \sin \omega} \quad \text{and} \quad \frac{dr}{d\omega} = \frac{-r \cos \omega}{\kappa r u + \sin \omega}, \tag{4.7}$$

where ω can be seen in Figure 4.1. With relation $\omega - \psi = \pi$, equations (4.6) and (4.7) are equivalent.

Moreover, the arc length parametric representation is used by McCuan and Treinen in the study of $3D$ floating ball in [17], is as follows:

$$\frac{du}{ds} = \sin\psi, \quad \frac{dr}{ds} = \cos\psi \quad \text{and} \quad \frac{d\psi}{ds} = \kappa u - \frac{\sin\psi}{r}. \tag{4.8}$$

The systems of DEs (4.6), (4.7) and (4.8) are equivalent. They all work in both the graph case and the non-graph case[1]. In practice, the equations (4.6) have the best numerical performance, and therefore, we choose the system of DEs in (4.6) as the governing equation.

Remark 4.1. *For the exterior problem, given a radial distance $\bar{r}$ and its corresponding inclination angle $\bar{\omega}$, and boundary condition $\lim_{r\to\infty} u = 0$, Elcrat, Neel and Siegel show that there is a unique solution of $u(r)$ on $r \geq \bar{r}$ for equations (4.8) in [3].*

4.2 $3D$ Floating Vertical Cylinder

In this section, we consider a vertical cylinder with radius a and length $2a$ floating on an infinite bath (see Figure 4.2). We allow the cylinder to only move in the vertical direction. This is similar to the configuration is in Chapter 2, where h is the height of centre and γ is the contact angle. The geometric constraint can be expressed as

$$\gamma - \psi_0 = \frac{\pi}{2}. \tag{4.9}$$

The fluid height $u(\psi)$ and the radial distance from the vertical axis $r(\psi)$ can be parametrized by the inclination angle ψ based on the system of DEs (4.6) with boundary conditions:

$$\lim_{r\to\infty} u = 0 \quad \text{and} \quad r(\psi_0) = a, \tag{4.10}$$

where a is the radius of the cylinder.

---

[1]The graph case means the fluid interface is a graph, the non-graph case means the fluid interface is not a graph.
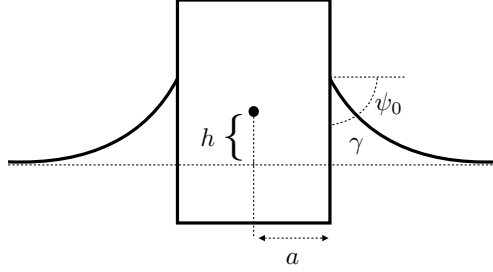
Figure 4.2: The cross-section of a floating vertical cylinder.

4.2.1   The Shooting Method for Fluid Height u When $\kappa = 1$

Since both governing equations (4.1) and (4.6), with boundary conditions in (4.10), are non-linear, the analytic solution has not been obtained yet. Based on the scaling transformation discussed in section 4.1, it will be sufficient to consider $\kappa = 1$ case. For the boundary value problem of ODEs, the shooting method can be applied. Heartland and Hartley [10] give an approximate to the solution for $r \gg a$, which can be treated as a good initial guess for the shooting method. The approximation is obtained as follows.

Since $\frac{du}{dr} \to 0$, as r is sufficiently large, equation (4.1) can be approximated by

$$\frac{u'}{\sqrt{1 + (u')^2}} + \frac{ru''}{\left(\sqrt{1 + (u')^2}\right)^3} = ru$$

$$\Rightarrow \quad u'' + \frac{1}{r}u' - u = 0. \tag{4.11}$$

Equation (4.11) is the modified Bessel's equation and has the solution:

$$u(r) = CK_0(r) + \bar{C}I_0(r). \tag{4.12}$$

With $\lim\limits_{r \to \infty} u = 0$, $\bar{C}$ has to be zero since $I_0(r) \to \infty$ as $r \to \infty$. For large r, the solution can be approximated by

$$u(r) \approx CK_0(r), \tag{4.13}$$

where C is a constant. Since $K_0(10) \approx 10^{-5}$, $r \to r^* = 10$ is good enough as a boundary condition instead of $r \to \infty$.

The shooting method has the following algorithm:

58

1. Guess a small $C = c_0{}^2$, and define the initial condition $\left(u^*(\psi^*), r^*(\psi^*) \right) = \left(c_0 K_0(r^*), r^* \right)$, where $\psi^* = \arctan(u'(r^*))$.

2. Define a function $f(C; \psi^*, u^*, r^*) = r(\psi_0) - a$, where $r(\psi_0)$ can be obtained by integrating the system (4.6) with respect to ψ backwards to ψ_0.

3. Solve $f(C; \psi^*, u^*, r^*) = 0$ for C using fsolve such that $u = CK_0(r)$ gives the correct height u_{true} at $r = r^*$.

4. Based on the true values $\left(u_{true}, r^* \right)$ and good approximation $\psi^* = -\arctan(CK_1(r^*))$, we integrate the system (4.6) backwards with respect to ψ from ψ^* to ψ_0 and obtain the numerical solutions as follows:

$$\{u_i\}_{i=0}^N, \ \ \{r_i\}_{i=0}^N \ \text{and} \ \{\psi_i\}_{i=0}^N. \tag{4.14}$$

The Figure 4.3 shows the Shooting method algorithm. Moreover, pseudocode is provided in Appendix G, and the Figure 4.3 also shows our shooting method with $\gamma = \frac{\pi}{4}$, $r^* = 10$ and initial guess $c_0 = 10^{-2}$.
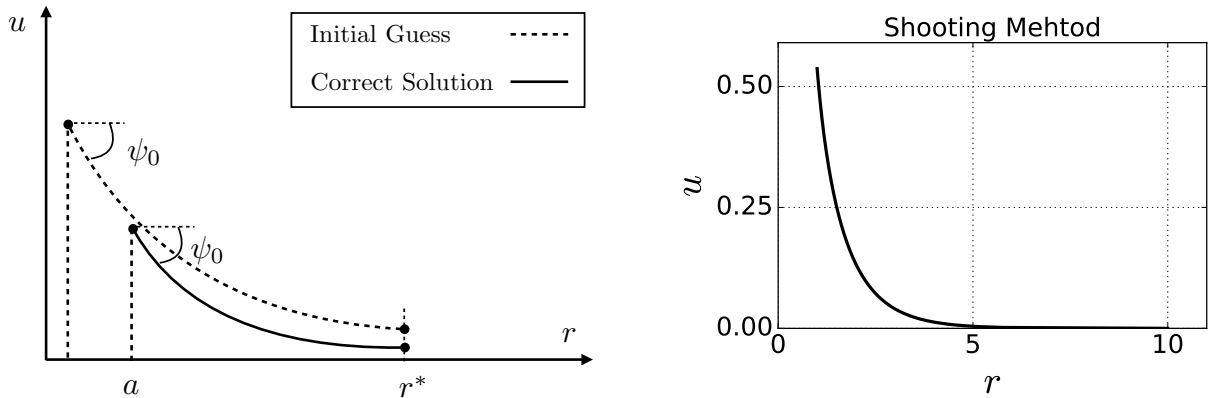
Figure 4.3: The shooting method algorithm and the fluid height $u(r)$.

---

[2]In practice, $c_0 = 10^{-2}$ is a good value for the initial guess.

4.2.2 Numerical Computation of $\hat{E}_T$

The shooting method gives the numerical solutions for $u(\psi)$ and $r(\psi)$, say,

$$\{u_i\}_{i=0}^N, \quad \{r_i\}_{i=0}^N \quad \text{and} \quad \{\psi_i\}_{i=0}^N. \tag{4.15}$$

We also discretize the height of centre $h \in [u_0 - a, u_0 + a]$: $\{h_i\}_0^N$. The density of the cylinder is ρ_s, the density of the liquid is ρ, and the density ratio α is define as $\alpha = \frac{\rho_s}{\rho}$, The acceleration due to gravity is g and acts in the downward direction. We introduce the characteristic energy $E_c = \pi\sigma a^2$ and dimensionless parameters: $\hat{h}_i = \frac{h_i}{a}$, $\hat{u}_i = \frac{u_i}{a}$, $\hat{r} = \frac{r}{a}$ and Bond number $\mathcal{B} = \kappa a^2$. We numerically compute the dimensionless total energy $\hat{E}_T$:

- The body potential energy is:

$$E_G = \rho_s \pi a^2 (2a) gh$$
$$\Rightarrow \quad E_{Gi} = E_c \mathcal{B}(2\alpha\hat{h}_i)$$
$$\Rightarrow \quad \hat{E}_{Gi} = 2\mathcal{B}\alpha\hat{h}_i. \tag{4.16}$$

- The wetting energy is:

$$E_W = -\cos\gamma\sigma|\Sigma|$$
$$\Rightarrow \quad E_{Wi} = -\cos\gamma\sigma\left[(2\pi a)(u_0 + a - h_i) + \pi a^2\right]$$
$$\Rightarrow \quad \hat{E}_{Wi} = -\cos\gamma\left[2(\hat{u}_0 - \hat{h}_i) + 3\right]. \tag{4.17}$$

- The surface tension energy is:

  As the height h varies, the shape of the fluid interface is unchanged, and E_σ can be computed through integrating ψ. The trapezoidal rule is applied on approximating the integration:

$$E_\sigma = \sigma \int_0^{2\pi} d\theta \int_a^\infty \left(\sqrt{1 + u_r^2} - 1\right) r\, dr$$
$$\Rightarrow \quad E_\sigma = 2\pi\sigma\left(\underbrace{\int_{\psi_0}^{\psi^*} S_\sigma(\psi; r, u)\, d\psi}_{(1)} + \underbrace{\int_{\psi^*}^0 S_\sigma(\psi; r, u)\, d\psi}_{(2)}\right)$$
$$\Rightarrow \quad \hat{E}_{\sigma i} \approx \left(\frac{\psi^* - \psi_0}{N}\right) \sum_{k=0}^{N-1} \left[\hat{S}_\sigma(\psi_k; r_k, u_k) + \hat{S}_\sigma(\psi_{k+1}; r_{k+1}, u_{k+1})\right], \quad (4.18)$$

where the integrands are $S_\sigma(\psi; r, u) = \left(\sqrt{1 + \tan^2 \psi} - 1 \right) \frac{r^2 \cos \psi}{ru - \sin \psi}$ and $\hat{S}_\sigma(\psi; r, u) = \left(\sqrt{1 + \tan^2 \psi} - 1 \right) \frac{\hat{r}^2 \cos \psi}{\mathcal{B} \hat{r} \hat{u} - \sin \psi}$. (2) can be approximated by $C \int_{r*}^{\infty} K_0(r) dr$, which is much smaller than the value of (1), so we can ignore it.

- The fluid potential energy is:

$$E_F = E_{F1} + E_{F2}$$

$$\Rightarrow E_F = \rho g \int_0^{2\pi} d\theta \int_a^{\infty} \frac{u^2}{2} r \, dr + \rho g \int_0^{2\pi} d\theta \int_0^a \frac{(a - h)^2}{2} r \, dr$$

$$\Rightarrow E_F = \pi \rho g \left(\underbrace{\int_a^{r*} u^2 r \, dr}_{(3)} + \underbrace{\int_{r*}^{\infty} u^2 r \, dr}_{(4)} \right) + \frac{1}{2} \pi \rho g a^2 (a - h)^2$$

$$\Rightarrow \hat{E}_{Fi} \approx \mathcal{B} \left(\frac{\hat{r}^* - 1}{2N} \right) \sum_{k=0}^{N-1} \left[(\hat{u}_k)^2 \hat{r} + (\hat{u}_{k+1})^2 \hat{r}_{k+1} \right]$$

$$+ \mathcal{B} \frac{(1 - \hat{h}_i)^2}{2}. \tag{4.19}$$

In addition, (4) can be approximated by $C^2 \int_{r*}^{\infty} \frac{K_0^2(r)}{2} r \, dr$, which is much smaller than the value of (3), so we can ignore it.

Thus, $\hat{E}_T$ has the expression:

$$\hat{E}_T = \hat{E}_G + \hat{E}_W + \hat{E}_\sigma + \hat{E}_F. \tag{4.20}$$

In Figure 4.4, we give an example of $\hat{E}_T$ vs h and $\hat{E}_T$ admits the minimum at $\hat{h} \approx -0.193$, thus it is stable.

In the analysis of total force F_T in vertical direction, we introduce the characteristic force $F_c = \pi \sigma a$. We can compute the dimensionless total force $\hat{F}_T$:

1. The gravitational force is:

$$
\begin{aligned}
F_G &= -\rho_m \pi a^2 (2a) g \\
&= -\pi \sigma (2\mathcal{B}\alpha) \\
\Rightarrow \hat{F}_G &= -2\mathcal{B}\alpha.
\end{aligned}
\tag{4.21}
$$

61
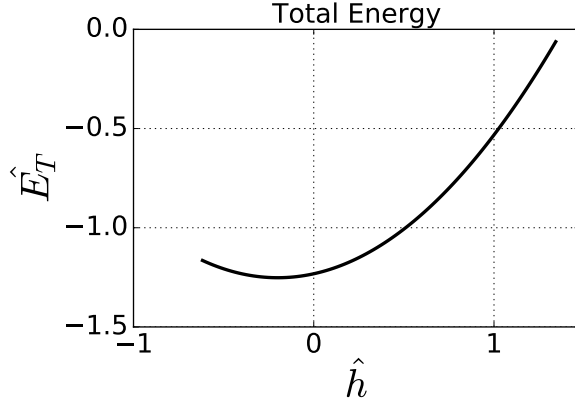
Figure 4.4: $\hat{E}_T$ vs h with parameters: $a = 1, \alpha = 0.1, \mathcal{B} = 1$ and $\gamma = \frac{\pi}{3}$.

2. The surface tension force: since σ can also be interpreted as force per length,

$$
\begin{aligned}
F_\sigma &= -\sigma \cos\gamma (2\pi a) \\
\Rightarrow \hat{F}_\sigma &= -2\cos\gamma.
\end{aligned}
\tag{4.22}
$$

3. The buoyant force: based on the discussion of the buoyant force in Appendix B,

$$
\begin{aligned}
F_B &= \rho g \pi a^2 (a - h) \\
\Rightarrow \hat{F}_B &= \mathcal{B}(1 - \hat{h}).
\end{aligned}
\tag{4.23}
$$

The dimensionless total force $\hat{F}_T$ in the vertical direction can be expressed as follows:

$$
\begin{aligned}
\hat{F}_T &= \hat{F}_G + \hat{F}_\sigma + \hat{F}_B \\
&= \mathcal{B}(1 - \hat{h} - 2\alpha) - 2\cos\gamma.
\end{aligned}
\tag{4.24}
$$

Moreover, $\frac{d\hat{E}_T}{d\hat{h}}$ has the analytic expression

$$
\frac{d\hat{E}_T}{d\hat{h}} = 2\cos\gamma - B(1 - \hat{h} - 2\alpha),
\tag{4.25}
$$

which leads to the relation $\hat{F}_T = -\frac{d\hat{E}_T}{d\hat{h}}$.

4.3 Discussion of the $3D$ Floating Ball

A challenging problem, the $3D$ floating ball, is introduced in this section. Since it is radially symmetric, the cross sectional configuration of the $3D$ floating ball is the same as the configuration of $2D$ cylinder case.
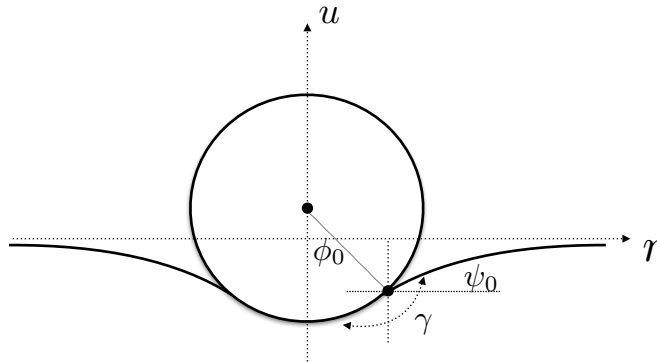
Figure 4.5: The cross sectional configuration of the $3D$ floating ball.

The shooting method can also be employed to obtain the fluid height. Differing from the one-to-one relation between h and ϕ_0 for the $2D$ floating cylinder, the relation of h and ϕ_0 is not monotonic in the $3D$ floating ball case (see Figure 4.6). Recall that the height h has the form:

$$h = a\cos\phi_0 + u_0, \tag{4.26}$$

where a is the radius of the ball, u_0 is the fluid height at the contact point, which can be computed by the shooting method.

The following example shows that the system admits two different configurations with the same $h = -1.3$ and contact angle $\gamma = \frac{\pi}{2}$.

The non-monotonic relation between h and ϕ_0 makes it more difficult to study the total energy E_T of the floating ball. The relation $-\frac{dE_T}{dh} = F_T$ has not been proved in floating ball case. We cannot give a convincing explanation of this unexpected result, and therefore, more study is expected for the floating ball problem.
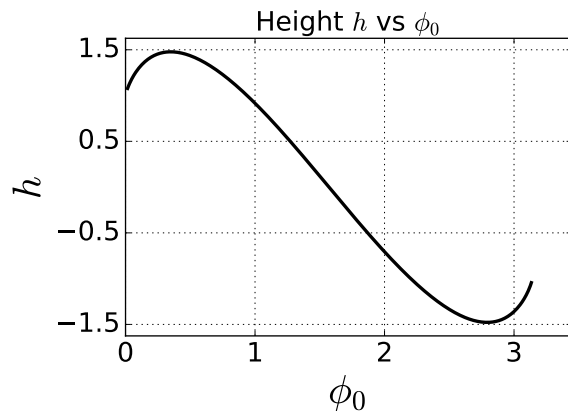
Figure 4.6: Non-monotonic relation of ϕ_0 and h, with parameters: $\mathcal{B} = 1$, $\gamma = \frac{\pi}{2}$ and $a = 1$.
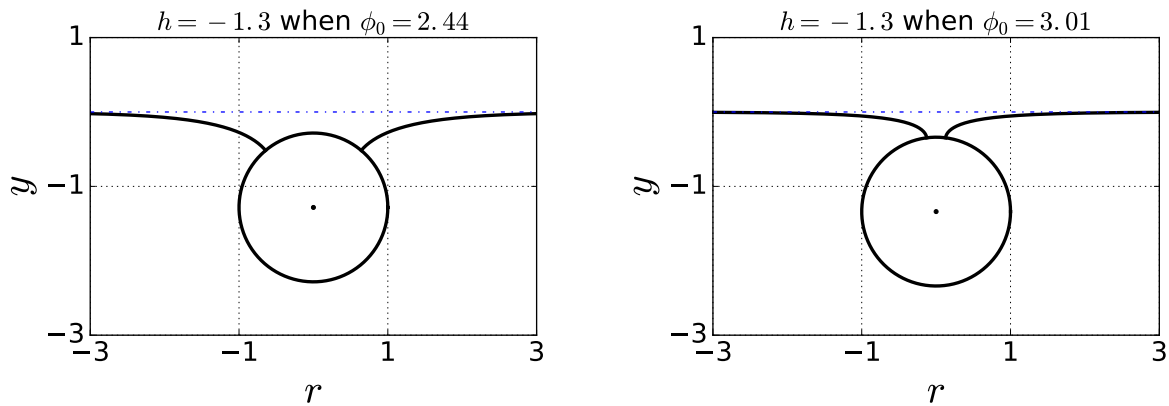
Figure 4.7: Two different configurations with same $h = -1.3$.

Chapter 5

Conclusions and Future Work

In this thesis, the floating configurations and their stability of both two-dimensional and three-dimensional objects on infinite reservoir are studied. The conclusions can be summarized as follows.

5.1 $2D$ Floating Cylinder Problem

The fluid height $u(\psi)$ and horizontal distance $x(\psi)$ can be analytically parametrized by the inclination angle ψ. With the geometric constraint $\psi_0 = \phi_0 + \gamma - \pi$ and the height h, which is defined as the displacement from the centre of the cylinder to the reference fluid level, the relative total energy E_T can be expressed only in terms of the wetting angle ϕ_0. Based on the one-to-one correspondence between h and ϕ_0, we investigate the relation between E_T and the vertical total force F_T, that is $-\frac{dE_T}{dh} = F_T$. The sign equivalence, $\operatorname{sign}(\frac{dE_T}{d\phi_0}) = \operatorname{sign}(F_T)$ and $\operatorname{sign}\left(\frac{d^2 E_T}{d\phi_0^2}(\bar{\phi}_0)\right) = \operatorname{sign}\left(\frac{dF_T}{d\phi_0}(\bar{\phi}_0)\right)$, gives a more convenient way to minimize E_T.

In the total force analysis, we assume the surface tension force F_σ exists only along the fluid interface, which contradicts Young's diagram. The result is consistent with Finn's assertion in [2]. Archimedes' principle only holds when the fluid surface is flat. With surface tension, the buoyant force F_B can be approached by the Divergence Theorem, which gives an analogue to Archimedes' principle.

In the analysis of the numbers of equilibria and their stability behaviour, we introduce two dimensionless parameters $\mathcal{A} = \frac{m}{a^2 \rho}$ and $\mathcal{C} = \sqrt{\kappa}a$. The numbers of equilibria can

be shown on $\mathcal{AC}$ plane. In Section 2.12, several examples with typical values of γ are discussed and the boundary curves between the regions with different numbers of equilibria are obtained numerically.

The $\hat{F}_T$ curve depends on ϕ_0, $\mathcal{A}$, $\mathcal{C}$ and γ. We summarize the numbers and the stability behaviour of equilibrium points in the following cases:

1. When $\gamma \geq \frac{\pi}{2}$, $\hat{F}_T$ admits at most two equilibrium points $\bar{\phi}_{01}$ and $\bar{\phi}_{02}$, the smaller equilibrium point $\bar{\phi}_{01}$ is stable and the larger equilibrium point $\bar{\phi}_{02}$ is unstable. In addition, if $\hat{F}_T$ admits only one equilibrium point $\bar{\phi}_0$ and $\frac{d\hat{F}_T}{d\phi_0}(\bar{\phi}_0) > 0$, it is stable. If $\frac{d\hat{F}_T}{d\phi_0}(\bar{\phi}_0) = 0$, it is unstable.

2. When $\gamma < \frac{\pi}{2}$, if $\frac{d\hat{F}_T}{d\phi_0}(\pi) < 0$, $\hat{F}_T$ behaves the same as $\hat{F}_T$ with $\gamma \geq \frac{\pi}{2}$. If $\frac{d\hat{F}_T}{d\phi_0}(\pi) > 0$, $\hat{F}_T$ admits at most one equilibrium point $\bar{\phi}_0$ and therefore, it is stable except $\bar{\phi}_0 = \pi$.

Moreover, we discuss the limitation of the model. When $\gamma = \frac{\pi}{2}$, there is always no intersection of the fluid interfaces, and when $\gamma \neq \frac{\pi}{2}$, intersection may happen. We give two typical Figures to illustrate the intersection region with $\gamma = \frac{\pi}{4}$ and $\gamma = \frac{3\pi}{4}$ (see Figure 2.21). Moreover, the stable equilibrium point never lies in the intersection region, while the unstable equilibrium point may lie in the intersection region.

5.2 $2D$ Floating Square with Rotation

The no surface tension case is first considered in the $2D$ floating square with rotation. We introduce the height of centre h (same as h in Chapter 2) and clock-wise rotational angle from the vertical axis θ. We define the solid/liquid density ratio $\alpha = \frac{\rho_s}{\rho} \in (0, \frac{1}{2}]$, which results in two different configurations: one corner immersed and two corners immersed. Since the fluid interface is flat, Archimedes' principle gives the height in equilibrium h^*. The relative total energy E_T in force balance depends only on θ. We summarize the stability based on minimizing $E_T(\theta)$ as follows:

1. When two corners are immersed, E_T admits two critical points $\theta^* = 0$ and $\theta^* = \arccos\left(\frac{1}{\sqrt{12\alpha - 12\alpha^2 - 1}}\right)$. If $\theta^* = 0$, θ^* is stable if $0 < \alpha \leq \frac{1}{2} - \frac{1}{2\sqrt{3}}$ and θ^* is unstable if $\frac{1}{2} - \frac{1}{2\sqrt{3}} < \alpha \leq \frac{1}{2}$. If $\theta^* = \arccos\left(\frac{1}{\sqrt{12\alpha - 12\alpha^2 - 1}}\right)$, α must belongs to $\left[\frac{1}{2} - \frac{1}{\sqrt{6}}, \frac{1}{4}\right]$ and θ^* is stable.

2. When one corner is immersed, E_T admits two critical points $\theta^* = \frac{\pi}{4}$ and $\theta^* = \frac{1}{2}\arcsin\left(\frac{16\alpha}{9-16\alpha}\right)$. If $\theta^* = \frac{\pi}{4}$, θ^* is stable if $\frac{9}{32} \le \alpha \le \frac{1}{2}$ and θ^* is unstable if $0 < \alpha < \frac{9}{32}$. If $\theta^* = \frac{1}{2}\arcsin\left(\frac{16\alpha}{9-16\alpha}\right)$, α belongs to $\left[\frac{1}{4}, \frac{9}{32}\right]$ and θ^* is stable.

With surface tension, it is difficult to analyze all cases and only $\gamma = \frac{\pi}{4}$ is considered. We introduce the characteristic energy $E_{square} = \rho_s a^3 g$ and the dimensionless variable $\mathcal{S} = \frac{\sigma}{\sqrt{\kappa}\rho_s a^3 g}$. The dimensionless $\hat{E}_T$ depends on two variable $\hat{h}$ and θ. Through the numerical computation, we give two typical examples:

1. When $\mathcal{S} = 0.1$, $(h^*, \theta^*) = \left(\frac{1}{2} - \frac{10 + 2\sqrt{2}\sqrt[3]{5}}{40}, 0\right)$ is a critical point, which is a saddle point; thus it is unstable by the second derivative test.

2. When $\mathcal{S} = 10$, there is no critical point for $\hat{h} \in [-1, 1]$, $\phi_0 \in [0, \pi]$.

5.3 $3D$ Floating Vertical Cylinder and Ball

Two axisymmetric examples are discussed in the $3D$ floating objects section, one is a vertical cylinder allowed to move only in the vertical direction, the other is a floating ball. With scaling transformation $u(r) = \frac{1}{\sqrt{\kappa}}w(\sqrt{\kappa}r)$, the solutions of the capillary equation (4.1) can be obtained based on the $\kappa = 1$ case. The shooting method is applied to obtain the parametrized solutions of the fluid height $u(\psi)$ and the radial distance $r(\psi)$.

In the vertical cylinder case, the shape of the fluid interface is independent of the vertical position of the cylinder. With $\alpha = 0.1$, $a = 1$ and $\gamma = \frac{\pi}{3}$, the minimum $\hat{E}_T$ occurs at $\hat{h}^* \approx -0.193$, which is a stable equilibrium. Moreover, the relation $-\frac{d\hat{E}_T}{d\hat{h}} = \hat{F}_T$ holds in general.

The floating ball case is different from the $2D$ cylinder case. The non-monotonic relation between ϕ_0 and h causes difficulties. We give an example with data $a = 1$, $\kappa = 1$ and $\gamma = \frac{\pi}{2}$, and give two configurations (one is $\phi_0 = 2.44$ and the other is $\phi_0 = 3.01$) with the same height $h = -1.3$.

5.4 Future Work

Several aspects can be considered for future work:

1. More numerical analysis in looking forward to the study of the numbers and stability of the equilibrium points in both $2D$ and $3D$ models.

2. In the $2D$ case, the floating cylinder with polygonal cross-section and surface tension present is also worth studying.

3. For the $3D$ floating ball, $F_T = 0$ and minimizing E_T seem to give different results. We can not give a convincing explanation for the unexpected results, and more study is required.

APPENDICES

Appendix A

E_T of the $2D$ Cylinder

In this part, the detailed derivation of both surface tension energy E_σ and the fluid potential energy E_F are given when the interface is a graph and when it is a non-graph.

A.1   Surface Tension Energy E_σ

In section 2.3, the surface energy E_σ is defined of the form:

$$E_\sigma = 2\sigma \lim_{x_1 \to \infty} \left[\int_{x_0}^{x_1} \sqrt{1 + \left(\frac{du}{dx}\right)^2} \, dx - \int_0^{x_1} dx \right]. \tag{A.1}$$
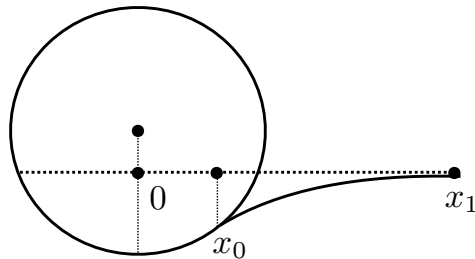
Figure A.1: Computation of relative surface tension energy.

- When the fluid interface is a graph, the inclination angle ψ ranges from $-\frac{\pi}{2}$ to $\frac{\pi}{2}$, from Equation (2.2), the chain rule gives $\frac{d\psi}{dx} = \frac{\kappa u}{\cos\psi} = -2\frac{\sqrt{\kappa}\sin\frac{\psi}{2}}{\cos\psi}$. With inclination angle $\tan\psi = \frac{du}{dx}$, E_σ can be achieved.

$$
\begin{aligned}
E_\sigma &= 2\sigma \lim_{x_1\to\infty} \left[\int_{x_0}^{x_1} \sqrt{1 + \left(\frac{du}{dx}\right)^2}\, dx - \int_0^{x_1} dx \right] \\
&= 2\sigma \lim_{x_1\to\infty} \left[\int_{x_0}^{x_1} \sqrt{1 + \left(\frac{du}{dx}\right)^2}\, dx - (x_1 - x_0) - a\sin\phi_0 \right] \\
&= 2\sigma \lim_{x_1\to\infty} \left[\int_{x_0}^{x_1} \sqrt{1 + \left(\frac{du}{dx}\right)^2} - 1\, dx \right] - 2\sigma a\sin\phi_0 \\
&= 2\sigma \lim_{\psi_1\to 0} \left\{ \int_{\psi_0}^{\psi_1} \left(\sqrt{1 + \tan^2\psi} - 1 \right) \left(\frac{-\cos\psi}{2\sqrt{\kappa}\sin\frac{\psi}{2}} \right) d\psi \right\} - 2\sigma a\sin\phi_0 \\
&= 2\sigma \lim_{\psi_1\to 0} \left\{ -\frac{1}{2\sqrt{\kappa}} \int_{\psi_0}^{\psi_1} \left(\frac{1}{\sin\frac{\psi}{2}} - \frac{\cos\psi}{\sin\frac{\psi}{2}} \right) d\psi \right\} - 2\sigma a\sin\phi_0 \\
&= 4\frac{\sigma}{\sqrt{\kappa}} \left(1 - \cos\frac{\psi_0}{2} \right) - 2\sigma a\sin\phi_0.
\end{aligned}
$$

- When the fluid interface is not a graph, we have to assume that there is no intersection of the fluid interfaces, i.e. the fluid interfaces on either side of the cylinder do not intersect. In addition, the inclination angle $\psi \in [-\pi, \pi]$.

- Case 1: $\psi_0 > 0$,

$$
\begin{aligned}
E_\sigma &= 2\sigma \lim_{x_1 \to \infty} \left[\int_{x_0}^{x_1} \sqrt{1 + \left(\frac{du}{dx}\right)^2}\, dx - \int_0^{x_1} dx \right] \\
&= 2\sigma \lim_{\psi_1 \to 0} \left[\int_{\psi_1}^{\psi_0} \sqrt{\left(\frac{dx}{d\psi}\right)^2 + \left(\frac{du}{d\psi}\right)^2}\, d\psi - \int_0^{x_1} dx \right] \\
&= 2\sigma \lim_{\psi_1 \to 0} \left[\int_{\psi_1}^{\psi_0} \frac{1}{\sqrt{\kappa}} \sqrt{\frac{\cos^2 \psi}{4 \sin^2 \frac{\psi}{2}} + \cos^2 \frac{\psi}{2}}\, d\psi - \int_{\psi_0}^{\psi_1} \left(-\frac{1}{2\sqrt{\kappa}}\right) \frac{\cos \psi}{\sin \frac{\psi}{2}}\, d\psi \right] - 2\sigma a \sin \phi_0 \\
&= 2\sigma \left(\frac{1}{2\sqrt{\kappa}}\right) \lim_{\psi_1 \to 0} \int_{\psi_1}^{\psi_0} \left\{ \frac{1}{\sin \frac{\psi}{2}} - \frac{\cos \psi}{\sin \frac{\psi}{2}} \right\} d\psi - 2\sigma a \sin \phi_0 \\
&= 4 \frac{\sigma}{\sqrt{\kappa}} \left(1 - \cos \frac{\psi_0}{2}\right) - 2\sigma a \sin \phi_0.
\end{aligned}
$$

- Case 2: $\psi_0 < 0$,

$$
\begin{aligned}
E_\sigma &= 2\sigma \lim_{x_1 \to \infty} \left[\int_{x_0}^{x_1} \sqrt{1 + \left(\frac{du}{dx}\right)^2}\, dx - \int_0^{x_1} dx \right] \\
&= 2\sigma \lim_{\psi_1 \to 0} \left[\int_{\psi_1}^{\psi_0} \sqrt{\left(\frac{dx}{d\psi}\right)^2 + \left(\frac{du}{d\psi}\right)^2}\, d\psi - \int_0^{x_1} dx \right] \\
&= 2\sigma \lim_{\psi_1 \to 0} \left[\int_{\psi_1}^{\psi_0} \frac{1}{\sqrt{\kappa}} \sqrt{\frac{\cos^2 \psi}{4 \sin^2 \frac{\psi}{2}} + \cos^2 \frac{\psi}{2}}\, d\psi - \int_{\psi_0}^{\psi_1} \left(-\frac{1}{2\sqrt{\kappa}}\right) \frac{\cos \psi}{\sin \frac{\psi}{2}}\, d\psi \right] - 2\sigma a \sin \phi_0 \\
&= 2\sigma \left(\frac{1}{2\sqrt{\kappa}}\right) \lim_{\psi_1 \to 0} \int_{\psi_0}^{\psi_1} \left\{ -\frac{1}{\sin \frac{\psi}{2}} + \frac{\cos \psi}{\sin \frac{\psi}{2}} \right\} d\psi - 2\sigma a \sin \phi_0 \\
&= 4 \frac{\sigma}{\sqrt{\kappa}} \left(1 - \cos \frac{\psi_0}{2}\right) - 2\sigma a \sin \phi_0.
\end{aligned}
$$

In summary, we have the surface energy:

$$
E_\sigma = 4 \frac{\sigma}{\sqrt{\kappa}} \left(1 - \cos \frac{\psi_0}{2}\right) - 2\sigma a \sin \phi_0. \tag{A.2}
$$

A.2   Fluid Potential Energy E_F

In section 2.3, we break the fluid potential energy E_F into two parts.

$$E_F = \underbrace{2\rho g \int_0^{x_0} \frac{y^2}{2} dx}_{E_{F1}} + \underbrace{2\rho g \int_{x_0}^{\infty} \frac{u^2}{2} dx}_{E_{F2}} . \tag{A.3}$$

Where y is the vertical height of the bottom of the cylinder and u is the fluid height.

$$u(\psi) = -\frac{2}{\sqrt{\kappa}} \sin \frac{\psi}{2}. \tag{A.4}$$

$$y = a \cos \phi - h. \tag{A.5}$$
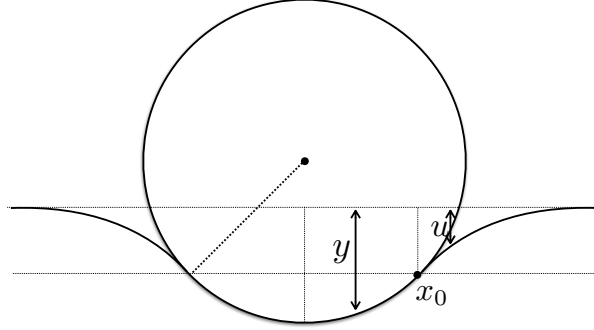
Figure A.2: Computation of relative potential energy.

$$\begin{aligned}
E_{F_2} &= 2\rho g \int_{x_0}^{\infty} \frac{u^2}{2} dx \\
&= \rho g \int_{\psi_0}^{0} \left(-\frac{2}{\sqrt{\kappa}} \sin \frac{\psi}{2} \right)^2 \left(-\frac{1}{2\sqrt{\kappa}} \frac{\cos \psi}{\sin \frac{\psi}{2}} \right) d\psi \\
&= -\frac{2\sigma}{\sqrt{\kappa}} \int_{\psi_0}^{0} \sin \frac{\psi}{2} \cos \psi d\psi \\
&= -\frac{2\sigma}{\sqrt{\kappa}} \left(\frac{2}{3} - \cos \frac{\psi_0}{2} + \frac{1}{3} \cos \frac{3\psi_0}{2} \right).
\end{aligned}$$

73

With the identity $\cos \frac{3\psi_0}{2} = \cos \frac{\psi_0}{2}(2\cos \psi_0 - 1)$,

$$E_{F_2} = -\frac{4\sigma}{3\sqrt{\kappa}}\left(1 - 2\cos \frac{\psi_0}{2} + \cos \frac{\psi_0}{2}\cos \psi_0\right). \tag{A.6}$$

For E_{F1},

$$
\begin{aligned}
E_{F_1} &= 2\rho g \int_0^{x_0} \frac{y^2}{2}dx \\
&= \rho g \int_0^{\phi_0} (a\cos \phi - h)^2 a\cos \phi d\phi \\
&= \rho g \int_0^{\phi_0} \left(a\cos \phi - a\cos \phi_0 + \frac{2}{\sqrt{\kappa}}\sin \frac{\psi_0}{2}\right)^2 a\cos \phi d\phi \\
&= \frac{1}{12}\rho g a^3 \sin 3\phi_0 - \rho g a^3 \phi_0 \cos \phi_0 + \frac{3}{4}\rho g a^3 \sin \phi_0 - a^2\sqrt{\sigma \rho g}\sin \frac{\psi_0}{2}\sin 2\phi_0 \\
&\quad + 2a^2\sqrt{\sigma \rho g}\phi_0 \sin \frac{\psi_0}{2} + 4\sigma a \sin^2 \frac{\psi_0}{2}\sin \phi_0.
\end{aligned}
$$
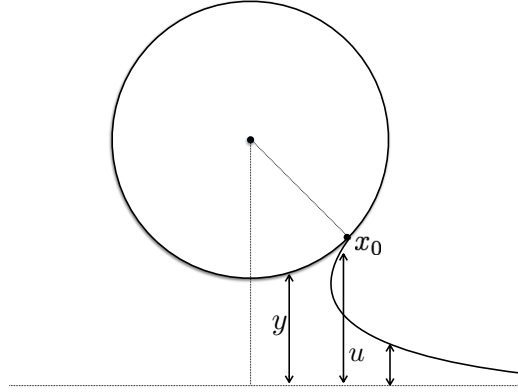
Figure A.3: A non-graph case.

If the fluid interface is not a graph (Figure A.3), the formula (A.3) also works. But in addition, we have to assume that there is no intersection of the fluid interfaces. The fluid

potential energy E_F has the form:

$$E_F = E_{F_1} + E_{F_2} = -\frac{4\sigma}{3\sqrt{\kappa}}\left(1 - 2\cos\frac{\psi_0}{2} + \cos\frac{\psi_0}{2}\cos\psi_0\right)$$
$$+\frac{1}{12}\rho g a^3 \sin 3\phi_0 - \rho g a^3 \phi_0 \cos\phi_0 + \frac{3}{4}\rho g a^3 \sin\phi_0 - a^2\sqrt{\sigma\rho g}\sin\frac{\psi_0}{2}\sin 2\phi_0$$
$$+2a^2\sqrt{\sigma\rho g}\phi_0 \sin\frac{\psi_0}{2} + 4\sigma a \sin^2\frac{\psi_0}{2}\sin\phi_0.$$

Appendix B

Analysis of the Buoyant Force

In this part, we will examine how Archimedes' principle works in no surface tension case and another way to approach buoyant force using the Divergence theorem.

From section 2.5, the buoyant force has the form:

$$F_B = \hat{k} \cdot \int_\Sigma \vec{F} ds. \tag{B.1}$$

Where the centripetal component pressure $\vec{F} = \rho g y \hat{n}_c$, $\hat{n}_c$ is the outer unit normal of the cylinder, $\hat{k}$ is the unit vertical vector pointing upward and Σ is the wetted region of the cylinder.
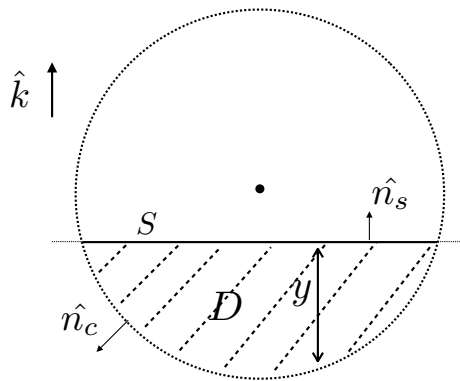
Figure B.1: Archimedes' principle.

- If no surface tension exists (as shown in Figure B.1),

$$
\begin{aligned}
F_B &= \hat{k} \cdot \int_{\Sigma} \vec{F} ds \\
&= \int_{\Sigma} \left(\rho g y \hat{k} \right) \cdot \hat{n} ds + \underbrace{\int_{S} \left(\rho g y \hat{k} \right) \cdot \hat{n} ds}_{=0} \\
&= \int_{\Sigma \cup S} \left(\rho g y \hat{k} \right) \cdot \hat{n} ds \\
&= \int_{D} \rho g dA = \rho g \left| D \right|.
\end{aligned}
$$

On the boundary S, $\int_{S} (\rho g \hat{k}) \cdot \hat{n} ds = 0$ since $y = 0$ on free fluid level. $\partial D = \Sigma \cup S$ and $\hat{n} \in \{\hat{n}_c, \hat{n}_s\}$ is the outer normal of ∂D. When the Divergence theorem is applied, $F_B = \rho g |D|$ which is consistent with Archimedes' principle.

- If surface tension is present (as shown in Figure B.2),
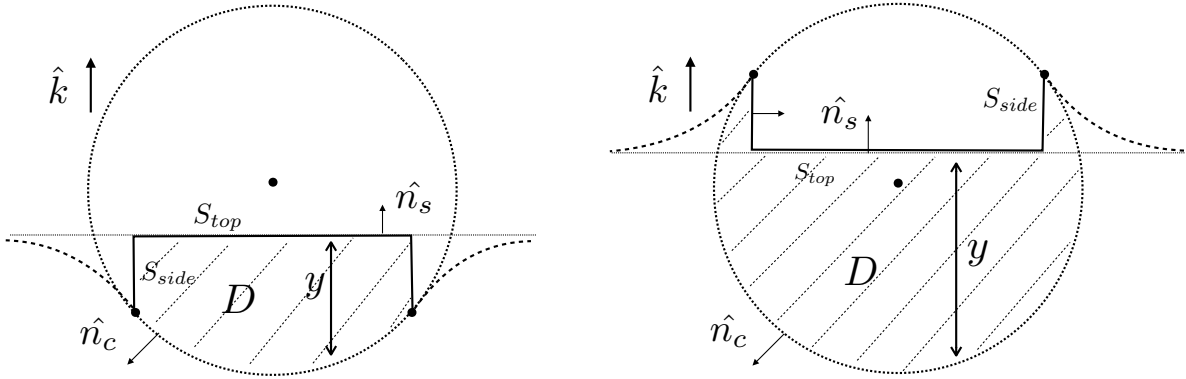
Figure B.2: The buoyant force when surface tension is present.

$$
\begin{aligned}
F_B &= \hat{k} \cdot \int_{\Sigma} \vec{F} ds \\
&= \int_{\Sigma} \left(\rho g y \hat{k} \right) \cdot \hat{n}_c ds + \underbrace{\int_{S_{top}} \left(\rho g y \hat{k} \right) \cdot \hat{n}_s ds}_{=0} + \underbrace{\int_{S_{side}} \left(\rho g y \hat{k} \right) \cdot \hat{n}_s ds}_{=0} \\
&= \int_{\Sigma \cup S_{top} \cup S_{side}} \left(\rho g y \hat{k} \right) \cdot \hat{n} ds \\
&= \int_D \rho g \, dA = \rho g |D|.
\end{aligned}
$$

On the boundary S_{top}, $\int_S \left(\rho g \hat{k} \right) \cdot \hat{n}_s ds = 0$ since $y = 0$ on free fluid level and $\int_{S_{side}} \left(\rho g y \hat{k} \right) \cdot \hat{n}_s ds = 0$ since $\hat{k}$ and $\hat{n}_s$ are orthogonal. $\partial D = \Sigma \cup S_{top} \cup S_{side}$ and $\hat{n} \in \{ \hat{n}_c, \hat{n}_s \}$ is the outer normal of ∂D. When the Divergence theorem is applied, $F_B = \rho g |D|$, This is not consistent with Archimedes' principle anymore. The enclosed area is no longer the immersed region due to the presence of surface tension.

Appendix C

Relation between $-\frac{dE_T}{dh}$ and F_T

Firstly, we take derivative of E_T in terms of ϕ_0,

$$
\begin{aligned}
\frac{dE_T}{d\phi_0}(\phi_0) &= -mga\sin\phi_0 - mg\sqrt{\frac{\sigma}{\rho g}}\sin\left(\frac{\phi_0 + \gamma}{2}\right) \\
&\quad - 2\sigma a \sin\phi_0 \sin(\phi_0 + \gamma) - 2\sigma\sqrt{\frac{\sigma}{\rho g}}\sin(\phi_0 + \gamma)\sin\left(\frac{\phi_0 + \gamma}{2}\right) \\
&\quad - 4\sigma a \sin\left(\frac{\phi_0 + \gamma}{2}\right)\cos\left(\frac{\phi_0 + \gamma}{2}\right)\sin\phi_0 - 4a^2\sqrt{\sigma\rho g}\sin^2\phi_0 \cos\left(\frac{\phi_0 + \gamma}{2}\right) \\
&\quad - \frac{1}{2}\rho g a^3 \sin\phi_0 \sin 2\phi_0 - \frac{1}{2}a^2\sqrt{\sigma\rho g}\sin\left(\frac{\phi_0 + \gamma}{2}\right)\sin 2\phi_0 \\
&\quad + \rho g a^3 \phi_0 \sin\phi_0 + \sqrt{\sigma\rho g}a^2\phi_0 \sin\left(\frac{\phi_0 + \gamma}{2}\right).
\end{aligned}
$$

After arranging the terms, we factor out the common term:

$$
a\sin\phi_0 + \sqrt{\frac{\sigma}{\rho g}}\sin\left(\frac{\phi_0 + \gamma}{2}\right). \tag{C.1}
$$

$$\frac{dE_T}{d\phi_0}(\phi_0) = -mg\left\{ a\sin\phi_0 + \sqrt{\frac{\sigma}{\rho g}}\sin\left(\frac{\phi_0+\gamma}{2}\right) \right\}$$

$$-2\sigma\sin(\phi_0+\gamma)\left\{ a\sin\phi_0 + \sqrt{\frac{\sigma}{\rho g}}\sin\left(\frac{\phi_0+\gamma}{2}\right) \right\}$$

$$-4a\sqrt{\sigma\rho g}\cos\left(\frac{\phi_0+\gamma}{2}\right)\sin\phi_0\left\{ a\sin\phi_0 + \sqrt{\frac{\sigma}{\rho g}}\sin\left(\frac{\phi_0+\gamma}{2}\right) \right\}$$

$$-\frac{1}{2}\rho g a^2 \sin 2\phi_0\left\{ a\sin\phi_0 + \sqrt{\frac{\sigma}{\rho g}}\sin\left(\frac{\phi_0+\gamma}{2}\right) \right\}$$

$$+\rho g a^2 \phi_0\left\{ a\sin\phi_0 + \sqrt{\frac{\sigma}{\rho g}}\sin\left(\frac{\phi_0+\gamma}{2}\right) \right\}.$$

When the chain rule is applied, we multiple one more term $\frac{d\phi_0}{dh}$:

$$-\frac{dE_T}{d\phi_0}\frac{d\phi_0}{dh} = -\left\{ -mg - 2\sigma\sin(\phi_0+\gamma) - 4a\sqrt{\sigma\rho g}\cos\left(\frac{\phi_0+\gamma}{2}\right)\sin\phi_0 \right.$$

$$\left. -\frac{1}{2}\rho g a^2 \sin 2\phi_0 + \rho g a^2\phi_0 \right\}\left\{ a\sin\phi_0 + \sqrt{\frac{\sigma}{\rho g}}\sin\left(\frac{\phi_0+\gamma}{2}\right) \right\}$$

$$\left\{ -\frac{1}{a\sin\phi_0 + \sqrt{\frac{\sigma}{\rho g}}\sin(\frac{\phi_0+\gamma}{2})} \right\}$$

$$= -mg - 2\sigma\sin(\phi_0+\gamma) - 4a\sqrt{\sigma\rho g}\cos\left(\frac{\phi_0+\gamma}{2}\right)\sin\phi_0$$

$$-\frac{1}{2}\rho g a^2 \sin 2\phi_0 + \rho g a^2\phi_0$$

$$= F_T.$$

Therefore, we find the relation between $-\frac{dE_T}{dh}$ and the vertical total force F_T:

$$-\frac{dE_T}{dh} = F_T. \tag{C.2}$$

Appendix D

Asymptotic Series of ϕ_0^* and $\mathcal{A}^*$

D.1 As $\mathcal{C} \to 0$

Consider the regular asymptotic series $\phi_0^* = \pi + a_1\mathcal{C} + a_2\mathcal{C}^2 + \dots$ and plug the series into $\frac{d\hat{F}_T}{d\phi_0}(\phi_0^*) = 0$.

$$
\frac{d\hat{F}_T}{d\phi_0}(\phi_0^*) = \sigma \left[-\frac{\sqrt{2}\mathcal{C}}{2} \cos \frac{\phi_0^*}{2} - \frac{\sqrt{2}\mathcal{C}}{2} \sin \frac{\phi_0^*}{2} + 2\sin \phi_0^* - \frac{3\sqrt{2}\mathcal{C}}{2} \cos \frac{3\phi_0^*}{2} \right.
$$
$$
\left. + \frac{3\sqrt{2}\mathcal{C}}{2} \sin \frac{3\phi_0^*}{2} - \mathcal{C}^2 \cos 2\phi_0^* + \mathcal{C}^2 \right] = 0.
$$

$\Rightarrow$

$$
-\frac{\sqrt{2}}{2}\mathcal{C} \cos \left[\frac{1}{2}(\pi + a_1\mathcal{C} + a_2\mathcal{C}^2 + \dots) \right] - \frac{\sqrt{2}}{2}\mathcal{C} \sin \left[\frac{1}{2}(\pi + a_1\mathcal{C} + a_2\mathcal{C}^2 + \dots) \right]
$$
$$
+ 2\sin \left[\pi + a_1\mathcal{C} + a_2\mathcal{C}^2 + \dots \right] - \frac{3\sqrt{2}}{2}\mathcal{C} \cos \left[\frac{3}{2}(\pi + a_1\mathcal{C} + a_2\mathcal{C}^2 + \dots) \right]
$$
$$
+ \frac{3\sqrt{2}}{2}\mathcal{C} \sin \left[\frac{3}{2}(\pi + a_1\mathcal{C} + a_2\mathcal{C}^2 + \dots) \right] - \mathcal{C}^2 \cos \left[2(\pi + a_1\mathcal{C} + a_2\mathcal{C}^2 + \dots) \right] + \mathcal{C}^2 = 0.
$$

$\Rightarrow$

$$\frac{\sqrt{2}}{2}\mathcal{C}\sin\left[\frac{1}{2}(a_1\mathcal{C} + a_2\mathcal{C}^2 + ...)\right] - \frac{\sqrt{2}}{2}\mathcal{C}\cos\left[\frac{1}{2}(a_1\mathcal{C} + a_2\mathcal{C}^2 + ...)\right]$$

$$-2\sin\left[a_1\mathcal{C} + a_2\mathcal{C}^2 + ...\right] - \frac{3\sqrt{2}}{2}\mathcal{C}\sin\left[\frac{3}{2}(a_1\mathcal{C} + a_2\mathcal{C}^2 + ...)\right]$$

$$-\frac{3\sqrt{2}}{2}\mathcal{C}\cos\left[\frac{3}{2}(a_1\mathcal{C} + a_2\mathcal{C}^2 + ...)\right] - \mathcal{C}^2\cos\left[2(a_1\mathcal{C} + a_2\mathcal{C}^2 + ...)\right] + \mathcal{C}^2 = 0.$$

We consider the power series expansions for Sine and Cosine at 0.

$$\cos(x) = 1 - \frac{x^2}{2} + \frac{x^4}{24} + ...$$

$$\sin(x) = x - \frac{x^3}{6} + ...$$

Let $P = a_1\mathcal{C} + a_2\mathcal{C}^2 + ...$

$$\frac{\sqrt{2}}{2}\mathcal{C}\left[\frac{1}{2}P - \frac{1}{6}(\frac{1}{2}P)^3 + ...\right] - \frac{\sqrt{2}}{2}\mathcal{C}\left[1 - \frac{1}{2}(\frac{1}{2}P)^2 + \frac{1}{24}(\frac{1}{2}P)^4 + ...\right] - 2\left[P - \frac{1}{6}P^3 + ...\right]$$

$$-\frac{3\sqrt{2}}{2}\mathcal{C}\left[\frac{3}{2}P - \frac{1}{6}(\frac{3}{2}P)^3 + ...\right] - \frac{3\sqrt{2}}{2}\mathcal{C}\left[1 - \frac{1}{2}(\frac{3}{2}P)^2 + \frac{1}{24}(\frac{3}{2}P)^4 + ...\right]$$

$$-\mathcal{C}^2\left[1 - \frac{1}{2}(2P)^2 + \frac{1}{24}(2P)^4 + ...\right] + \mathcal{C}^2 = 0.$$

We sort each term and obtain:

$\mathcal{O}(1) : 0;$

$\mathcal{O}(\mathcal{C}) : -2\sqrt{2} - 2a_1 = 0 \quad \rightarrow \quad a_1 = -\sqrt{2};$

$\mathcal{O}(\mathcal{C}^2) : -2\sqrt{2}a_1 - 2a_2 = 0 \quad \rightarrow \quad a_2 = 2;$

$\mathcal{O}(\mathcal{C}^3) : -2\sqrt{2}a_2 + \frac{7}{4}\sqrt{2}a_1^2 - 2a_3 + \frac{1}{3}a_1^3 = 0 \quad \rightarrow \quad a_3 = -\frac{7}{12}\sqrt{2};$

82

So $\phi_0^* = \pi - \sqrt{2}\mathcal{C} + 2\mathcal{C}^2 - \frac{7}{12}\sqrt{2}\mathcal{C}^3 + \mathcal{O}(\mathcal{C}^4)$ as $\mathcal{C} \to 0$.

As $\mathcal{C} \to 0$,

$$\phi_0^* = \pi - \sqrt{2}\mathcal{C} + 2\mathcal{C}^2 - \frac{7}{12}\sqrt{2}\mathcal{C}^3 + \mathcal{O}(\mathcal{C}^4). \tag{D.1}$$

We substitute ϕ_0^* in (D.1) into $\hat{F}_T = 0$ to get $\mathcal{A}^*$, where $\mathcal{A}^* = \frac{b_0}{\mathcal{C}^2} + \frac{b_1}{\mathcal{C}} + b_2 + b_3\mathcal{C} + b_4\mathcal{C}^2 + ...$

$\mathcal{O}(1) : -b_0 + 2 = 0 \quad \to \quad b_0 = 2;$

$\mathcal{O}(\mathcal{C}) : -b_1 = 0 \quad \to \quad b_1 = 0;$

$\mathcal{O}(\mathcal{C}^2) : -b_2 + 2 + \pi = 0 \quad \to \quad b_2 = 2 + \pi;$

$\mathcal{O}(\mathcal{C}^3) : -b_3 - 2\sqrt{2} = 0 \quad \to \quad b_3 = -2\sqrt{2};$

$\mathcal{O}(\mathcal{C}^4) : -b_4 + 2 = 0 \quad \to \quad b_4 = 2;$

Therefore $\mathcal{A}^* = \frac{2}{\mathcal{C}^2} + 2 + \pi - 2\sqrt{2}\mathcal{C} + \mathcal{O}(\mathcal{C}^2)$ as $\mathcal{C} \to 0$.

In summary, as $\mathcal{C} \to 0$,

$$\mathcal{A}^* = \frac{2}{\mathcal{C}^2} + 2 + \pi - 2\sqrt{2}\mathcal{C} + \mathcal{O}(\mathcal{C}^2).$$
$$\phi_0^* = \pi - \sqrt{2}\mathcal{C} + 2\mathcal{C}^2 - \frac{7}{12}\sqrt{2}\mathcal{C}^3 + \mathcal{O}(\mathcal{C}^4).$$

D.2 As $\mathcal{C} \to \infty$

Consider $\phi_0^* = \pi + \frac{a_1}{\mathcal{C}^{\frac{1}{2}}} + \frac{a_2}{\mathcal{C}} + \frac{a_3}{\mathcal{C}^{\frac{3}{2}}} + ...$ and plug the series into $\frac{d\hat{F}_T}{d\phi_0}(\phi_0^*) = 0$.

$$\frac{d\hat{F}_T}{d\phi_0}(\phi_0^*) = \sigma\left[-\frac{\sqrt{2}\mathcal{C}}{2}\cos\frac{\phi_0^*}{2} - \frac{\sqrt{2}\mathcal{C}}{2}\sin\frac{\phi_0^*}{2} + 2\sin\phi_0^* - \frac{3\sqrt{2}\mathcal{C}}{2}\cos\frac{3\phi_0^*}{2}\right.$$

$$\left. +\frac{3\sqrt{2}\mathcal{C}}{2}\sin\frac{3\phi_0^*}{2} - \mathcal{C}^2\cos 2\phi_0^* + \mathcal{C}^2\right] = 0.$$

$\Rightarrow$

$$-\frac{\sqrt{2}}{2}\mathcal{C}\cos\left[\frac{1}{2}(\pi + \frac{a_1}{\mathcal{C}^{\frac{1}{2}}} + \frac{a_2}{\mathcal{C}} + \frac{a_3}{\mathcal{C}^{\frac{3}{2}}} + ...)\right] - \frac{\sqrt{2}}{2}\mathcal{C}\sin\left[\frac{1}{2}(\pi + \frac{a_1}{\mathcal{C}^{\frac{1}{2}}} + \frac{a_2}{\mathcal{C}} + \frac{a_3}{\mathcal{C}^{\frac{3}{2}}} + ...)\right]$$

$$+2\sin\left[\pi + \frac{a_1}{\mathcal{C}^{\frac{1}{2}}} + \frac{a_2}{\mathcal{C}} + \frac{a_3}{\mathcal{C}^{\frac{3}{2}}} + ...\right] - \frac{3\sqrt{2}}{2}\mathcal{C}\cos\left[\frac{3}{2}(\pi + \frac{a_1}{\mathcal{C}^{\frac{1}{2}}} + \frac{a_2}{\mathcal{C}} + \frac{a_3}{\mathcal{C}^{\frac{3}{2}}}...)\right]$$

$$+\frac{3\sqrt{2}}{2}\mathcal{C}\sin\left[\frac{3}{2}(\pi + \frac{a_1}{\mathcal{C}^{\frac{1}{2}}} + \frac{a_2}{\mathcal{C}} + \frac{a_3}{\mathcal{C}^{\frac{3}{2}}}...)\right] - \mathcal{C}^2\cos\left[2(\pi + \frac{a_1}{\mathcal{C}^{\frac{1}{2}}} + \frac{a_2}{\mathcal{C}} + \frac{a_3}{\mathcal{C}^{\frac{3}{2}}}...)\right] + \mathcal{C}^2 = 0.$$

$\Rightarrow$

$$\frac{\sqrt{2}}{2}\mathcal{C}\sin\left[\frac{1}{2}(\frac{a_1}{\mathcal{C}^{\frac{1}{2}}} + \frac{a_2}{\mathcal{C}} + \frac{a_3}{\mathcal{C}^{\frac{3}{2}}} + ...)\right] - \frac{\sqrt{2}}{2}\mathcal{C}\cos\left[\frac{1}{2}(\frac{a_1}{\mathcal{C}^{\frac{1}{2}}} + \frac{a_2}{\mathcal{C}} + \frac{a_3}{\mathcal{C}^{\frac{3}{2}}} + ...)\right]$$

$$-2\sin\left[\frac{a_1}{\mathcal{C}^{\frac{1}{2}}} + \frac{a_2}{\mathcal{C}} + \frac{a_3}{\mathcal{C}^{\frac{3}{2}}} + ...\right] - \frac{3\sqrt{2}}{2}\mathcal{C}\sin\left[\frac{3}{2}(\frac{a_1}{\mathcal{C}^{\frac{1}{2}}} + \frac{a_2}{\mathcal{C}} + \frac{a_3}{\mathcal{C}^{\frac{3}{2}}}...)\right]$$

$$-\frac{3\sqrt{2}}{2}\mathcal{C}\cos\left[\frac{3}{2}(\frac{a_1}{\mathcal{C}^{\frac{1}{2}}} + \frac{a_2}{\mathcal{C}} + \frac{a_3}{\mathcal{C}^{\frac{3}{2}}}...)\right] - \mathcal{C}^2\cos\left[2(\frac{a_1}{\mathcal{C}^{\frac{1}{2}}} + \frac{a_2}{\mathcal{C}} + \frac{a_3}{\mathcal{C}^{\frac{3}{2}}}...)\right] + \mathcal{C}^2 = 0.$$

Consider the power series expansions for Sine and Cosine at 0.

$$\cos(x) = 1 - \frac{x^2}{2} + \frac{x^4}{24} + ...$$

$$\sin(x) = x - \frac{x^3}{6} + ...$$

Let $P = \frac{a_1}{\mathcal{C}^{\frac{1}{2}}} + \frac{a_2}{\mathcal{C}} + \frac{a_3}{\mathcal{C}^{\frac{3}{2}}} + ...$

$$\frac{\sqrt{2}}{2}\mathcal{C}\left[\frac{1}{2}P - \frac{1}{6}(\frac{1}{2}P)^3 + ...\right] - \frac{\sqrt{2}}{2}\mathcal{C}\left[1 - \frac{1}{2}(\frac{1}{2}P)^2 + \frac{1}{24}(\frac{1}{2}P)^4 + ...\right] - 2\left[P - \frac{1}{6}P^3 + ...\right]$$

$$-\frac{3\sqrt{2}}{2}\mathcal{C}\left[\frac{3}{2}P - \frac{1}{6}(\frac{3}{2}P)^3 + ...\right] - \frac{3\sqrt{2}}{2}\mathcal{C}\left[1 - \frac{1}{2}(\frac{3}{2}P)^2 + \frac{1}{24}(\frac{3}{2}P)^4 + ...\right]$$

$$-\mathcal{C}^2\left[1 - \frac{1}{2}(2P)^2 + \frac{1}{24}(2P)^4 + ...\right] + \mathcal{C}^2 = 0.$$

84

Sorting each term and obtain:

$\mathcal{O}(\mathcal{C}): -2\sqrt{2} + 2a_1{}^2 = 0 \quad \rightarrow \quad a_1 = 2^{\frac{1}{4}}\text{(invalid) or } a_1 = -2^{\frac{1}{4}}\text{(valid, } \phi_0^* < \pi);$

$\mathcal{O}(\mathcal{C}^{\frac{1}{2}}): -2\sqrt{2}a_1 + 4a_2a_1 = 0 \quad \rightarrow \quad a_2 = \frac{\sqrt{2}}{2};$

$\mathcal{O}(1): -2\sqrt{2}a_2 + \frac{7}{4}\sqrt{2}a_1{}^2 - \frac{2}{3}a_1{}^4 + 2a_2{}^2 + 4a_1a_3 = 0 \quad \rightarrow \quad a_3 = \frac{7}{24}2^{-\frac{1}{4}};$

Therefore,

$$\phi_0^* = \pi - \frac{2^{\frac{1}{4}}}{\mathcal{C}^{\frac{1}{2}}} + \frac{\frac{\sqrt{2}}{2}}{\mathcal{C}} + \frac{\frac{7}{24}(2^{-\frac{1}{4}})}{\mathcal{C}^{\frac{3}{2}}} + \mathcal{O}(\mathcal{C}^{-\frac{1}{2}}) \quad \text{as} \quad \mathcal{C} \to \infty. \tag{D.2}$$

Then we plug ϕ_0^* in (D.2) into $\hat{F}_T = 0$ to get $\mathcal{A}^*$, where $\mathcal{A}^* = b_0 + \frac{b_1}{\mathcal{C}^{\frac{1}{2}}} + \frac{b_2}{\mathcal{C}} + \frac{b_3}{\mathcal{C}^{\frac{3}{2}}} + \frac{b_4}{\mathcal{C}^2} + \dots$

$\mathcal{O}(\mathcal{C}^2): -b_0 + \pi = 0 \quad \rightarrow \quad b_0 = \pi;$

$\mathcal{O}(\mathcal{C}^{\frac{3}{2}}): -b_1 = 0 \quad \rightarrow \quad b_1 = 0;$

$\mathcal{O}(\mathcal{C}): -b_2 = 0 \quad \rightarrow \quad b_2 = 0;$

$\mathcal{O}(\mathcal{C}^{\frac{1}{2}}): -b_3 + \frac{4}{3}2^{\frac{3}{4}} = 0 \quad \rightarrow \quad b_3 = \frac{4}{3}2^{\frac{3}{4}};$

$\mathcal{O}(1): b_4 = 0;$

$\mathcal{O}(\mathcal{C}^{\frac{1}{2}}): b_5 = -\frac{1}{6}2^{\frac{1}{4}};$

In summary, as $\mathcal{C} \to \infty$,

$$\mathcal{A}^* = \pi + \frac{\frac{4}{3}2^{\frac{3}{4}}}{\mathcal{C}^{\frac{3}{2}}} + \mathcal{O}(\mathcal{C}^{-\frac{1}{2}}).$$

$$\phi_0^* = \pi - \frac{2^{\frac{1}{4}}}{\mathcal{C}^{\frac{1}{2}}} + \frac{\frac{\sqrt{2}}{2}}{\mathcal{C}} + \frac{\frac{7}{24}2^{-\frac{1}{4}}}{\mathcal{C}^{\frac{3}{2}}} + \mathcal{O}(\mathcal{C}^{-2}).$$

Appendix E

No Intersection for $\gamma = 0$

In Section 2.12.1, Theorem 2.4 shows the equilibrium point(if it exists) never lies in intersection region. The proof is shown as follows.

Theorem. *If there exists $\bar{\phi}_0$ such that $\hat{F}_T(\bar{\phi}_0) = 0$, then $I(\bar{\phi}_0, \mathcal{C}) > 0$ for any given $\mathcal{C}$*

Proof. With $\gamma = 0$,

$$\hat{F}_T(\phi_0) = -\mathcal{A}\mathcal{C}^2 - 2\mathcal{C}\sin\frac{\phi_0}{2} - 2\sin\phi_0 - 2\mathcal{C}\sin\frac{3\phi_0}{2} - \frac{1}{2}\mathcal{C}^2\sin 2\phi_0 + \mathcal{C}^2\phi_0.$$

The smallest $\bar{\phi}_0$ appears when $\mathcal{A} = 0$. Suppose $\bar{\phi}_{0\,\text{min}}$ is the smallest equilibrium point for given $\mathcal{C}$. If we can prove $I(\bar{\phi}_{0\,\text{min}}, \mathcal{C}) > 0$, then all equilibrium points $\bar{\phi}_0$ never lie in intersection region.

$$\hat{F}_T(\bar{\phi}_{0\,\text{min}}) = -2\mathcal{C}\sin\frac{\bar{\phi}_{0\,\text{min}}}{2} - 2\sin\bar{\phi}_{0\,\text{min}} - 2\mathcal{C}\sin\frac{3\bar{\phi}_{0\,\text{min}}}{2} - \frac{1}{2}\mathcal{C}^2\sin 2\bar{\phi}_{0\,\text{min}} + \mathcal{C}^2\bar{\phi}_{0\,\text{min}} = 0.$$

We only need to consider $\bar{\phi}_{0\,\text{min}} \in [0, \frac{\pi}{2}]$. Since the intersection never occurs for $\gamma = 0$ and $\bar{\phi}_{0\,\text{min}} \in (\frac{\pi}{2}, \pi]$, therefore we suppose $\bar{\phi}_{0\,\text{min}} \in [0, \frac{\pi}{2}]$.

The equation $\hat{F}_T(\bar{\phi}_{0\,\text{min}}) = 0$ turns out to be the quadratic equation in $\mathcal{C}$.

$$\left(\bar{\phi}_{0\,\text{min}} - \frac{1}{2}\sin 2\bar{\phi}_{0\,\text{min}}\right)\mathcal{C}^2 - 2\left(\sin\frac{\bar{\phi}_{0\,\text{min}}}{2} + \sin\frac{3\bar{\phi}_{0\,\text{min}}}{2}\right)\mathcal{C} - 2\sin\bar{\phi}_{0\,\text{min}} = 0.$$

Moreover,

$$\bar{\phi}_{0\,\min} - \frac{1}{2}\sin 2\bar{\phi}_{0\,\min} \geq 0, \quad `` ='' \text{ holds only } \bar{\phi}_{0\,\min} = 0,$$

$$2\left(\sin\frac{\bar{\phi}_{0\,\min}}{2} + \sin\frac{3\bar{\phi}_{0\,\min}}{2}\right) > 0.$$

We can solve for $\mathcal{C}$:

$$\mathcal{C} = \frac{2\left(\sin\frac{\bar{\phi}_{0\,\min}}{2} + \sin\frac{3\bar{\phi}_{0\,\min}}{2}\right) \pm \sqrt{\left[2\left(\sin\frac{\bar{\phi}_{0\,\min}}{2} + \sin\frac{3\bar{\phi}_{0\,\min}}{2}\right)\right]^2 + 8\left(\bar{\phi}_{0\,\min} - \frac{1}{2}\sin 2\bar{\phi}_{0\,\min}\right)\sin\bar{\phi}_{0\,\min}}}{2\left(\bar{\phi}_{0\,\min} - \frac{1}{2}\sin 2\bar{\phi}_{0\,\min}\right)}.$$

Only $+$ is valid (we require $\mathcal{C}$ being positive). And we have $\mathcal{C} > \frac{2(\sin\frac{\bar{\phi}_{0\,\min}}{2} + \sin\frac{3\bar{\phi}_{0\,\min}}{2})}{\bar{\phi}_{0\,\min} - \frac{1}{2}\sin 2\bar{\phi}_{0\,\min}}$ then plug in $I(\bar{\phi}_{0\,\min}, \mathcal{C})$.

$$
\begin{aligned}
I(\bar{\phi}_{0\,\min}, \mathcal{C}) \;>\; & \frac{2(\sin\frac{\bar{\phi}_{0\,\min}}{2} + \sin\frac{3\bar{\phi}_{0\,\min}}{2})}{\bar{\phi}_{0\,\min} - \frac{1}{2}\sin 2\bar{\phi}_{0\,\min}}\sin\bar{\phi}_{0\,\min} - \sqrt{2} - \ln\left(\tan\frac{\pi}{8}\right) \\
& + 2\sin\left(\frac{\bar{\phi}_{0\,\min}}{2}\right) + \ln\left[-\tan\left(\frac{\bar{\phi}_{0\,\min} - \pi}{4}\right)\right] \\
\;>\; & 0.
\end{aligned}
$$

Therefore, $I(\bar{\phi}_0, \mathcal{C}) > 0$. $\qquad\qquad\qquad\qquad\qquad\qquad\qquad\qquad\qquad\qquad\qquad\square$

Appendix F

$\hat{E}_T$ of the Square with Rotation

Similar to what we did in Section 2.3, we are going to compute the dimensionless total energy $\hat{E}_T$ of in terms of $\hat{h} = \frac{h}{a}$ and θ. In addition, the characteristic energy E_{square} and a dimensionless variable $\mathcal{S}$ are introduced in (F.6).

- The body potential energy is:
$$E_G = \rho' a^2 g h. \tag{F.1}$$

- The wetting energy is:

$$
\begin{aligned}
E_W &= -\cos\gamma\sigma|\Sigma| \\
&= -\cos\gamma\sigma\left[|AC| + |DE| + |CD| + |LA| + |RE|\right] \\
&= -\cos\gamma\sigma\left[2a - \frac{2h}{\cos\theta} - \frac{\frac{2}{\sqrt{\kappa}}\sin\frac{\psi_{10}}{2} + \frac{2}{\sqrt{\kappa}}\sin\frac{\psi_{20}}{2}}{\cos\theta}\right] \\
&= 2\cos\gamma\sigma\left[\frac{h}{\cos\theta} + \frac{\sqrt{2}\cos\frac{\theta}{2}(\sin\frac{\gamma}{2} - \cos\frac{\gamma}{2})}{\sqrt{\kappa}\cos\theta} - a\right]. \tag{F.2}
\end{aligned}
$$

88

- The surface tension energy is:

$$
\begin{aligned}
E_\sigma &= \sigma \int_{N_x}^{\infty} \left[\sqrt{1 + \left(\frac{du_1}{dx}\right)^2} - 1 \right] dx + \sigma \int_{-\infty}^{M_x} \left[\sqrt{1 + \left(\frac{du_2}{dx}\right)^2} - 1 \right] dx - \sigma|MN| \\
&= \sigma \int_0^{\psi_{10}} \left[\sqrt{1 + \tan^2 \psi_1} - 1 \right] \frac{\cos \psi_1}{\kappa u_1} d\psi_1 + \sigma \int_0^{\psi_{20}} \left[\sqrt{1 + \tan^2 \psi_2} - 1 \right] \frac{\cos \psi_2}{\kappa u_2} d\psi_2 \\
&\quad - \sigma \left[a\cos\theta + a\sin\theta\tan\theta - \frac{2}{\sqrt{\kappa}} \tan\theta \left(\sin\frac{\psi_{10}}{2} - \sin\frac{\psi_{20}}{2} \right) \right] \\
&= 2\frac{\sigma}{\sqrt{\kappa}} \left(1 - \cos\frac{\psi_{10}}{2} \right) + 2\frac{\sigma}{\sqrt{\kappa}} \left(1 - \cos\frac{\psi_{20}}{2} \right) \\
&\quad - \sigma \left[a\cos\theta + a\sin\theta\tan\theta - \frac{2}{\sqrt{\kappa}} \tan\theta \left(\sin\frac{\psi_{10}}{2} - \sin\frac{\psi_{20}}{2} \right) \right] \\
&= 2\frac{\sigma}{\sqrt{\kappa}} \left[2 - \sqrt{2}\cos\frac{\theta}{2} \left(\sin\frac{\gamma}{2} + \cos\frac{\gamma}{2} \right) \right] \\
&\quad - \sigma \left[a\cos\theta + a\sin\theta\tan\theta + \frac{2\sqrt{2}}{\sqrt{\kappa}} \tan\theta \sin\frac{\theta}{2} \left(\sin\frac{\gamma}{2} + \cos\frac{\gamma}{2} \right) \right].
\end{aligned}
\tag{F.3}
$$

- The fluid potential energy is:

$$
\begin{aligned}
E_F &= \rho g \int_{N_x}^{\infty} \frac{u_1{}^2}{2} dx + \rho g \int_{-\infty}^{M_x} \frac{u_2{}^2}{2} dx - \int_{\triangle AML} \rho g y \, dA + \int_{\triangle ENR} \rho g y \, dA - \int_{ACDN} \rho g y \, dA \\
&= -\frac{\sigma}{\sqrt{\kappa}} \left[\frac{4}{3} - \left(\cos\frac{\psi_{10}}{2} + \cos\frac{\psi_{20}}{2} \right) + \frac{1}{3} \left(\cos\frac{3\psi_{10}}{2} + \cos\frac{3\psi_{20}}{2} \right) \right] \\
&\quad - \rho g \left(\text{Area}_{AML} \right) \bar{y}_{\triangle AML} + \rho g \left(\text{Area}_{ENR} \right) \bar{y}_{\triangle ENR} - \rho g \left(\text{Area}_{ACDE} \right) h_B,
\end{aligned}
\tag{F.4}
$$

where h_B can be calculated by equation (3.24). Thus

$$
\begin{aligned}
E_F &= -\frac{\sigma}{\sqrt{\kappa}} \left[\frac{4}{3} - \sqrt{2}\cos\frac{\theta}{2} \left(\sin\frac{\gamma}{2} + \cos\frac{\gamma}{2} \right) + \frac{\sqrt{2}}{3}\cos\frac{3\theta}{2} \left(\sin\frac{3\gamma}{2} - \cos\frac{3\gamma}{2} \right) \right] \\
&\quad + \frac{4\sigma}{3\sqrt{\kappa}} \tan\theta \left[\sin^3 \left(\frac{\gamma+\theta}{2} - \frac{\pi}{4} \right) - \sin^3 \left(\frac{\gamma-\theta}{2} - \frac{\pi}{4} \right) \right] \\
&\quad + \rho g a^3 \left[\frac{1}{12\cos\theta} + \frac{1}{2}\left(\frac{h}{a}\right)^2 \frac{1}{\cos\theta} - \frac{1}{2}\left(\frac{h}{a}\right) + \frac{1}{24}\frac{\cos 2\theta}{\cos\theta} \right].
\end{aligned}
\tag{F.5}
$$

89

We introduce the characteristic energy E_{square} and a dimensionless variable $\mathcal{S}$,

$$E_{square} = \rho_s a^3 g \quad \text{and} \quad \mathcal{S} = \frac{\sigma}{\sqrt{\kappa \rho_s a^3 g}}. \tag{F.6}$$

In addition, the term $\sigma a = \sqrt[3]{\frac{\mathcal{S}^2}{\alpha}} E_{square}$.

$$E_G = E_{square} \hat{h}. \tag{F.7}$$

$$E_W = E_{square} \left\{ 2 \cos \gamma \left[\sqrt[3]{\frac{\mathcal{S}^2}{\alpha}} \left(\frac{\hat{h}}{\cos \theta} - 1 \right) + \sqrt{2} \mathcal{S} \frac{\cos \frac{\theta}{2} (\sin \frac{\gamma}{2} - \cos \frac{\gamma}{2})}{\cos \theta} \right] \right\}. \tag{F.8}$$

$$E_\sigma = E_{square} \left\{ 2\mathcal{S} \left[2 - \sqrt{2} \cos \frac{\theta}{2} \left(\sin \frac{\gamma}{2} + \cos \frac{\gamma}{2} \right) \right] - \sqrt[3]{\frac{\mathcal{S}^2}{\alpha}} \left(\cos \theta + \sin \theta \tan \theta \right) \right.$$
$$\left. -2\sqrt{2} \mathcal{S} \tan \theta \sin \frac{\theta}{2} \left(\sin \frac{\gamma}{2} + \cos \frac{\gamma}{2} \right) \right\}. \tag{F.9}$$

$$E_F = E_{square} \left\{ \mathcal{S} \left[-\frac{4}{3} + \sqrt{2} \cos \frac{\theta}{2} \left(\sin \frac{\gamma}{2} - \cos \frac{\gamma}{2} \right) + \frac{\sqrt{2}}{3} \cos \frac{3\theta}{2} \left(\sin \frac{3\gamma}{2} - \cos \frac{3\gamma}{2} \right) \right] \right.$$
$$+ \frac{4}{3} \mathcal{S} \tan \theta \left[\sin^3 \left(\frac{\gamma+\theta}{2} - \frac{\pi}{4} \right) - \sin^3 \left(\frac{\gamma-\theta}{2} - \frac{\pi}{4} \right) \right]$$
$$\left. + \frac{1}{\alpha} \left[\frac{1}{12 \cos \theta} + \frac{\hat{h}^2}{2 \cos \theta} - \frac{1}{2} \hat{h} + \frac{\cos 2\theta}{24 \cos \theta} \right] \right\}. \tag{F.10}$$

In summary, the non-dimensional $\hat{E}_T$ can be written as

$$\hat{E}_T(\hat{h}, \theta; \mathcal{S}, \theta) = \frac{E_G + E_W + E_\sigma + E_F}{E_{square}}. \tag{F.11}$$

Appendix G

Python Code of the Shooting Method

```python
## import libraries.
import numpy as np
from scipy.integrate import odeint
from scipy import special
from scipy.optimize import fsolve

## steps
N =400

## set contact angle to be pi/3
gamma = np.pi/3

## define radius of cylinder as a
## define radial distance boundary r_star
a = 1.
r_star = 10. ## 10 is good enough

## non-dimensionlize r
r_star = r_star/a

## define capillary length
kappa = 1.

## initial guess
```

```python
c0 = 10**-2

## geometric constraint
## define the inclination angle at contact point
psi0 = gamma-np.pi/2.

## define governing equation
## z = [r u]
def ODEmodel(z,psi):
    drdpsi = z[0]*np.cos(psi)/(kappa*z[0]*z[1]-np.sin(psi))
    dudpsi = z[0]*np.sin(psi)/(kappa*z[0]*z[1]-np.sin(psi))
    return [drdpsi,dudpsi]

## define shooting function
def func14(c,r_star,psi0):
    r0 = a
    steps = N
    if psi0 > 0:
        u_star = -c*special.k0(r_star)
        psi_star = np.arctan(c*special.k1(r_star))
        z0 = np.array([r_star,u_star])

        # integrate from psi* to psi0

        psi = np.linspace(psi_star,psi0,steps)
        z = odeint(ODEmodel,z0,psi)

    else:   #psi0<0
        u_star = c*special.k0(r_star)
        psi_star = -np.arctan(c*special.k1(r_star))
        z0 = np.array([r_star,u_star])

        # integrate from psi* to psi0

        psi = np.linspace(psi_star,psi0,steps)
        z = odeint(ODEmodel,z0,psi)
    return z[-1,0]-r0
```

```
## define root finding function
def fcn(c):
    return func14(c,r_star,psi0)

## solve root finding function to obtain the
## coefficient c
c = fsolve(fcn,c0)

## generate the fluid interface
if psi0 >0:
    u_star = -c*special.k0(r_star)
    z0 = np.array([r_star,u_star])
    psi_star = np.arctan(c*special.k1(r_star))
    psi = np.linspace(psi_star,psi0,N)
    z = odeint(ODEmodel,z0,psi)
else: #psi0<0
        u_star = c*special.k0(r_star)
        z0 = np.array([r_star,u_star])
        psi_star = -np.arctan(c*special.k1(r_star))
        psi = np.linspace(psi_star,psi0,N)
        z = odeint(ODEmodel,z0,psi)

## thus r = z[:,0] and u = z[:,1]

## save the data
np.savetxt('shape.txt', np.c_[z[:,0],z[:,1],psi], delimiter=',')
```

References

[1] Mohammad Abolhassani. On the stability of floating bodies. https://www.researchgate.net/publication/236157800_On_the_satiability_of_floating_bodies, 2011.

[2] Rajat Bhatnagar and Robert Finn. Equilibrium configurations of an infinite cylinder in an unbounded fluid. *Phys. Fluids*, 18(4):047103, 7, 2006.

[3] Alan Elcrat, Robert Neel, and David Siegel. Equilibrium configurations for a floating drop. *J. Math. Fluid Mech.*, 6(4):405–429, 2004.

[4] Paul Erdös, Gérard Schibler, and Roy C. Herndon. Floating equilibrium of symmetrical objects and the breaking of symmetry. part 1: Prisms. *American Journal of Physics*, 60(4):335–345, 1992.

[5] Robert Finn. *Equilibrium capillary surfaces*. Springer-Verlag, New York, 1986.

[6] Robert Finn. The contact angle in capillarity. *Phys. Fluids*, 18(4):047102, 7, 2006.

[7] Robert Finn. On young's paradox, and the attractions of immersed parallel plates. *Physics of Fluids*, 22(1), 2010.

[8] Robert Finn, John McCuan, and Henry C. Wente. Thomas Young's surface tension diagram: its history, legacy, and irreconcilabilities. *J. Math. Fluid Mech.*, 14(3):445–453, 2012.

[9] W. Gifford and L. Scriven. On the attraction of floating particles. *Chem. Eng. Sci.*, 26:287–&, 1971.

[10] Stanley Hartland and Richard W. Hartley. *Axisymmetric fluid-liquid interfaces*. Amsterdam ; New York : Elsevier Scientific Pub. Co., 1976.

[11] Kevin Hemphill. Bubble development of known radius from capillary surfaces. Master's thesis, Wichita State University, The U.S., 1991.

[12] Todd M Kemp and David Siegel. Floating bodies in two dimensions without gravity. *Physics of Fluids*, 23(4):043303, 2011.

[13] Steven G Krantz and Harold R. Parks. *A primer of real analytic functions*. Boston : Birkhäuser., 2002.

[14] John Uri. Lloyd. A study in pharmacy. *Journal of the American Pharmaceutical Association*, 13(6):508–519, 1924.

[15] Ivan Lunati. Young's law and the effects of interfacial energy on the pressure at the solid-fluid interface. *Physics of Fluids*, 19(11), 2007.

[16] Antonin Marchand, Joost H. Weijs, Jacco H. Snoeijer, and Bruno Andreotti. Why is surface tension a force parallel to the interface? *American Journal of Physics*, 79(10):999–1008, 2011.

[17] John McCuan and Ray Treinen. Capillarity and Archimedes' principle of flotation. *Pacific J. Math.*, 265(1):123–150, 2013.

[18] Yulii D. Shikhmurzaev. On young's (1805) equation and finn's (2006) 'counterexample'. *Physics Letters A*, 372(5):704 – 707, 2008.

[19] Ray Treinen. A free boundary problem for capillary surfaces arising from the equilibrium of a floating drop. Master's thesis, Wichita State University, The U.S., 2001.

[20] Thomas I. Vogel. Symmetric unbounded liquid bridges. *Pacific J. Math.*, 103(1):205–241, 1982.

[21] Wikipedia. Centroid — Wikipedia, the free encyclopedia, 2015. [Online; accessed August 2015].

[22] Thomas Young. An essay on the cohesion of fluids. *Philosophical Transactions of the Royal Society of London*, 95:65–87, 1805.